

Membrane Tube Formation by Motor Proteins
Forces and Dynamics

Membrane Tube Formation by Motor Proteins

Forces and Dynamics

Proefschrift

TER VERKRIJGING VAN
DE GRAAD VAN DOCTOR
AAN DE UNIVERSITEIT LEIDEN,
OP GEZAG VAN DE RECTOR MAGNIFICUS DR. D.D. BREIMER,
HOGLERAAR IN DE FACULTEIT DER WISKUNDE EN
NATUURWETENSCHAPPEN EN DIE DER GENEESKUNDE,
VOLGENS BESLUIT VAN HET COLLEGE VOOR PROMOTIES
TE VERDEDIGEN OP WOENSDAG 26 JANUARI 2005
TE KLOKKE 14.15 UUR

DOOR

Gerbrand Koster

GEBOREN TE WAGENINGEN IN 1974

Promotiecommissie:

Promotor: Prof. dr. M. Dogterom
Referent: Prof. dr. P. Bassereau (Institut Curie, France)
Overige leden: Prof. dr. T. Schmidt
Dr. C. Storm
Prof. dr. C.F. Schmidt (Vrije Universiteit Amsterdam)
Dr. K.N.J. Burger (Universiteit Utrecht)
Prof. dr. P.H. Kes

Membrane tube formation by motor proteins: forces and dynamics
Gerbrand Koster

Cover: Maria Heesen

ISBN 90-6464-975-8

A digital version of this thesis can be downloaded from <http://www.amolf.nl>

The work described in this thesis was performed at the FOM Institute for Atomic and Molecular Physics (AMOLF), Kruislaan 407, 1098 SJ Amsterdam. This work is part of the research program of the "Stichting voor Fundamenteel Onderzoek der Materie (FOM)", which is financially supported by the "Nederlandse organisatie voor Wetenschappelijk Onderzoek (NWO)".

“On ne voit bien qu’avec le cœur. L’essentiel est invisible pour les yeux”

—Antoine de Saint-Exupéry
(Le petit prince)

This thesis is partly based on the following articles:

- G. Koster, M. VanDuijn, B. Hofs, and M. Dogterom (2003),
Membrane tube formation from giant vesicles by dynamic association of motor proteins,
Proceedings of the National Academy of Sciences USA, **100**, 15583-15588 (Chapters 3 and 5)
- G. Koster, A. Cacciuto, I. Derényi, D. Frenkel, and M. Dogterom (2004),
Force barriers for membrane tube formation,
Submitted (Chapter 4)
- G. Koster, I. Derényi, and M. Dogterom,
Membrane tube formation and retraction: analysis of the force-extension curve,
In preparation (Chapter 4)
- G. Koster, M. VanDuijn, and M. Dogterom,
In vitro study of competition between plus-end and minus-end directed motors,
In preparation (Chapter 6)
- G. Koster,
Moleculaire motors geven vorm aan membranen in de cel,
Submitted (Samenvatting)

Contents

1	Introduction	9
1.1	Internal organization of cells	9
1.2	Spatial organization of membranes by motor proteins and the cytoskeleton	17
1.3	Thesis overview	19
2	Experimental set-up, procedures and data analysis	21
2.1	Preparations and purifications	21
2.2	Sample preparation	27
2.3	Apparatus	32
2.4	Data Analysis	36
3	Forces required to maintain membrane tubes	39
3.1	Mechanics of lipid bilayers	39
3.2	Membrane tension and fluctuations	45
3.3	Experimental determination of plateau forces	49
3.4	Discussion	61
4	Force barriers for membrane tube formation	63
4.1	Introduction	63
4.2	Theoretical analysis of overshoot forces	65
4.3	Experimental results and simulations	66
4.4	Discussion	77
5	Tubular membrane networks formed by dynamic association of motor proteins	79
5.1	Introduction	79
5.2	Experimental results	81
5.3	Dynamic association of motor proteins	89
5.4	Discussion	95
6	Competition between plus-end and minus-end directed motors	97
6.1	Introduction	98
6.2	Preliminary experimental results	99
6.3	Organizing microtubules	105
6.4	Discussion	109
7	Summary and general discussion	113
	Bibliography	121

Samenvatting	129
Nawoord	139
Curriculum Vitae	141

1 Introduction

The interior of cells shows a high level of compartmentalization, where membranes form the borders between the different compartments. The spatial organization of intracellular membranes is dependent on the dynamic interplay between the cytoskeleton, which provides a network of tracks throughout the cell, and motor proteins that can generate forces while moving on these tracks. A ubiquitous membrane shape is that of membrane tubes, which are formed when a localized force is exerted on a membrane. Membrane tubes form a significant part of intracellular compartments and transport intermediates. In cells, motor proteins have been shown to be important for the formation of tubes, but the exact mechanism is not well understood. To shed some light on this mechanism, we study in this thesis the forces and parameters that control tube formation in an in vitro experimental system. In this first chapter the different components that are important for the spatial organization of the cellular membranes will be introduced. Subsequently, we will discuss the widespread presence of membrane tubes. In the last section an overview of the subjects treated in the thesis will be presented.

1.1 Internal organization of cells

The basic building unit of living organisms is the cell. For different specialized tasks, different cell types are found in a variety of different shapes. The general organizing mechanisms and the machinery used for the proper functioning are however similar in different cell types. Eukaryotic cells (plant- and animal cells) are typically a few μm to 50 μm in size. Interestingly, even at these small scales, there is a clear organization of spatially and functionally separated compartments (organelles) for the different cellular functions. In these compartments, different components and functions are segregated from each other: DNA storage in the nucleus, ATP production in the mitochondria, synthesis of proteins and lipids in the endoplasmic reticulum (ER), and sorting of proteins for their final destinations in the Golgi apparatus. A much-simplified sketch of a eukaryotic cell is presented in Figure 1-1.

Introduction

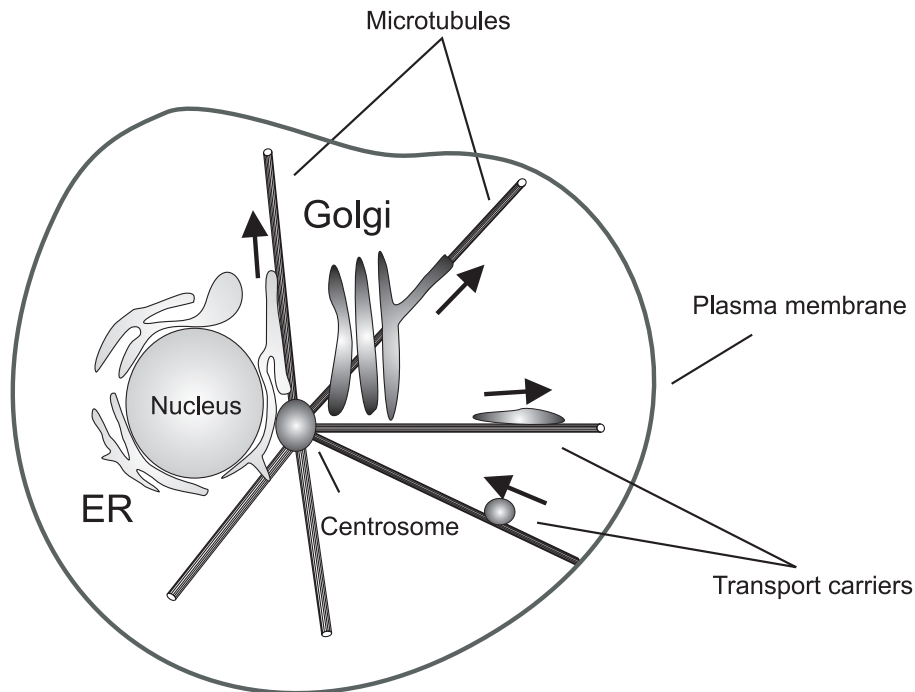


Figure 1-1. Sketch of the internal organization of a cell. The arrows indicate the movement of membrane compartments on the microtubule cytoskeleton.

Cells, and the organelles within them, are separated from each other and from the outside world by thin membranes. The main building blocks of these cellular membranes are lipids and proteins (Figure 1-3). One important mechanism through which different compartments are shaped and spatially distributed, is the action of motor proteins and the cytoskeleton (the skeleton of the cell). The cytoskeleton forms a dense network of tracks throughout the cell, and functions as an infrastructure for the movement of motor proteins that pull on membrane compartments. This results either in the movement of the membrane compartment through the cell, or in a deformation of the membrane compartment (for example the formation of a membrane tube) when there is an opposing force on the membrane (see Figure 1-1). In animal cells, the dominant cytoskeletal components for membrane organization are the microtubules and their associated motor proteins. These have been shown to be essential for the formation of extensive tubular networks throughout the cell and the membranes and microtubule cytoskeleton are closely colocalized (see Figure 1-2). In plant cells actin and the associated motor protein myosin are the most relevant components.

Introduction

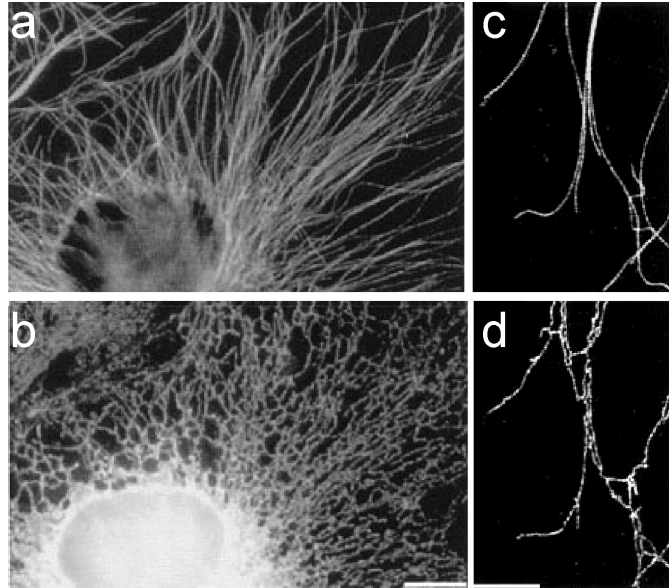


Figure 1-2. Fluorescently labeled microtubules (a) and endoplasmic reticulum (b) are distributed *in vivo* throughout the cell, and show a close colocalization (c and d). Adapted from [1]. The bar in (b) is 10 μm and the bar in (d) is 5 μm .

The mechanism through which the motor proteins form the tubes is poorly understood. In this thesis we will examine some of the basic physical mechanisms that govern membrane tube formation, and study under what conditions motor proteins can pull tubes along microtubules. In this section the three components that are crucial for the spatial organization of the cell (membranes, the cytoskeleton, and motor proteins) will be introduced.

Membranes

Cellular membranes consist of many different lipids and these membranes typically contain embedded (membrane) proteins and associated proteins (see Figure 1-3). Even though it incorporates many kinds of lipids and proteins, a membrane has a thickness of only ~ 5 nm. This limited thickness makes it a flexible structure that is easily deformable by forces in the piconewton regime and makes it susceptible to Brownian fluctuations. Lipids consist of a hydrophilic head and a hydrophobic tail. When dissolved in an aqueous solution, it is energetically favorable to shield the tail from the water molecules, while the heads prefer to be oriented towards the aqueous solution. This property of the lipids makes them self-

Introduction

assemble into a bilayer (consisting of two monolayers of lipids). In addition to the lipids, *in vivo* many proteins are embedded in the bilayer. This allows for the communication between the different sides of a membrane. In addition, certain proteins in the cytosol can interact directly with the lipid bilayer or with the proteins embedded within this membrane.

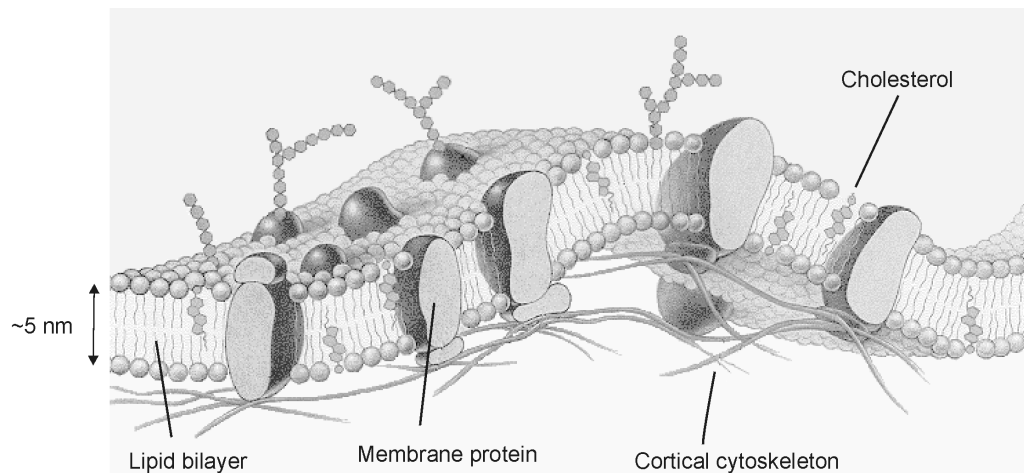


Figure 1-3. Sketch of a membrane and associated proteins (adapted from [2]).

A crucial property of lipid bilayers is their two-dimensional liquid nature (above a certain temperature). This allows for the lateral diffusion of molecules in the membrane, a property that lies at the heart of the dynamic and flexible nature of the membrane. It is essential for proper cell functioning [3], for the several shapes a membrane can adopt, and for many processes where molecules diffuse on the membrane surface to explore the adjacent space and find the right interaction partner. Even though the bilayer behaves in many respects as a two-dimensional fluid, the mobility of different molecules is restricted by several factors. Most lipids and proteins cannot cross over to the complementary monolayer, and the composition of the two monolayers is actively maintained through transport of lipids by proteins from one layer to the other [4]. Furthermore, membranes may contain substructures often referred to as rafts [5] and, depending on the composition of the membranes, the properties of the lipids can induce phase separation into different domains [6]. In addition, the underlying cortical cytoskeleton and associated proteins limit the diffusion of molecules in the membrane as well [7].

Introduction

The microtubule cytoskeleton

As mentioned above, an important component for the internal organization of the cell is the cytoskeleton. This skeleton is present throughout the whole cell, providing it with mechanical rigidity and defining the shape of the cell. In addition, it is important for the movement of cells, for cell division, and it provides an infrastructure for the movement of motor proteins that transport vesicles through the cell and shape the different organelles [8]. There are three types of cytoskeletal filaments in eukaryotic cells: microtubules, actin filaments, and intermediate filaments. These filaments polymerize from protein sub-units and can reach length scales comparable to the dimensions of the whole cell. The essential role of the cytoskeleton is underlined by the fact that cytoskeletal proteins are highly conserved in evolution, and are found in all eukaryotic cells [8], presumably because of the key role these cytoskeletal filaments play in the many cell processes described above.

In this thesis we focus on the role of microtubules (MTs), and therefore we will give a more detailed description of them in this section. MTs polymerize from alpha-beta tubulin dimers. The dimers are 8 nm long and assemble in such a way that they form a polarized tubule of 25 nm diameter with (on average) 13 filaments (see Figure 1-4). This structure makes MTs the stiffest cytoskeletal component, and the polymerization process of MTs itself has been shown to be able to exert significant forces [9].

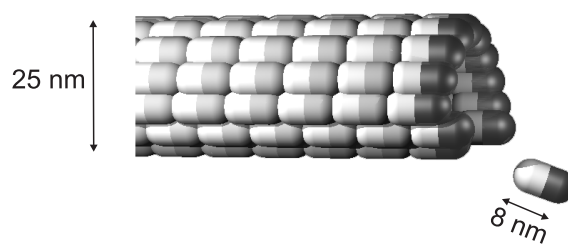


Figure 1-4. Sketch of a microtubule (adapted from [10]). A tubulin dimer is 8 nm long, and consists of an α (light) and a β monomer, which can be in a GTP-bound state (black) or in a GDP-bound state (gray). The dimers polymerize into a tubule with a diameter of 25 nm.

In vivo MTs are highly dynamic structures, with alternating periods of growth and shrinkage [11]. This so-called dynamic instability is fueled by the hydrolysis of GTP. It has an important role in the exploration of the environment, and the positioning of the microtubule-

Introduction

organizing center (see below) near the center of the cell [12]. MTs are intrinsically asymmetric. One end is called the plus-end (because of the higher growth velocity), and the other the minus-end [11]. This asymmetry of the filament is recognized by motor-proteins, which move in either the minus- or the plus-end direction on these tracks.

In most animal cells, an important characteristic of MTs is that they are organized in a radial array (aster-shape) that spreads out throughout a large part of the cell (see e.g. Figure 1-2a). MTs are nucleated at the MT organizing-center (the centrosome) near the nucleus, resulting in the plus-ends of the MTs pointing towards the periphery. This aster structure provides a polarized infrastructure throughout the cytoplasm along which cytoskeletal motor proteins can move. In addition, it defines a general coordinate system, which is used to position the organelles. For example, the positioning of the Golgi apparatus near the nucleus has been suggested to be (partly) caused by the action of minus-end directed motors [13-15], and the ER is spread throughout the cell on the MT network by the action of plus-end directed motors [16].

Motor proteins

Motor proteins are the engines of the cell. These proteins convert the chemical energy, which is released by removal of a phosphate group from ATP or GTP, to conformational changes of their structure. The use of chemically stored energy for force generation by proteins is a general method used in cells to perform work. This energy may for example be used for the translocation of material through a membrane [17] or the pinching off of membranous cargo carriers [18]. We will be concerned here with the cytoskeletal motor proteins that interact with, and move along the cytoskeleton.

Based on homology studies (comparison of the genetic sequence) there are three main families of motor proteins: the kinesins, the dyneins, and the myosins [19]. The myosins move along actin filaments and have many important functions in cells, and are best known for their function in muscle movement. In addition, many of the processes that are carried out by MTs and associated proteins in animal cells, are executed by myosins and the actin network in plant cells [20].

Introduction

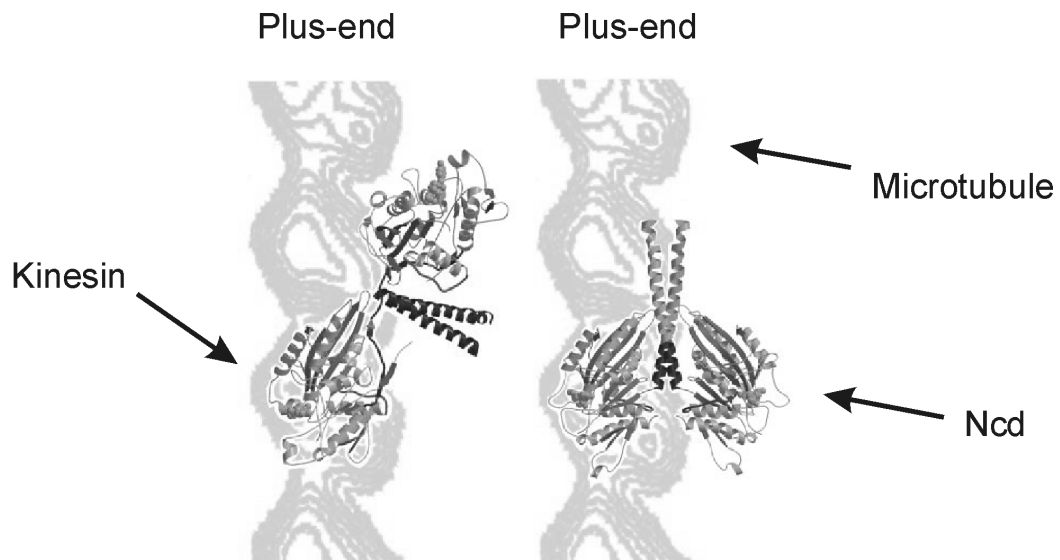


Figure 1-5. Kinesin (left) and ncd (right) docked to a microtubule protofilament (adapted from [21]). The kinesin and ncd structures were determined with crystallography and fitted to the tubulin dimers. Kinesin moves to the plus-end and ncd to the minus-end.

The kinesin and dynein motor proteins are responsible for movement and transport along MTs. Kinesins move towards the plus-end and dyneins move towards the minus-end. There are, however, exceptions to this directionality: the kinesin-family protein ncd (nonclaret disjunctional, [22-24]) moves on MTs in the minus-end direction. Presumably due to a different positioning of the (directionality of) the heads with respect to each other [21], see Figure 1-5.

The kinesin motor protein family is large [25, 26], and new members of the family are frequently discovered by screening of the genomes of many organisms. MT motor proteins can be characterized by common structural properties. In general, a motor protein consists of a part that provides the interaction with the MT (the head of the protein), a tail that provides the association of the motor protein with the object it needs to transport, and a neck connecting head and tail. Although motor proteins can exert force as a monomer, many of them are found as dimers [19]. This results in a protein complex with two heads, which allows in principle for the movement on a MT while keeping one head attached to the MT all the time. The details of

Introduction

this movement are heavily debated [19, 27-29], but it is clear that dimerization increases the number of steps that can be taken before the motor dissociates from the MT. Because MTs are formed from 8-nm-long dimers of alpha and beta-tubulin, the filaments of MTs have an 8 nm periodicity. It has been shown that kinesin moves in 8 nm steps on this lattice [30]. The number of steps taken before detachment is stochastically distributed, with on average ~100 steps (800 nm), when no force is present. When studied in bead assays or sliding assays [19], conventional kinesin can move up to 1 $\mu\text{m/s}$. However, the exact speed depends on several parameters like, for example, the kind of kinesin, the presence of several factors in the solution, the ATP concentration, the temperature, and the opposing force. When an external force is applied to kinesin (e.g. with optical tweezers), the number of steps the motor can take decreases. When the force is increased, at some point a maximum force is reached where the motor cannot move anymore (the stall force). For kinesin this stall force is approximately 6 pN [31, 32]. Dynein has been studied in less detail because of its more complex structure, which consists of a complex of several proteins [26]. However a recent study suggests that dynein moves in a processive way and can exert forces up to 1.1 pN [33]. Far less is known about the properties of ncd. The speed of MT sliding in a ncd-gliding assay has been measured to be 0.1-0.15 $\mu\text{m/s}$ in the minus-end direction [23], and ncd has been shown to be non-processive. Upon each contact with the MT a power stroke is made which moves the ncd over a distance of ~9 nm and subsequently the motor detaches [34].

The properties of individual motor proteins are being unraveled at a rapid pace. How multiple motor proteins cooperate, interact, and coordinate their activities has however received far less attention. If individual motor proteins cannot move processively by themselves, they may do so by functioning together in groups. An example of this is the long-distance movement by motor activity in muscle. The individual myosin motors in muscle do not move processively, but in groups their activity results in large-scale movement. Furthermore, many organelles are observed to move over larger distances than one motor may be expected to move [35]. This occurs without detaching from cytoskeletal filaments, suggesting that multiple motors are working together. The general cooperative effects of motor protein functioning are badly understood. It is becoming clear that such collaborative functioning is important for the spatial distribution of organelles. For example, multiple motors of opposite directionality are present on organelles, and it is yet unclear how their interaction is orchestrated [36].

1.2 Spatial organization of membranes by motor proteins and the cytoskeleton

The different organelles in cells have characteristic shapes, which are dynamic in the sense that they are constantly being remodeled and deformed. Most notably, for this study, are the typical dynamic morphologies of the endoplasmic reticulum (ER) and the Golgi apparatus. The ER is often described as consisting of two different parts: the rough ER and the smooth ER. The rough part consists of flat sacs covered with ribosomes, whereas the smooth part consists of a network of interconnected membrane tubes. These tubes give the ER its characteristic appearance of a netlike labyrinth, which colocalizes with the MT cytoskeleton (see Figure 1-2, [1]). In the smooth ER, new tubes are continuously being formed and existing ones disappear [37] by the action of motor proteins that move along MTs (see Figure 1-6, [38]).

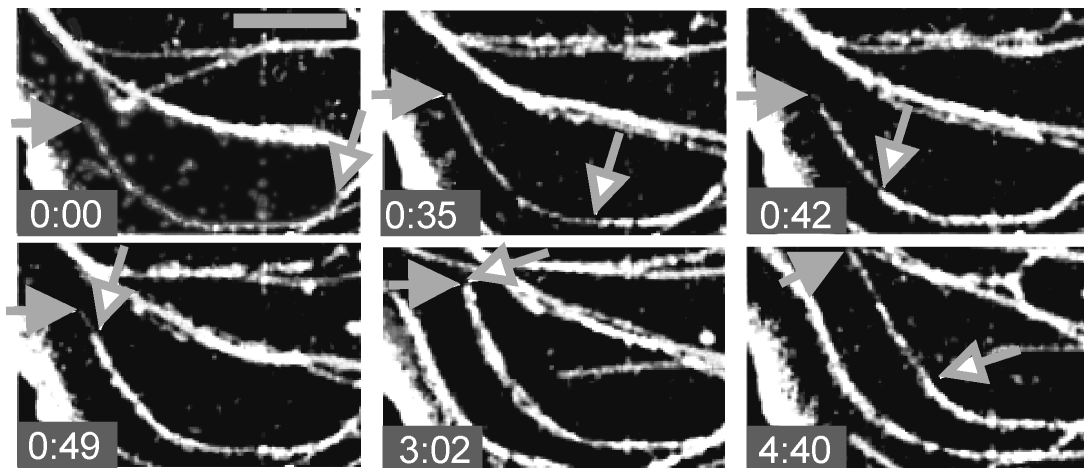


Figure 1-6. A membrane tube from the ER is pulled along a microtubule (adapted from [38]). The solid arrow indicates the tip of the MT and the open arrow indicates the tip of the membrane tube. At 4:40 the tube has retracted to halfway the MT. Time is in minutes and seconds, and the bar is 5 μm .

The importance of motors and the cytoskeleton is demonstrated by experiments in which the expression of kinesin is suppressed [16] or when MTs are depolymerized [39]. In both cases the tubular membrane network retracts towards the cell center and no tubes are being formed anymore. Even though the important role of motor proteins and the cytoskeleton for

Introduction

membrane tube formation is well-established, it should be noted that there are other mechanisms through which curvature may be imposed on membranes that result in shape changes. One may for example think of the assembly of a protein coat with an intrinsic curvature on the membrane, or proteins or lipids that change the local composition of one of the monolayers [40, 41]. Similar tubular networks can also be observed in cell extracts. In such studies, different fractions of the cell contents are acquired by centrifugation. These cell-free systems allow for obtaining insight in the relevant molecules for the formation of networks and simplify observation and analysis [42-44]. They have recently also allowed for the determination of the forces required to form tubes from Golgi and ER membranes [45].

The Golgi apparatus is often characterized as a stack of flattened membrane sacs. Like the ER, the Golgi apparatus is also a dynamic organelle (Figure 1-7). On one side (the *cis* part), membranous cargo carriers that arrive from the ER fuse with the Golgi membrane. On the *trans* side of the Golgi, tubulovesicular membrane compartments pinch off for further transport [46]. Motor proteins that move along MTs have been suggested to form and extend these tubes.

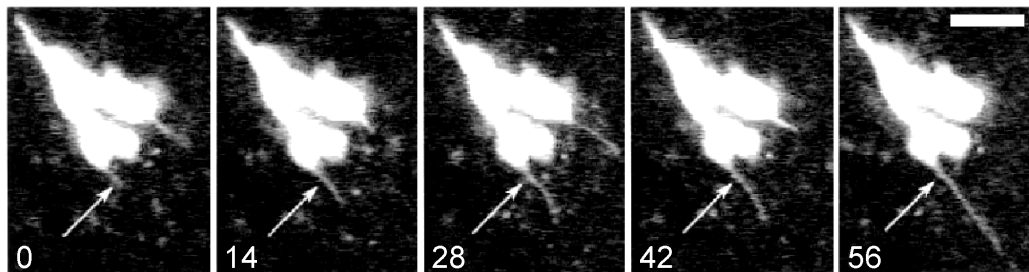


Figure 1-7. A GFP labeled tube is formed from the Golgi apparatus. Adapted from [46]. Bar is 3 μm and time in seconds.

In addition to the shaping of larger organelles, motor proteins and the cytoskeleton are essential for intracellular transport. The compartmentalization of the cell requires the movement of material between the different organelles. Cargo carriers for intracellular transport are small membrane compartments. Historically, it was thought that all cargo carriers had a spherical shape, and were around 100 nm in size. Recent advances in microscopy, especially the specific fluorescent labeling of proteins (GFP technology [47]) have led to the observation that transport carriers in fact have many different shapes. For example, large parts of tubes formed from the Golgi apparatus are cleaved off at once, and

Introduction

subsequently transported [46, 48]. This process of cleavage, the correct movement to the target organelle and the subsequent fusion are intricate processes themselves that require the activity and assembly of protein complexes and cofactors on the membrane [49, 50].

1.3 Thesis overview

We have described the complex and dynamical nature of membranes and the function of membrane compartments in the cell. Evidence from *in vivo* studies and studies in cell extracts clearly demonstrate the significance of motor proteins and the cytoskeleton in the shaping of tubular membrane compartments. The composition and the properties of cells and extracts are however complex. This makes it difficult to distinguish the essential components for the formation of tubular membranes from secondary factors involved in processes that precede or follow tube formation. The exact mechanism through which membrane tubes are formed is therefore difficult to understand from such complex systems. Studying tube formation in a system of reconstituted purified components *in vitro* makes it easier to grasp the different parameters that are essential for tube formation. This allows for the determination of the minimal components and the relevant physical parameters required for the formation of membrane tubes.

We have studied the forces and dynamics involved in the deformation and spatial distribution of membranes, where we have especially focused on tube formation. We will present experimental results obtained with synthetic vesicles of a controlled composition and purified motor proteins and MTs. In chapter 2 we will describe the experimental methods used for the work presented in this thesis. In chapter 3 we will examine the forces required for the maintenance of membrane tubes after they have been formed. Based on available theory, we will describe the relevant parameters that determine the tube force. Experiments with optical tweezers demonstrate that (as expected from energy minimization) the bending rigidity and the membrane tension are the relevant parameters that determine the tube forces.

We extend the study on the forces involved in tube formation in chapter 4, where we focus on the force required for the initial formation of a membrane tube. We demonstrate that an initial force barrier exists, which can be several times larger than the force required to

Introduction

maintain the tube. This initial tube barrier is overlooked in many studies, but in fact may provide cells with a powerful mechanism to control the shapes of membrane compartments.

In chapter 5 we show that purified motor proteins and MTs are sufficient to form membrane tubes from membranes. This system allows for a systematic study on the influence of force and motor concentration on the extent of tube formation. We found that multiple motors must work together for the formation of tubes. To explain the results, we discuss a mechanism through which motor proteins may form dynamic clusters that can exert enough force to form tubes.

In vivo, different motor proteins of opposite directionality are present on membranes, and are important for the spatial organization and distribution of membrane compartments. In chapter 6 we describe an experimental assay to study the competition between plus-end and minus-end directed motor proteins in a system of reconstituted purified components. In the concluding chapter 7 we will suggest potential future experiments and we will conclude by discussing possible biological implications of the studies presented in this thesis, and the regulatory mechanisms they suggest for cellular control.

2 Experimental set-up, procedures and data analysis

In this chapter, the experimental methods and protocols that were used for the experiments discussed in chapters 3-6 will be described. We will start with a description of the protocols that were used to obtain the giant vesicles, the microtubules and the motor proteins used in the experiments. Next, the assays developed for the study of the formation of membrane tubes with optical tweezers and motor proteins will be described. Finally, we will discuss the methods used for the analysis of the results from these assays.

2.1 Preparations and purifications

Electroformation of giant unilamellar vesicles

Giant Unilamellar Vesicles (GUVs) were formed by the electroformation (EF) method [51]. In this method the formation of giant vesicles ($>10\ \mu\text{m}$ diameter) is stimulated by the application of an alternating electric field. We used a modified version of the ramped voltage protocol described in [52]. The mechanisms behind the EF method are not fully understood [53], but the yield of GUVs is higher and they have a more monodisperse diameter than with other methods for vesicle formation [54]. When GUV formation is observed under a microscope, as a first step small vesicles can be observed to form. These vesicles vibrate with the frequency of the applied voltage and fuse with neighboring vesicles to progressively form larger ones. It was empirically determined that the (slow) stepwise increase in amplitude of the voltage results in a good and fast vesicle yield [52]. The protocol is as follows:

Lipids were acquired in lyophilized form from Avanti Polar Lipids in 1 mg aliquots and cholesterol was bought from Sigma-Aldrich, both were stored at -20°C . The lyophilized lipids were dissolved in chloroform and stored at -80°C and used for typically a period of 2 months. To make giant unilamellar vesicles, 150 μl of lipids (the exact composition depends on the experiment, see Table 2.1) was diluted and mixed. Next 75 μl of this solution was spin-coated

Experimental set-up, procedures and data analysis

(2000 rpm) onto each of two Indium Tin Oxide (ITO) coated glass slides (2 x (~7.5 x 4.5) cm²) (gift from E. Helfer and D. Chatenay¹, Strasbourg, France). Next, the slides were placed in vacuum (N86 KT.18, KNF-Verder, Vleuten, NL) for 1.5 hours to remove the chloroform. The two lipid-covered slides were subsequently mounted face to face on a frame to construct the electroformation chamber (Figure 2-1a). In this electroformation chamber the slides are separated by a 1 mm Teflon spacer. After the EF chamber was filled with ~2 ml of a solution of 200 mM sucrose in deionized water, it was closed with sealing wax (Vitrex, Omnilabo, Breda, NL).

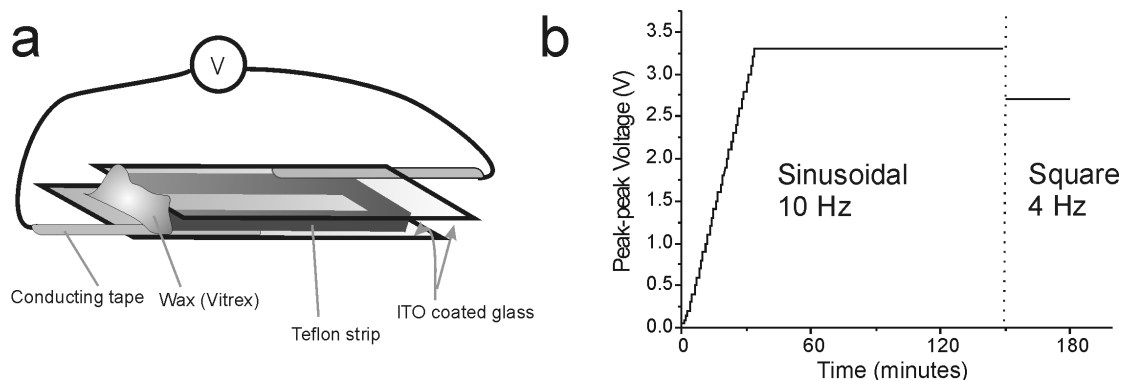


Figure 2-1. (a) Sketch of the electroformation cell (the frame is not shown). (b) Applied peak-peak voltage for the electroformation.

Next, an AC voltage was applied to the slides through conducting tape to grow the vesicles (Figure 2-1b). The computer-controlled voltage was generated by a function generator (TTi, Thurlby Thandar instruments, type TG420). The peak-peak amplitude of a 10 Hz sinusoidally modulated voltage was increased in 35 minutes to 3.3 V ($V_{\text{rms}} \sim 1.1$ V), and was kept at this value for 115 minutes. Finally, a 4 Hz square wave of 2.7 V ($V_{\text{rms}} \sim 1.1$ V) was applied for 30 minutes, in order to detach the vesicles from the surfaces. To prevent reattachment, rapidly after the square wave had stopped, the vesicles were removed with a 1 ml pipette from the EF chamber, stored in amber glass vials at 4° C, and used within 1 week. Figure 2-2 shows 2 examples of vesicles formed with the EF method.

¹ I would like to thank Emmanuèle Helfer and Didier Chatenay for initial help with the electroformation method.

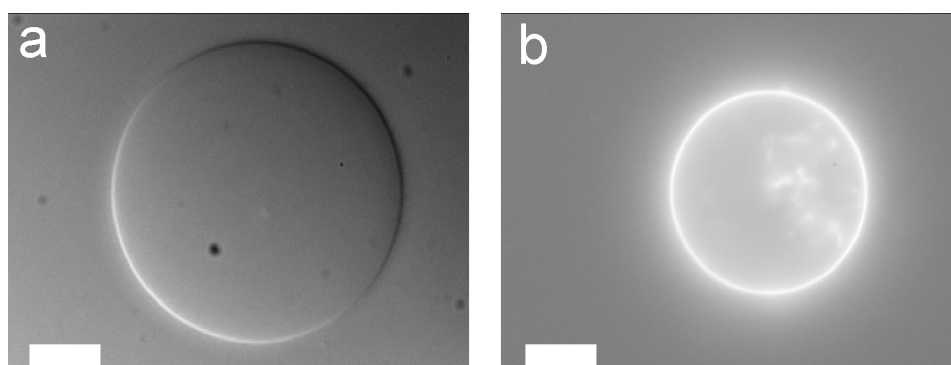


Figure 2-2. Vesicles formed by the EF method. (a) VE-DIC image of a vesicle. (b) Fluorescence image of a vesicle. The bars are 10 μm .

In the experiments vesicles of several compositions were used. We used 1,2-Dioleoyl-*sn*-Glycero-3-Phosphocholine (DOPC), 1,2-Dioleoyl-*sn*-Glycero-3-Phosphoethanolamine-N-(Cap Biotinyl) (DOPE-Biotin), cholesterol, and 1,2-Dioleoyl-*sn*-Glycero-3-Phosphoethanolamine-N-(Lissamine Rhodamine B Sulfonyl) (Ammonium Salt) (DOPE-rhodamine) (see Figure 2-3).

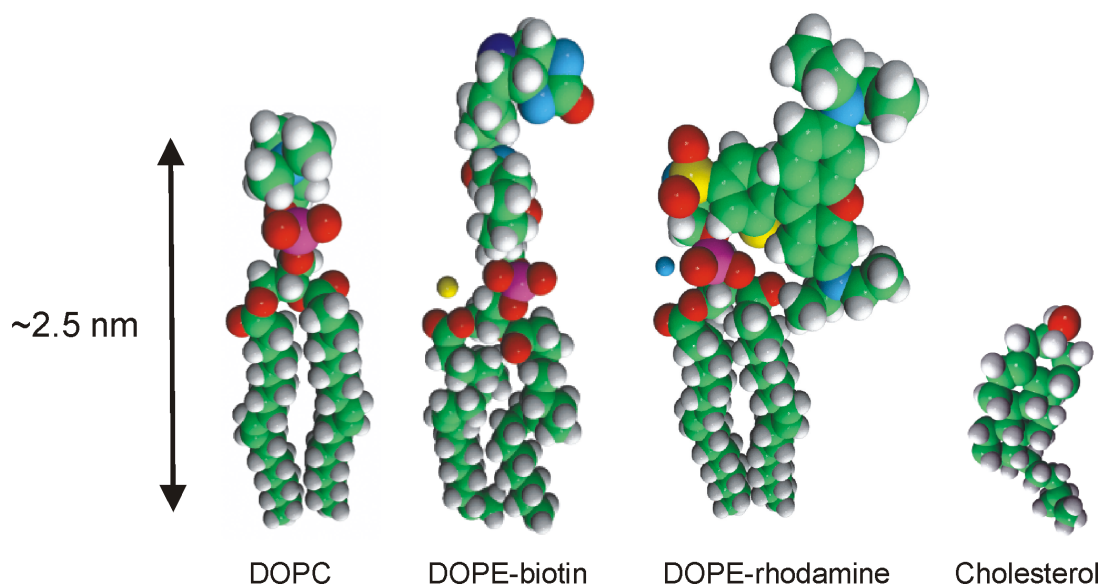


Figure 2-3. Sketches (space filled) of the different components of the vesicles (images kindly provided by Avanti Polar Lipids, Inc).

Experimental set-up, procedures and data analysis

To make the different vesicles, we varied the composition of the lipids in the solution that was spin-coated on the ITO slides (see Table 2.1). It should be noted that more than 10% of charged lipids in the mixture [55], or the presence of high salts in the solution in which the vesicles are formed, prevents their proper formation [53, 56].

Lipid (mol%)	DOPC	DOPE-Biotin	Cholesterol	DOPE-Rhodamine	Remark
Vesicle type					
DOPC	96.3	3.7			Chapter 3-6
DOPC-Chol	57.2	2.8	40		Chapter 3 and 5 Also used for streptolysin pores
DOPC-Rho	96.7	3.1		0.2	Chapter 4
MW	786	1105	387	1301	
Charge	Neutral	Negative (-1)	Neutral	Negative (-1)	

Table 2.1. Composition of the different vesicles used.

Microtubule preparation

Microtubules (MTs) were grown from 2 different batches of tubulin. For the experiments in chapter 5 tubulin was purified from pig brain by 2 cycles of cold and warm centrifugation followed by phosphocellulose chromatography [12, 57, 58]. For the experiments in chapter 6 tubulin (Bovine, #TL238) was purchased from Cytoskeleton (Denver, USA). Microtubules were grown by incubating tubulin (~4 mg/ml) in MRB80 (80 mM K-PIPES, 4 mM MgCl₂, 1 mM EGTA, pH = 6.8) with 1mM GTP for 30 minutes at 35° C. Next, MTs were stabilized by mixing them 1:9 (v/v) with MRB80 containing 10 μM taxol. During the experiments, taxol was added in all buffers used when MTs were present.

Kinesin preparation

We used a truncated and biotinylated version of kinesin from *Drosophila melanogaster* (Kinesin-1, [59], see also <http://www.proweb.org/kinesin/>). The plasmid was a kind gift of

Experimental set-up, procedures and data analysis

François Nédélec and Thomas Surrey (Heidelberg, Germany) and was originally created in the lab of J. Gelles (Brandeis University, USA). It contains the first 401 residues of the kinesin heavy chain (slightly modified from plasmid pEY4, [60]), where a triple hemagglutinin tag [61], and the biotin carboxyl carrier protein (BCCP) for the attachment of biotin were incorporated. This kinesin was expressed in *E. coli* and purified as described [61, 62] (see Figure 2-4). In the several kinesin purifications the final yield of kinesin varied. Typically ~200 µg was collected (~350 µl of 650 µg/ml). The kinesin moved microtubules in a gliding assay at speeds of ~0.5-1 µm/s.

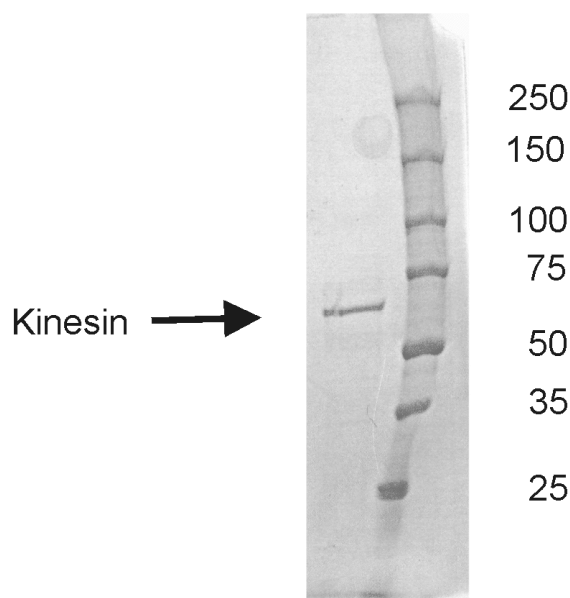


Figure 2-4. Gel showing the purified biotinylated kinesin. On the right the protein standard is shown (Biorad, 161-0372).

Ncd preparation

A biotinylated ncd was constructed in our laboratory by Martijn van Duijn. In brief, the (his-tagged) ncd created by DeCastro [24] was cut out of the pRSET-NCD195-kan plasmid (kind gift from R. Stewart, University of Utah, USA), and inserted into Promega Pinpoint Xa2, which contains a “biotin purification tag region” that allows for the attaching of a biotin to the protein. Because the plasmid was unstable during expression, PCR with a mutagenic primer was used to amplify the coding sequence and add a restriction site. After digestion with NdeI

Experimental set-up, procedures and data analysis

and *ClaI*, the fragment was inserted into a pEY4 vector, from which the kinesin sequence had first been removed by digestion with the same enzymes. Subsequently, the biotinylated *ncd* construct was expressed in *E. coli* (BL21). Induction conditions were optimized to 10 μM IPTG at 28°C (rather than the 100 μM at 27°C used for the kinesin expression, [61, 62]) to minimize protein degradation during expression. The purification was done with the same protocol as for the biotinylated-kinesin purification. Typically 60-80 μg was obtained (~600 $\mu\text{g/ml}$). The activity of the (truncated) biotinylated *ncd* was verified by the formation of membrane tubes by the *ncd* motor. Tubes were formed at a low velocity (~0.03 $\mu\text{m/s}$), see also chapter 6.

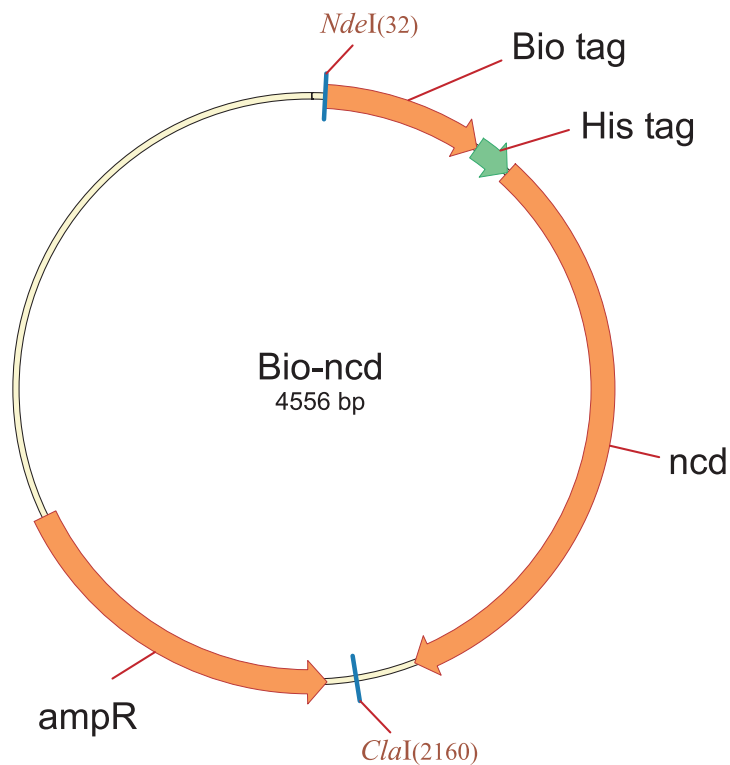


Figure 2-5. Bio-ncd plasmid.

2.2 Sample preparation

Flow-cell

All experiments were done in a (simple) flow-cell set-up [63]. A flow-cell of a certain volume (10 μl or 20 μl) was constructed by drawing two parallel lines of vacuum grease (Hivac-G, Shin-Etsu, Japan) approximately 5 mm apart (~ 10 mm for a 20 μl flow-cell) on a microscope slide and by mounting a glass coverslip (24x24 mm^2) on top. For experiments where the surface-properties need to be comparable (for example in titration or for parallel control experiments), coverslips can be used efficiently by constructing multiple 10 μl (flow-cell)-lanes on the same slide (see Figure 2-6). Next, 10 μl of a solution was introduced into the flow-cell by capillary action, and the coverslip was pressed down to make this volume fill the whole cell (the cell will have a height of approximately 100 μm). The solution in the flow-cell can now be replaced by presenting the new solution on one side of the cell and, at the same time, removing the original solution (by absorbing it with a piece of tissue) from the other end. After the last solution was flown in, the cell was closed using either paraffin or nail polish.

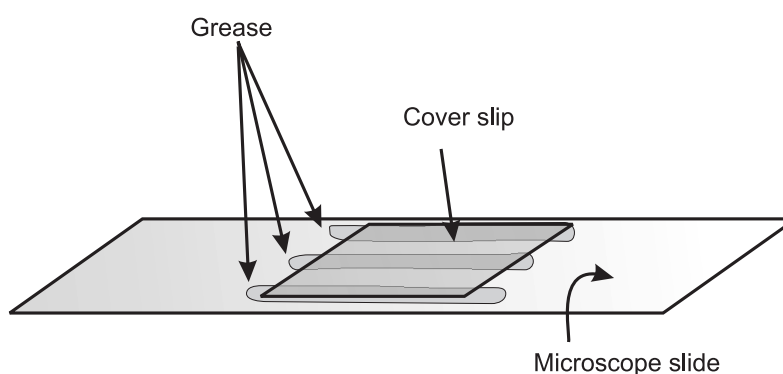


Figure 2-6. Sketch of a flow-cell with two parallel lanes.

The interaction properties of the vesicles and microtubules with the coverslip depend on the treatment of the coverslip. Before use, the coverslips were cleaned by loading them into a Teflon holder, placing this holder in ~ 400 ml NaOH (2M) in ethanol and sonicating for 5 minutes. Next, the coverslips were rinsed in ~ 400 ml ddH₂O, transferred to a new beaker with

Experimental set-up, procedures and data analysis

~400 ml ddH₂O and sonicated for 5 minutes. Finally, the coverslips were removed from the beaker, rinsed with ddH₂O (squirt bottle), rinsed with ethanol (squirt bottle), and dried at 100°C in an oven for 15 minutes.

Next, depending on the experiment, the coverslips were treated with casein and/or BSA to passivate the surface, or were coated with (positively charged) poly-L-lysine (polylysine) to enhance the interaction with microtubules, which are negatively charged at pH = 6.8. There are different methods to apply polylysine (PL) to the coverslip, resulting in different properties of the coverslip:

- PL-spin. In this method 200 µl of polylysine (2 µg/ml) in ethanol was spin coated (4000 rpm, 15 s) onto the coverslips. Next, the coverslips were stored in a container box. This method was used for the experiments used in chapter 5.
- PL-dip. In this method 600 µl of polylysine (0.1%, Sigma-Aldrich) is dissolved in 300 ml ethanol (final concentration 2 µg/ml). The NaOH cleaned coverslips are next (in a Teflon holder) placed in this solution for 15 minutes, and subsequently dried in an oven at 100° C. The coverslips are stored in a container box. This coating method was used for the experiments in chapter 6.
- PL-flow. This is the strongest coating method. After a flow-cell was constructed, and just before the experiment, polylysine (0.1 %) was flown into the flow-cell and incubated for 5 minutes. Next, the cell was rinsed with 5-10 flow-cell volumes of buffer. This method made microtubules adhere strongly to the surface (but unfortunately also the vesicles, see chapter 6).

Assay for force determination of tube formation with optical tweezers

A 20 µl flow-cell was constructed with a NaOH cleaned coverslip. Casein (2.5 mg/ml) in MRB40-Iso (40 mM K-Pipes, 1 mM EGTA, 4 mM MgCl₂, and 112 mM glucose) was flown in to coat the surface and prevent the vesicles from exploding on the surface. For the experiments on plateau forces (chapter 3) a mixture was made of 10 µl vesicle solution (centrifuged, see below), 9 µl MRB40-Iso, and 1 µl streptavidin-coated polystyrene bead solution (20x diluted, 2.17 µm diameter, SVP-20-5, Spherotech, Libertyville, USA). If required for the experiment, streptolysin O was added to this mixture shortly before use. For the experiments on force barriers for tube formation (chapter 4) a mixture was made consisting of 10 µl vesicle solution (centrifuged), 9 µl MRB40-Iso, 1 µl streptavidin coated

Experimental set-up, procedures and data analysis

polystyrene bead solution (5x diluted, SVP-40-5, 4.09 μm diameter), and 0.4 μl oxygen scavenger (200 mM DTT, 10 mg/ml catalase, 20 mg/ml glucose-oxidase) [63], in buffer.

After flowing the bead-vesicle mixture into the flow-cell, one bead was grabbed with the optical tweezers (see below) and pressed against a vesicle to make a connection. This same bead was next pressed against the coverslip surface, and held there for approximately 30 seconds. This makes an attachment to the surface that is strong enough for tube formation experiments in approximately 50% of the cases. Subsequently, another bead was grabbed with the tweezers, and after the vesicle was in contact with the bead for several seconds, a tube was formed by displacing the immobilized vesicle for 10 μm at a velocity of 0.1 - 1 $\mu\text{m/s}$ using a piezo stage (P-730.4C, Physik Instrumente, Karlsruhe, Germany) and holding it at this distance. The force on the bead was determined from the recorded bead displacement data after the experiment was finished (see section 2.4).

Before using the vesicles, their concentration was increased by centrifugation. This was done as follows: 200 μl of vesicle solution was mixed with 400 μl MRB40-Iso in an Eppendorf tube, and centrifuged at 4500g for 1 minute. All but 50 μl of the supernatant was removed and 500 μl of MRB40-Iso was added, and the tube was centrifuged again. The bottom ~ 20 μl , containing the concentrated vesicles, was used for the experiment. We found that coating the Eppendorf tube with casein (2.5 mg/ml) before the centrifugation process (and subsequently rinsing it with MRB40-Iso), strongly increased the amount of vesicles retrieved. Presumably, this is because vesicles will otherwise be lost by adhering to the tube. An important additional advantage of the centrifugation step is that the success rate for bead attachment to the vesicle is enhanced. This is presumably due to the fact that the centrifugation removes small vesicle debris that would otherwise attach to streptavidin on the bead, preventing its attachment to the vesicle.

Assay for membrane tube formation by motor proteins

In this assay membrane tubes are formed from giant vesicles by the movement of linked motor proteins on immobilized microtubules. We used the following protocol:

First, the flow-cell was prepared and coated with microtubules and casein. A flow-cell (10 μl) was constructed with a polylysine coverslip (PL-spin). Next, pre-grown taxol-stabilized microtubules (MTs) were flown in and incubated for 5 minutes to adhere to the surface. MTs that did not stick to the surface were removed by flushing 2 times with MRB40-Iso. Finally,

Experimental set-up, procedures and data analysis

α -casein (2.5 mg/ml) in MRB40 was flown in and incubated for 5 minutes to minimize the interaction of the vesicles with the coverslip. If the coverslip was not coated, the vesicles were observed to either strongly adhere to the surface (making a highly tensed “hemisphere shaped” vesicle) or explode on the surface.

Second, a mixture (MIX) was prepared with the following components, dissolved in MRB40:

- 20 μ M taxol (for stability of the microtubules)
- 3 mM ATP (for motor protein activity)
- Oxygen scavenger (0.4 mg/ml catalase, 0.8 mg/ml glucose oxidase, and 8mM DTT) (to remove oxygen radicals that would damage the sample)
- 0.4 μ M biotin (to block the remaining biotin binding sites on the streptavidin)
- 4 μ M of C8-BODIPY 500/510-C5 (Molecular Probes) (as a hydrophobic fluorescent dye that stains the membrane)
- 109 mM glucose (to osmotically match the final solution in the flow-cell with the intravesicular buffer of 200 mM sucrose)

After these preparatory steps the final solution could be prepared. For the kinesin assay (chapter 5), 3 μ l of centrifuged vesicle solution was mixed with 1 μ l of streptavidin (50 μ g/ml, see below) in a tube. This solution was incubated for ~5 minutes to make the streptavidin adhere to the biotinylated vesicle (Figure 2-7). Next, 1 μ l of biotinylated kinesin (typically at 10 μ g/ml) was added and incubated for 5 minutes to adhere to the streptavidin on the vesicle. After the incubation of kinesin with the vesicles, 5 μ l of the prepared MIX was added to the 5 μ l of now kinesin-coated vesicles. This solution was flown into the flow-cell. In the case that an experiment was conducted with streptolysin pores in the vesicle, the streptolysin O (Sigma S-5265, to a final solution of 500 Units/ml) was added to the mixture just before flowing the final mixture into the flow-cell. The advantage is that this allows the vesicles to sediment to the coverslip surface and attach to the MTs during the time that the streptolysin has not formed pores yet (this typically takes ~3 minutes). The extent of tube formation was subsequently determined from snapshots in fluorescence (see section 2.4).

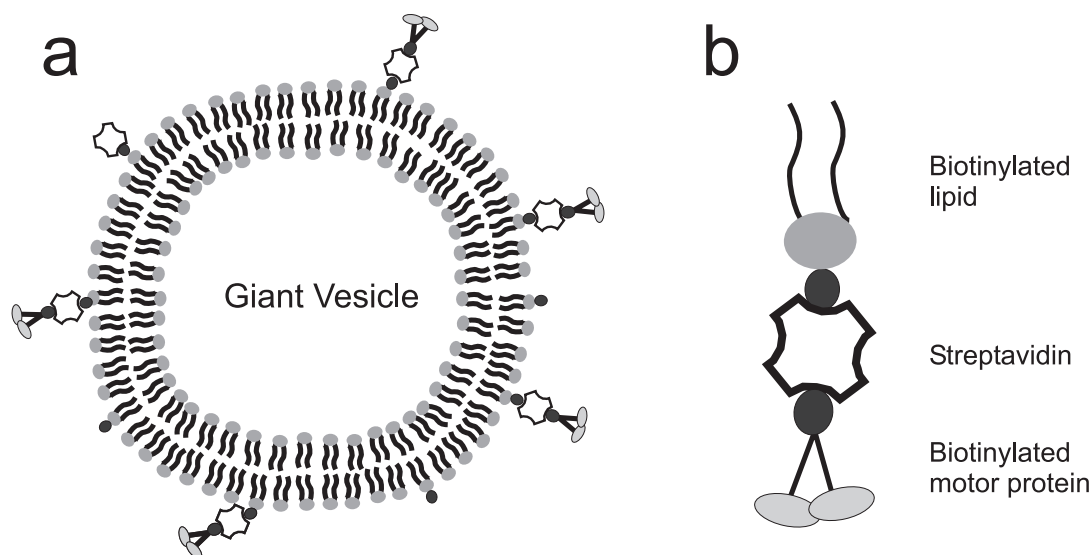


Figure 2-7. Sketch (not to scale) of the tube assay "construct". (a) Biotinylated motor proteins are linked to a giant vesicle through streptavidin. (b) Zoom of the motor-streptavidin-lipid complex that provides the connection.

As described above, the link between the motor proteins and the vesicle was made through streptavidin. We determined the concentration of streptavidin (in the final sample) that was required to form tubes with the protocol described above (the motor protein concentration is studied in more detail in chapter 5). To study this, we titrated 4 concentrations of streptavidin (logarithmic concentration steps) on DOPC vesicles versus 4 kinesin concentrations. Subsequently, the extent of tube formation from the motor-coated vesicles was determined at 20 minutes after insertion. The extent of tube formation was estimated by visual inspection and graded on a scale of 1 to 10. The results are shown in Figure 2-8 where the radius of a circle indicates the extent of tube formation. First of all, these results show a general trend towards the formation of larger networks with higher kinesin concentrations. An additional observation is that (as expected) a minimal concentration of streptavidin is required for tube formation. The data suggest that a streptavidin concentration of $\sim 5 \mu\text{g/ml}$ (in the sample) yields the highest number of tubes, and we therefore decided to use this streptavidin concentration for the experiments in chapter 5 and 6. Interestingly, a higher streptavidin

Experimental set-up, procedures and data analysis

concentration of 50 $\mu\text{g/ml}$ seems to lower the number of tubes again, possibly due to free streptavidin in the background that sequesters kinesin from the vesicle.

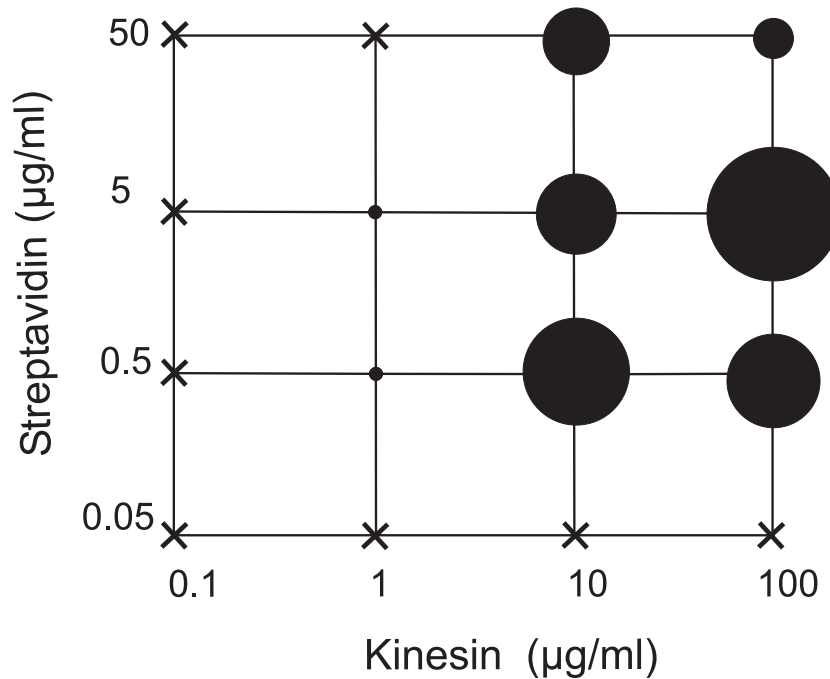


Figure 2-8. Extent of tube formation for different concentrations of kinesin and streptavidin in the tube assay as indicated by the diameter of the circle. Most tubes are formed around a streptavidin concentration of 5 $\mu\text{g/ml}$. A cross indicates that no tubes were formed.

2.3 Apparatus

Microscopy

Observations were done with video enhanced differential interference contrast (VE-DIC) and fluorescence microscopy on an inverted microscope (DMIRB, Leica, Rijswijk, NL), with a 100x oil-immersion objective (numerical aperture 1.3). For DIC microscopy the sample was illuminated with a (green filtered) 100 W mercury lamp through an oil immersion condenser. DIC images were acquired with a CCD camera (Kappa CF 8/4, Kappa Optoelectronics,

Experimental set-up, procedures and data analysis

Gleichen, Germany), contrast enhanced (C5510, Hamamatsu Photonics) and recorded on S-VHS videotape (25 fps) for offline analysis. If optimized, it is possible to visualize vesicles with DIC microscopy, but membrane tubes are difficult to observe. After contrast enhancement by image processing, tubes became clearly visible. At the same time, the image of the vesicle will however become distorted due to the excessive contrast. Part of the contrast is due to the difference in index of refraction between intravesicular and extravesicular buffer. If this contrast component is removed by forming streptolysin pores, it is however still possible to observe the bilayer of the vesicle (see e.g. Figure 3-9).

For the experiments reported in chapter 5, fluorescence images were recorded with a Kappa CF 8/4 DX CCD camera. Illumination was done with a 100 W mercury lamp and excitation through a filter cube (Leica, 513849). BODIPY was excited in blue (BP480/40), and emitted in green (filter BP527/30). For these experiment snapshots were taken and directly saved to disk and processed offline afterwards. For the patch size determination in chapter 4, a filter cube with exciter of 546/12 and emitter of 585/40 (41003, Chroma, Rockingham, USA) was used for the observation of rhodamine-labeled lipids. Images were acquired with a Kappa CF 8/4 camera, contrast enhanced (C5510, Hamamatsu) and movies were stored on S-VHS tape.

Optical tweezers set-up

Optical trapping [64-67] was done with an infrared laser beam (1064 nm, Nd:YVO₄, Spectra-Physics, Darmstadt, Germany), which was focused in the sample plane. This laser was coupled into the DMIRB microscope, with the diameter of the beam increased to slightly overfill the back aperture of the microscope objective for maximal trapping potential. Stiffness calibration of the tweezers was done by determining the roll-off frequency of a trapped bead (see below), as determined by the projection of the superimposed (low power) red laser (633 nm, HeNe, 1125P, Uniphase, San Jose, USA) on a quadrant photodiode. A schematic picture of the several components of the set-up is presented in Figure 2-9.

Experimental set-up, procedures and data analysis

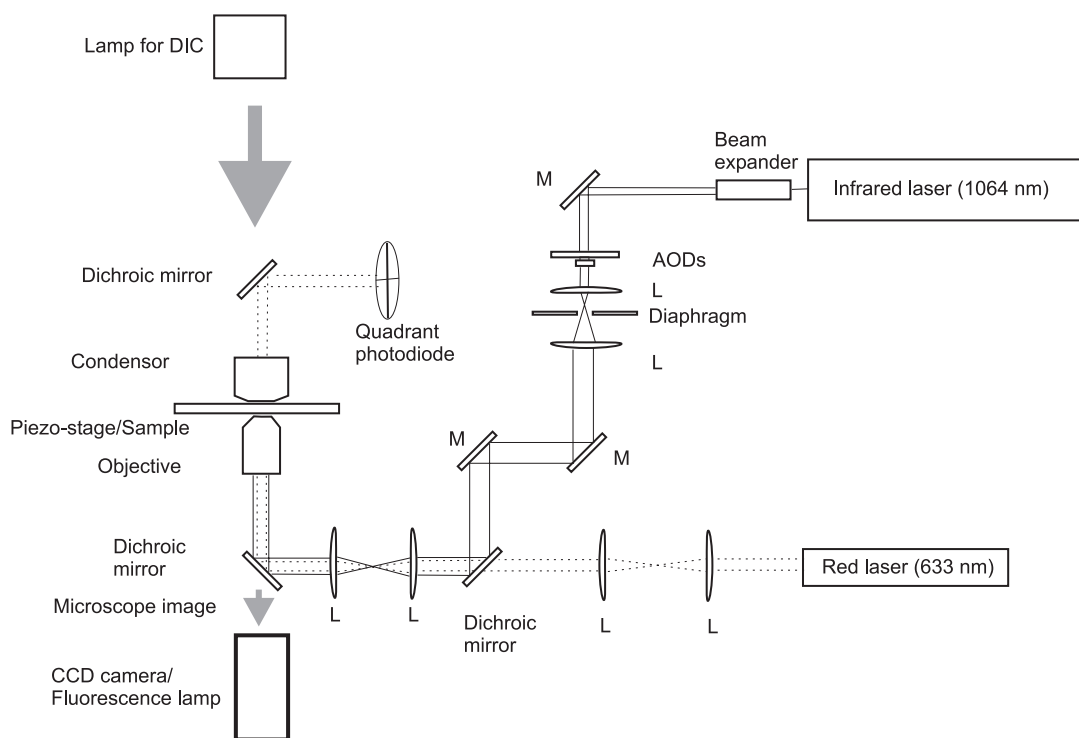


Figure 2-9. Optical tweezers set-up. The solid line indicates the infrared laser beam, and the dashed line the red laser beam. L = lens M = mirror.

Between the objective and the condenser, a Piezo stage (P-730.4C, Physik Instrumente, Karlsruhe, Germany) was mounted. This allowed high precision movement of the sample (with respect to the tweezers), and movement of the stage could be done at controlled velocities by computer control. The stiffness of the tweezers could be controlled by varying the power of the beam coming from the IR-laser, or through the AODs (Acousto-optic deflectors, IntraAction DTD-274HA6), which were present in the set-up for other experiments in the group. Typically the IR laser power was set between 0.2 W (minimum setting) and 4 W (higher powers could possibly damage the optics). Approximately 25% of this power reached the sample [68]. This resulted in typical trap stiffnesses of ~ 0.02 - 0.40 pN/nm for the polystyrene beads of 2 and 4 μm used in chapters 3 and 4. In the set-up a low power red laser is superimposed on the trapping laser beam for stiffness determination. After passing through the bead in the sample, this red laser was imaged onto a quadrant photodiode, and the power

spectrum of the Brownian fluctuations of the bead in the trap was digitally stored (home made software: “trap state queue”, developed by Astrid van der Horst in Labview).

The stiffness of the trap can be determined from the power spectrum of the thermal fluctuations by determining the roll-off frequency ($f_{roll-off}$) [66, 67], the characteristic frequency at which the Brownian motion of the bead is restricted by the tweezers (see Figure 2-10 for an example of a power spectrum). The relation is given by $\kappa_{trap} = 12\pi^2\eta af_{roll-off}$ [67], where η is the viscosity of the medium ($\sim 10^{-3}$ N.s/m², as the experiments were conducted >4 bead radii away from the surface [67]), and a is the radius of the bead. The roll-off frequency was determined offline by fitting a Lorentzian, $C_1/(f_{roll-off}^2 + f^2)$, to the spectrum [67], where C_1 is a constant. The amplitude of the lower frequencies is often enhanced by external disturbances and we ignored these frequencies ($< \sim 15$ Hz) for a better fit. A clear horizontal plateau should however still be present for a good fit. High frequencies (> 6000 Hz) were also ignored because of instrument noise and the presence of an anti-alias filter [69].

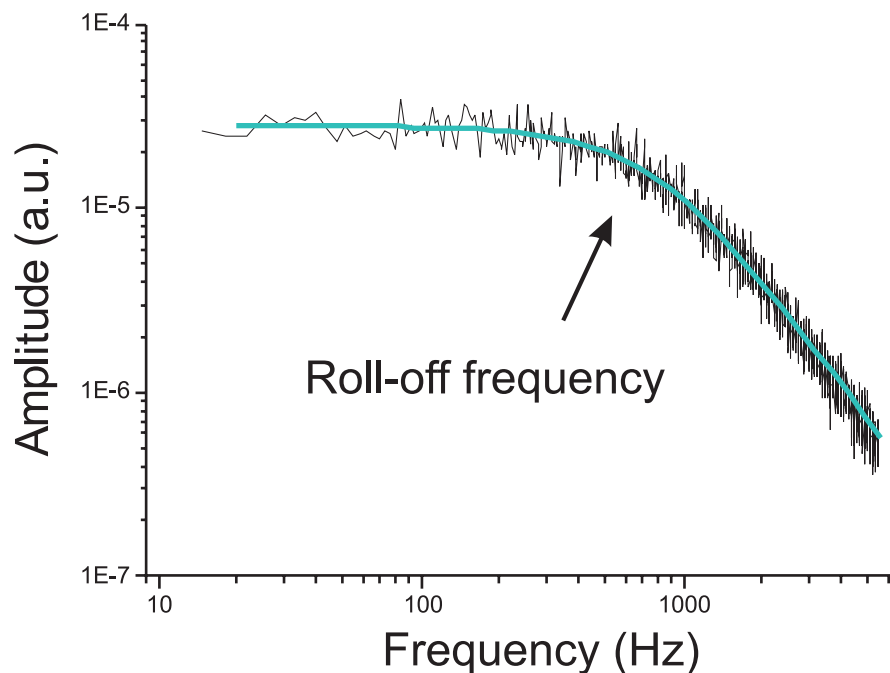


Figure 2-10. An example of a power spectrum. The roll-off frequency is ~ 800 Hz as determined by fitting a Lorentzian to the data.

2.4 Data Analysis

Determination of tube formation force with optical tweezers

At the beginning of each experiment, the position of a trapped streptavidin-coated polystyrene bead corresponding to a zero force in the trap was determined. Next, a vesicle was moved against the bead, and after holding it against the bead for several seconds, a tube was formed by displacing the vesicle 10 μm with the piezo stage and holding it at this distance. These several steps were observed with DIC microscopy and recorded on videotape for offline analysis.

The recorded time sequence was digitized with home-made software (“E&I framegrabber”, developed in IDL by Marco Konijnenburg), and was stored as a stack of images. The position of the bead could now be determined in each of these frames by cross-correlation analysis. To determine the bead position in the sequence of images, an image of the bead at the beginning of the experiment was saved as a template. This template was subsequently positioned on every possible position in the images of the stack, and the cross-correlation value was determined. This yielded a landscape of cross-correlation values. From this landscape all correlation values below half of the maximum value were deleted. From the resulting cross-correlation peak, the average position (each position weighted by its cross-correlation value) was determined, giving the position of the bead. This cross correlation analysis was done for all the frames in the stack, resulting in a time trace of the position of the bead, in pixels, at sub-pixel resolution [70]. These pixel values can be translated to nanometers (in the set-up we used: 88.75 nm/pixel horizontally and 81.5 nm/pixel vertically).

To determine the force on the bead from the deviation of the bead position from the trap center, the stiffness of the tweezers is required. Before each tube formation experiment we determined the power spectrum, which was stored to disk. In addition to the roll-off frequency, this power spectrum also provides a check for the quality of the trap, as the presence of debris (from the vesicles) distorts the spectrum. Together with the stiffness of the trap, the deviation from the center of the trap yields the force on the bead, $f = \kappa_{\text{trap}} \Delta x$.

Experimental set-up, procedures and data analysis

Determination of the total tube length pulled by motor proteins

The total length of the tubes pulled from vesicles was measured according to the following protocol² :

- A contiguous image of $\sim 300 \times 500 \mu\text{m}^2$ of the sample was made by acquiring a matrix (5x4) of fluorescent images and stitching overlapping images together using PanaVue ImageAssembler software (PanaVue, Canada) (see Figure 2-11a).
- By hand, lines were drawn along the lengths of all the tubes in the field of view (with the line tool in a separate layer in Paintshop Pro) (see Figure 2-11b for the superimposed image).

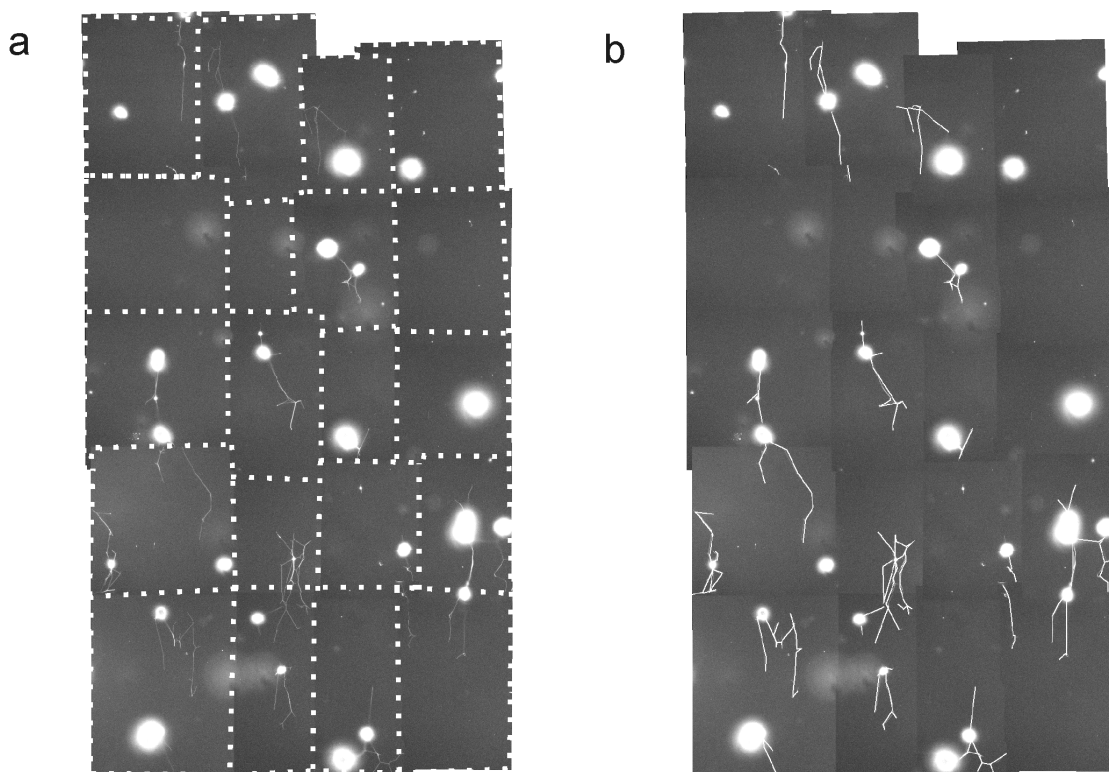


Figure 2-11. (a) Stitched microscopy images of vesicles from which tubes have formed (the white dashed lines are presented to show the stitching). (b) The same image with lines drawn by hand superimposed.

² I would like to thank Martijn van Duijn for the development of the quantification procedure.

Experimental set-up, procedures and data analysis

- The lines from the separate layer were saved as a bitmap file (.bmp). It is convenient for visibility to change the line-color to black.
- The bmp file was opened in the program Win Topo (free download at (<http://www.wburrows.demon.co.uk/softsoft/wintopo/index.htm>)). This program fits vectors to the lines, which can be saved as an ASCII file.
- In a spreadsheet program (MS Excel 2000), the total length of the vectors was determined by adding the length of each vector to obtain the total tube length.

3 Forces required to maintain membrane tubes

As discussed in the introduction, biological membranes assume complex morphologies that are essential for the proper functioning of the cell. They consist of different lipids and many proteins that associate with the membrane to fulfill their function. In certain cases membranes are supported by a cytoskeletal cortex, which provides additional structural rigidity. Because of this multitude of different components, potentially interacting with each other, it is difficult to get a basic understanding of the mechanisms and principles that control the morphology of such membranes. For a proper understanding of the relevant physics of membranes, lipid bilayer membranes have been studied under controlled conditions. Experimentally, procedures have been developed to make simplified membranes that consist of a limited number of lipids of choice. Methods were established to form giant vesicles of the size of cells, which are distinguishable by light microscopy. This has allowed for an analysis of the basic mechanisms and parameters that govern membrane mechanics. In parallel, theoretical tools have been developed to give a coarse grained description of the membrane. Such models take into account the energy cost to deform a membrane under certain boundary conditions, and have been able to describe many of the basic shapes that are found experimentally. In this chapter an overview will be given of the relevant theoretical and experimental knowledge concerning membranes that is relevant for this thesis. Next, the specific case of the mechanics of membrane tubes will be discussed. In the last part, our experimental findings on tube formation from giant vesicles by optical tweezers will be presented, and interpreted with respect to the theoretical predictions.

3.1 Mechanics of lipid bilayers

Membrane structures in cells assume complex morphologies. Such membranes consist of a mixture of different kinds of lipids, and are often covered with several types of membrane proteins. In addition, a cytoskeletal cortex sometimes supports these membranes. Adding to complexity, many of the cellular membranes are continuously being remodeled by the activity

Forces required to maintain membrane tubes

of piconewton force generators, and are therefore “out of equilibrium”. For a good understanding of the membranes *in vivo*, the basic organizing mechanisms of more simple membranes need to be understood first, and theoretical and experimental techniques have been developed to study the properties of model membranes.

When lipids are placed in an aqueous solution, they will try to shield their hydrophobic fatty acid tails from the water molecules. This can be achieved by forming aggregates of lipids. However, how they organize depends on several parameters, like the temperature, the concentration and specific properties of the lipid studied [71]. In most biological situations, the lipids prefer to form bilayers, which close on themselves to form isolated compartments (vesicles). There have been many experimental and theoretical studies on the variety of shapes that can be formed as a result of this self-assembly of the lipids. These have shed light on the basic organizing mechanisms and parameters that define the shape of a membrane. Even if the bilayers consist of only 1 kind of lipid, a large variety of membrane shapes can be observed [72-75]. In the following sections we will give an overview of the part of these findings that is relevant for the interpretation of our experimental results. We will start by describing the relevant theory.

Energy minimization defines the membrane shape

Membranes can be described theoretically by identifying the components that contribute to the free energy of the membrane system. The equilibrium shape of a vesicle can then be found by minimizing this energy with system-specific boundary conditions, like for example restrictions on the area and volume. Here, we will first introduce the spontaneous curvature (SC) model, next the more refined model of area difference elasticity (ADE), and finally the energy describing membrane tubes will be discussed. Although not all experimentally observed shapes and shape transitions can be explained by these descriptions, for most cases the predicted behavior agrees well with observations [76].

Historically, a theoretical description of membranes starts with the energy component due to the bending of the (thin) membrane sheet. In the earliest description (the *spontaneous curvature* model [77, 78]), the curvature of a membrane is characterized by the two principal curvatures, C_1 and C_2 (see e.g. [74]), which are defined as the reciprocal of the radii of curvature (R_1 and R_2) which characterize a surface, see Figure 3-1).

Forces required to maintain membrane tubes

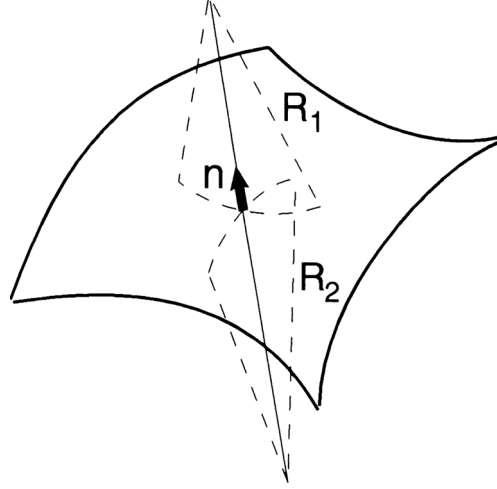


Figure 3-1. The radii of curvature of a surface. The vector *n* is the normal. Adapted from [74].

The energy of the membrane can be described as the integral of the curvature energy over the whole surface, *A*:

$$E = \frac{1}{2} \kappa \int dA (C_1 + C_2 - C_0)^2 + \kappa_g \int dA (C_1 C_2) \quad (3.1)$$

where κ is the parameter that defines how strongly the membrane resists bending (the bending rigidity modulus), C_0 is the spontaneous curvature (a preferred curvature of the membrane), and κ_g is the Gaussian bending modulus. In most studies, the Gaussian curvature term is dropped because it is a topological invariant; the value of this term depends only on the number of holes or handles through the vesicle. Since in our study this number is constant, it can be ignored [74] for energy-minimization purposes. So Equation (3.1) becomes:

$$E = \frac{1}{2} \kappa \int dA (C_1 + C_2 - C_0)^2 \quad (3.2)$$

Since a membrane is a bilayer (consisting of two monolayers of lipids), the description of a thin sheet is not always adequate. An additional term needs to be incorporated that takes into account the coupling between the two monolayers. When a bilayer is bent, the outer layer will be stretched (area per lipid increases) while the lipids of the inner monolayer are compressed.

Forces required to maintain membrane tubes

This differential stretching is the essence of the *area difference elasticity* model [79], also known as the generalized bilayer-couple model [80] and it contributes an additional term to the energy. The time scale of movement of lipids from one monolayer to the other (flip-flop) is slow on the timescale of experiments (e.g. [81], but see [82, 83] for tension-enhanced flip-flop rates). Equation (3.2) becomes:

$$E = \frac{1}{2} \kappa \int dA (C_1 + C_2 - C_0)^2 + \frac{\bar{\kappa} \pi}{2Ad^2} (\Delta A - \Delta A_0)^2 \quad (3.3)$$

where $\bar{\kappa}$ is the non-local bending modulus which sets the energy scale for resistance to the differential stretching of the separate monolayers, d is the thickness of the membrane, ΔA the area difference between the monolayers, and ΔA_0 the relaxed area difference between the monolayers. The shape of a membrane vesicle can now be determined by minimizing this energy, with certain boundary conditions imposed. This description has been used with success for the understanding of the several shapes that vesicles assume in equilibrium [76, 84].

Finally, there are contributions to the energy of a membrane which emerge from constraints on the surface area and the volume, which have to be included (e.g. [85]):

$$E = \frac{1}{2} \kappa \int dA (C_1 + C_2 - C_0)^2 + \frac{\bar{\kappa} \pi}{2Ad^2} (\Delta A - \Delta A_0)^2 + \sigma A - pV \quad (3.4)$$

where σ is the membrane tension (the energy cost for increasing the area of the vesicle), A is the surface area of the membrane, p the pressure difference between the inside and the outside of the vesicle, and V the volume.

Mechanics of membrane tubes

An important part of this thesis deals with the forces involved in the formation of a thin, highly curved membrane protrusion (see Figure 3-2), which can be formed when a localized force is applied to a membrane. The resulting membrane protrusions have been referred to as tether, tubule or tube. To distinguish them from cytoskeletal microtubules we will refer to them as either tubes or tethers. The same components that were identified to contribute to the

Forces required to maintain membrane tubes

free energy of a general membrane shape (Equation (3.4)) are applicable for a membrane tube. Since the tube is connected to the (much larger) vesicle, the vesicle effectively functions as a reservoir for area and volume for the membrane tube [85], and the membrane tube energy is given by Equation (3.5):

$$E_{tube} = \frac{1}{2} \kappa \int dA (C_1 + C_2 - C_0)^2 + \frac{\bar{\kappa} \pi}{2A_v d^2} (\Delta A - \Delta A_0)^2 + \sigma A - pV - f_0 L \quad (3.5)$$

Except for the area of the whole vesicle (A_v), all quantities in (3.5) refer to the membrane tube, and the properties of the vesicle determine the effective tension and pressure difference for the tube. Finally, f_0 is the force required to hold a tube of length L .

For membrane tubes much shorter than the vesicle radius, several contributions in (3.5) are negligible and it can be simplified. For a tube of length 10 μm , which is pulled from a giant vesicle of 10 μm radius, the induced area difference ΔA between the monolayers is well approximated by $\Delta A = 2\pi hL$, where h is the separation distance between the (neutral surfaces of) the two monolayers and L is the length of the tube. For a typical value of h (~ 3 nm, [86]), this area difference is less than 0.02%. The contribution due to differential stretching of the membrane may therefore be neglected [85]. The pressure component is negligible with respect to the other ones [80, 85] since the volume of the tether is negligible. Finally, the spontaneous curvature, C_0 , of the membrane is also set to zero since the two monolayers of the membranes used in our studies are made up of the same lipids and can be assumed to be symmetrically distributed over the monolayers.

When the above-described arguments and approximations are taken into account, the energy of the membrane tube can finally be written as

$$E_{tube} = \frac{1}{2} \kappa \int dA \left(\frac{1}{R_1} + \frac{1}{R_2} \right)^2 + \sigma A - f_0 L \quad (3.6)$$

where the curvatures have been replaced by the two radii of curvature. The shape and force of the membrane-tube system can be determined by minimization of the energy given in Equation (3.6). This involves the numerical solving of the shape equations for a membrane, the details of which can be found in [87].

Forces required to maintain membrane tubes

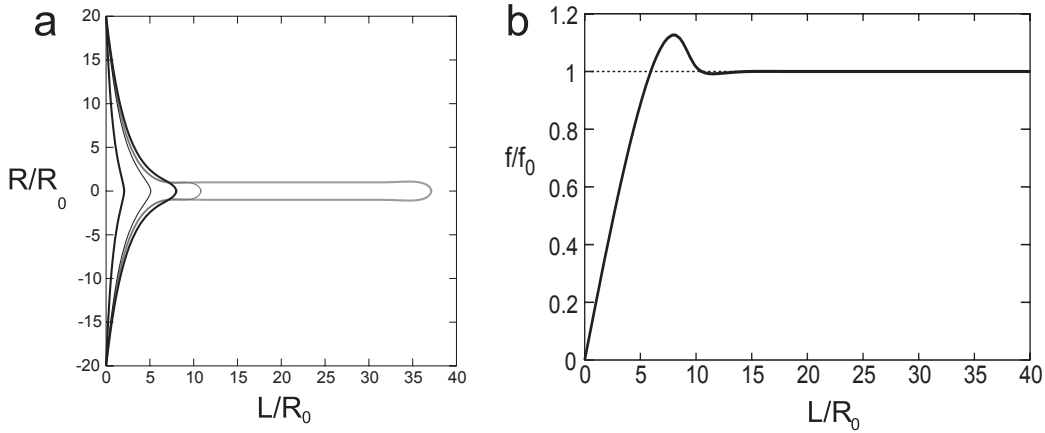


Figure 3-2. (a) Several shapes of an emerging tube when a point force is exerted on a flat membrane. Here R is the distance from the center of the membrane, R_0 is the radius of the tube, and L is the distance from the membrane. (b) The predicted force extension curve when a tube is formed from a flat circular membrane by a point force (adapted from [87]), f is the force required to deform the membrane and f_0 is the plateau force (see text).

Figure 3-2 shows the shapes that are assumed by a flat membrane when a point force is exerted on it, together with the corresponding force-extension curve. When the point force is moved away, the membrane starts to deform and the force increases while this happens. At a critical extension (around the force maximum) a tube is formed. At this moment, the force falls down to the *plateau force*. Moving the point force away further results in an extension of the tube. In this calculation the plateau force stays constant because the tension is taken to be constant. In experiments this is often not the case (see below). The details of the several shapes the membrane assumes in the process of tube formation and the corresponding forces will be discussed in detail in chapter 4.

The plateau force is determined by the membrane tension and the bending rigidity. Except for corrections at the tip and at the base, the tube can be assumed to be cylindrical [80, 87, 88]. For a cylinder, one radius of curvature is its radius (R_0) and the other radius of curvature is infinitely large. The area of a cylinder is $2\pi R_0 L$. Inserting this area into Equation (3.6), the energy for the membrane tube becomes:

$$E_{tube} = \left(\frac{\kappa}{2R_0^2} + \sigma \right) 2\pi R_0 L - f_0 L \quad (3.7)$$

Forces required to maintain membrane tubes

From (3.7) it can be seen that a smaller tube radius will lower the contribution of the surface tension component to the energy. In contrast, a smaller tube radius will increase the energy due to bending. The equilibrium radius will be determined by the competition between these contributions. The energy minimum can be found by minimizing Equation (3.7) with respect to R_0 and L , this yields:

$$R_0 = \sqrt{\frac{\kappa}{2\sigma}} \quad (3.8)$$

and

$$f_0 = 2\pi\sqrt{2\sigma\kappa} \quad (3.9)$$

Combining (3.8) and (3.9) reveals that the force is inversely proportional to the tube radius:

$$f_0 = \frac{2\pi\kappa}{R_0} \quad (3.10)$$

The inverse proportionality of the tube radius on the force (with the bending modulus as a proportionality constant) has been confirmed experimentally [89, 90], and can be used for determining the bending rigidity modulus.

3.2 Membrane tension and fluctuations

When tubes are pulled from a vesicle, membrane has to flow into the tube. The energy cost for this is determined by the membrane tension. In this section we will discuss that the effective membrane tension is related to the out-of-plane fluctuations of the membrane.

The experiments presented in this thesis are conducted on a scale at which Brownian motion is important. This is especially true for lipid bilayer membranes, which are easily deformed due to their small thickness (~ 5 nm), and small bending rigidity ($\sim 20 k_b T$). Because of this deformability, thermal noise will induce fluctuations perpendicular to the plane of the membrane. When a membrane is left to itself, without any constraints, the membrane tension

Forces required to maintain membrane tubes

is at a minimum and the membrane will show pronounced fluctuations around an average value [91]. The maximal amplitude of these fluctuations depends on the size of the bilayer, and the largest wavelength fluctuations have the largest amplitude [91, 92]. However, when constraints are imposed (for example by applying an external force, see Figure 3-3), the number of conformations the membrane can assume is reduced, and this results in an increase in the membrane tension.

The magnitude of the membrane tension depends on the excess area, which is not resolvable with (for example) light microscopy. Only large amplitude fluctuations will be resolvable. The membrane area that can be resolved by microscopy is defined as the *macroscopic* area [93] (see Figure 3-3). Contrary to this macroscopic area, the total number of lipids defines the total *microscopic* area of the membrane (if we assume that the distance between the lipids does not change, which is true for lower membrane tensions). The number of lipids in a lipid bilayer is constant because it is energetically unfavorable for them to move out of the membrane.

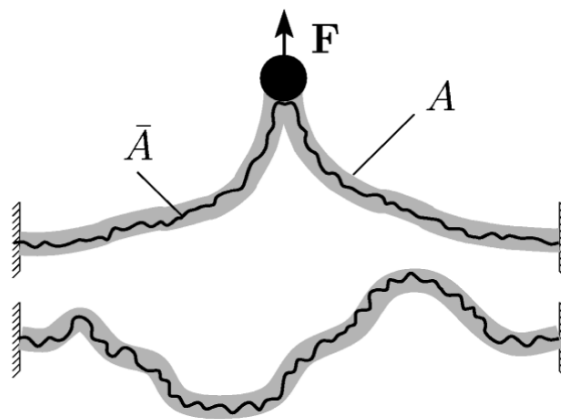


Figure 3-3. The microscopic area \bar{A} , and the macroscopic area A . The microscopic area is the real total area (determined by the number of lipids). The macroscopic area is the area resolved by the microscope [93]. F is an external force.

When a membrane is stretched by external forces, for example by micropipette suction or optical tweezers, two phases can be discerned. In the first phase, the (visible and non-visible) thermal undulations will be flattened, thereby lowering the entropy. In this entropic regime,

Forces required to maintain membrane tubes

the relationship between the fractional increase in visible area α and the tension, is given by [91, 93-95]:

$$\alpha = \frac{k_b T}{8\pi\kappa} \ln\left(1 + \frac{c\sigma A}{\kappa}\right) \quad (3.11)$$

where k_b is the Boltzmann constant, T is the temperature, c is a constant (~ 0.1 , [94]) and A is the macroscopic membrane area. Equation (3.11) can be rewritten [95]:

$$\sigma = \sigma_0 e^{\frac{8\pi\kappa}{k_b T} \alpha} \quad (3.12)$$

in which case σ_0 is the initial membrane tension.

When the macroscopic membrane area is increased even more, the tension will increase to values where the distance between the lipids in the membrane will increase. This results in an additional linear elastic response, where K determines the energy cost for area expansion. In this regime the relation between fractional area increase and the tension is mostly linear with a much smaller residual entropic component:

$$\alpha = \frac{k_b T}{8\pi\kappa} \ln\left(1 + \frac{c\sigma A}{\kappa}\right) + \frac{\sigma}{K} \quad (3.13)$$

This relationship has been verified in micropipette experiments [94-96] in which the macroscopic area of a giant unilamellar vesicle was increased by pipette suction. This method provides a sensitive means for the determination of the bending rigidity (κ).

Forces required to maintain membrane tubes

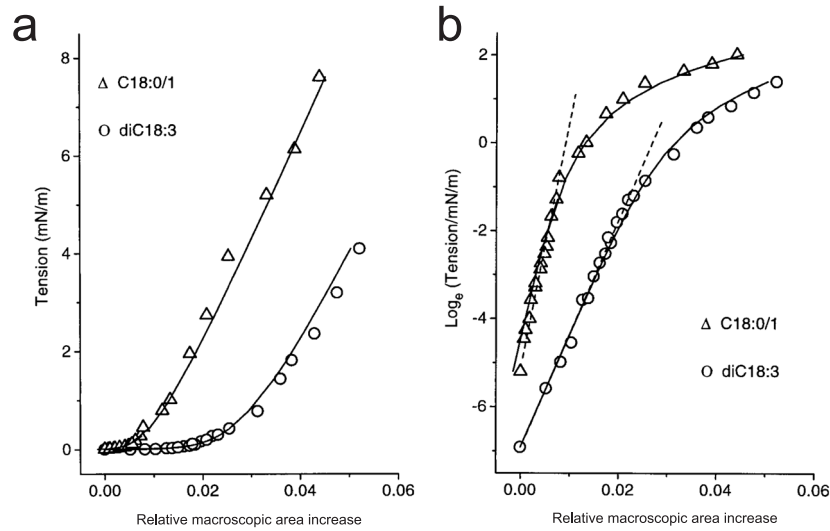


Figure 3-4. The membrane tension as a function of the area expansion [95] for two kinds of lipids. The same data are presented with linear (left) and exponential axes (right). At lower area expansions ($\sim <0.02$) the tension is determined by the reduction of thermal fluctuations, indicated by the exponential dependence. At higher area expansions the membrane is stretched.

In the low-tension regime, the stretching term in Equation (3.13) can be neglected; and the bending rigidity can therefore be determined by fitting the data with Equation (3.12) (see Figure 3-4). On the other hand, in the linear stretching regime the entropic component can be neglected and a value for the membranes stretching modulus can be obtained.

An important remark regarding experiments with synthetic vesicles should be made here. Although synthetic lipid bilayers are, in some ways, easier to study than cellular membranes, they do not necessarily behave as perfect model systems. An interesting point is that most vesicles in experimental studies are not as clean as is often theoretically described, and presumably contain excess area that could function as a lipid reservoir. This additional area has been referred to as “hidden” area [97, 98], but could also be due to microscopically small and therefore difficult to observe protrusions (see [72, 99, 100], and our own observations). Such small protrusions could be metastable and get incorporated into the membrane when the tension increases. In experiments in which the tension of the membrane is studied (e.g Figure 3-4), the membrane is therefore pre-stressed to remove this excess area, after which the analysis is done [95]. In our quantitative experiments on tube formation forces, we do not pre-stress the vesicles. Because hidden area could function as additional area that is incorporated during an experiment, the expansion of the macroscopic area could increase the membrane

tension more slowly than what may be expected based on theoretical descriptions, or than is measured in the above mentioned micropipette suction experiments.

3.3 Experimental determination of plateau forces

In this section we present experimental data obtained on the forces required to maintain a membrane tube that is formed from a giant vesicle. We will present measurements for DOPC vesicles, for DOPC vesicles with 40 % cholesterol, and for vesicles with pores formed by the peptide streptolysin O. These results provide a characterization of the vesicles with different properties, and show that our giant vesicles behave as expected from theory. The results will be used for the interpretation of motor-protein induced tube formation studies presented in chapter 5.

There are several sources that contribute to the force required for the pulling of a tube from a membrane. As described in the previous sections in this chapter, for short membrane tubes the membrane tension and the bending rigidity determine the plateau force at equilibrium. When tubes are formed at high velocities, there is a contribution due to the friction that arises when the monolayers of a bilayer slide with respect to each other. This has been shown [101, 102] in experiments where tubes were elongated at high speeds ($\sim 100 \mu\text{m/s}$). In this chapter we evaluate the forces to *maintain* a tube, after the dynamic components have relaxed. Inter-monolayer friction therefore does not play a role.

Pulling tubes with optical tweezers

Membrane tubes were formed from giant vesicles according to the following procedure. A mixture was made of biotin-labeled giant unilamellar vesicles (see section 2.1) in MRB40 with 112 mM glucose, and streptavidin coated polystyrene beads ($2.17 \mu\text{m}$ diameter), which was flown into a flow-cell (see section 2.2). Subsequently, the bottom surface of the flow-cell sample was searched for a vesicle of a reasonable size ($\sim 10 \mu\text{m}$ radius). Next, a bead was held against this vesicle with the optical tweezers. After a strong connection was made through biotin-streptavidin connections, this same bead was pressed against the surface of the flow-

Forces required to maintain membrane tubes

cell for ~ 1 minute to allow for a strong attachment to the (casein coated) coverslip. A practical remark here is that the success rate of bead attachment to the vesicle increased significantly if the vesicles were washed by centrifugation before usage. We suspect that small (non-visible) vesicles and lipid debris competed for the streptavidin on the bead if this was not done. For the force measurements, another bead was grabbed with the optical tweezers. This bead was positioned at a height halfway the vesicle, at a distance of $\sim 10 \mu\text{m}$ from the vesicle on the side opposite to the attached bead. Next, a power spectrum of the fluctuations of the bead was recorded for determination of the stiffness of the tweezers (see section 2.3).

The following experimental steps were recorded on videotape for offline analysis after the experiment was completed. First, the position of the bead in the optical tweezers corresponding to a zero force was recorded. Subsequently, the vesicle was moved against the trapped bead with the piezo-stage. After holding the vesicle against the bead for ~ 10 seconds, a tube was formed by displacing the vesicle at $1 \mu\text{m/s}$. After a tube had formed, the bead was kept at a fixed position for ~ 1 minute for the system to reach equilibrium (Figure 3-5).

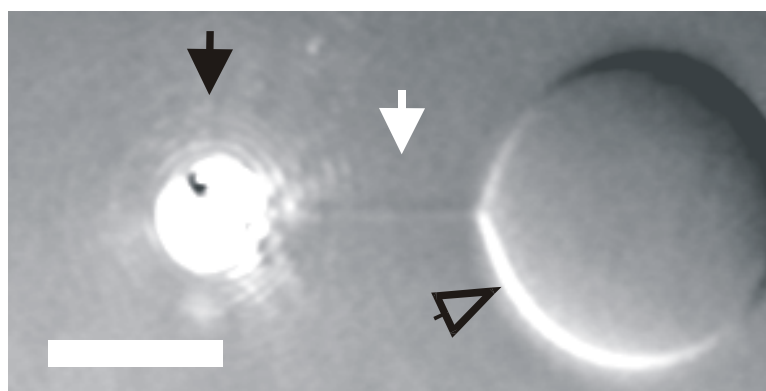


Figure 3-5. VE-DIC image of a DOPC vesicle (open arrow) from which a tube (white arrow) is pulled with a bead (black arrow) held in the optical tweezers. The contrast has been enhanced to make the tube visible. The bar is $5 \mu\text{m}$.

After a successful experiment had been finished, the deviation of the bead position from the trap center was tracked on the video images (section 2.3), with a dataset of bead position versus time as a result. Together with the stiffness of the tweezers (derived from the power spectrum), this yielded the force on the bead during the experiment.

Forces required to maintain membrane tubes

Plateau forces for DOPC vesicles

We first conducted tube formation experiments on DOPC vesicles (section 2.1). A typical example of the force on a bead during an experiment is shown in Figure 3-6. This figure shows the force connected with the different stages described above. Initially the bead is not connected to the vesicle, this determines the position of the bead corresponding to zero force (in Figure 3-6 this is the period between 0 and ~20 seconds). Next, the vesicle is moved against the bead, and during a couple of seconds streptavidin-biotin connections are established (at around 25 seconds). In the following phase (between 25 and 40 seconds), the vesicle is moved away from the bead. The force increases to a peak value, and when the tube is formed the force falls down to the lower plateau force. Next, the tube is extended for several micrometers (during which the force would sometimes increase a bit more, see below), and is subsequently held at a fixed distance to allow the membrane system to reach equilibrium.

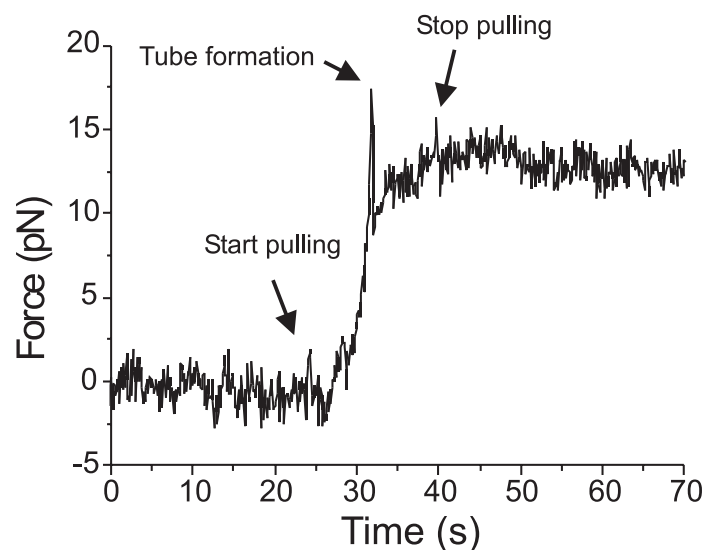


Figure 3-6. The force on a bead versus time when a tube is pulled from a DOPC vesicle. The bead is moved away from the vesicle starting at around 25 seconds. At 32 seconds a tube is formed. The bead movement stops around 40 seconds.

This characteristic shape of the “force-extension” curve is similar for all of the vesicles from which a tube is pulled. The details of the curves are however subject to variability. We observe different slopes for the rise in force before tube formation, different force barriers for

Forces required to maintain membrane tubes

tube formation, different plateau forces, and also different behaviors when the tube is elongated after the initial tube formation. Most of these characteristics will be discussed in chapter 4, where we will focus on the details of the formation of a tube and will discuss the shape of the force-extension curves in more detail. An important point for the plateau force measurements presented here, however, is the expected rise in force when a tube is elongated after the initial formation of the tube. This is expected because of an increase of the macroscopic area, which should reduce the amount of entropic undulations and possibly lead to stretching of the membrane. A small calculation shows that the extension of a 50 nm radius tube to 10 μm will require an extra area of $\sim 3 \mu\text{m}^2$ ($A_{\text{tube}} \approx 2\pi R_0 L$), which is small (but significant) with respect to the area of a vesicle of 10 μm radius, $\sim 1000 \mu\text{m}^2$ ($4\pi R_{\text{vesicle}}^2$). One would expect that the membrane tension, and therefore the plateau force would rise. For some vesicle we do observe a slow increase in the plateau force with extension of the tube (see e.g. Figure 3-6), but for others the force stays constant up to experimental resolution (see below). An explanation for this may be that “hidden-area” is incorporated into the total membrane area (see also section 3.2). When vesicles are observed with high contrast VE-DIC or fluorescence microscopy, we have observed small but significant “strings” of membrane material inside the vesicle. We have not systematically investigated the possible incorporation of these structures. Such anomalies could function as a reservoir of lipids when only prevented from being incorporated into the membrane by a small energy barrier. This incorporation into the vesicle could occur at experimental timescales, especially when the membrane is under tension. The timescales for such putative incorporations are not known but are expected to decrease with the applied force.

A concern regarding the determination of plateau forces are dynamic and relaxation effects that could play a role. In the 30 seconds after the initial tube has formed (Figure 3-6), the force first grows with elongation of the tube. After elongation has stopped a slow decrease of the plateau force can be observed, although it is hard to distinguish from the noise on the signal. Possible causes for this behavior could be the relaxation of a dynamic (friction) component, or accelerated flip-flop (movement of lipids from one monolayer to the other [83]). When a tube is formed, lipids will need to move into the tube from the main vesicle body. If a tube is formed at high velocity ($>1 \mu\text{m/s}$), this could mean that the membrane neck (at the vesicle-tube junction) functions as a bottleneck [102] for the lipids to flow through. We take care to minimize such effects by pulling at speeds of 1 $\mu\text{m/s}$ or less. It is generally accepted [83, and references therein] that lipids with a polar head group in the bilayer of

Forces required to maintain membrane tubes

synthetic vesicles do not move from one monolayer to the other on any reasonable timescale (unlike in *in vivo* membranes where the lipid-composition of monolayers is maintained by active transport, [4]). It was, however, shown that under tension, accelerated flip-flop can occur at experimental timescales of minutes [83]. Such a high-speed flip-flop would result in a disappearance of the (small!) non-local bending component that may be present in the force. Many parameters play a role for the exact behavior of the plateau force once a tube is formed. For the determination of the plateau forces we decided to take the average force value over the first 30 seconds after a tube has formed.

The plateau force measurements for 20 DOPC vesicles are shown in Table 3.1 (together with the force measurements for vesicles containing cholesterol and streptolysin vesicles, see below).

Vesicle #	DOPC plateau force (pN)	Cholesterol	Streptolysin
1	18.1	43.7	0.77
2	9.8	31	0.83
3	22.9	39.3	1.08
4	10.1	68	0.79
5	11.8	58	0.65
6	21	29	0.49
7	15.2	34	0.53
8	14	32	
9	6.8	20	
10	32.7	81	
11	21.4	37.3	
12	33.6		
13	35.9		
14	11.1		
15	19.8		
16	11		
17	9.9		
18	36		
19	12.9		
20	10.1		
Average \pm SD	18 \pm 10	43 \pm 18	0.73 \pm 0.22

Table 3.1 Plateau forces for vesicles of different composition: DOPC, DOPC + 40% cholesterol, and DOPC + 40 % cholesterol + Streptolysin O.

Forces required to maintain membrane tubes

A combination of the dynamic effects described above, and measurement errors due to noise on the determination of the bead position (Brownian motion and tracking noise) determines the error on the plateau force. Typically this results in an error of $\sim 10\%$. The average plateau force for DOPC vesicles is 18 ± 10 pN (average \pm standard deviation). The spread in these plateau forces is large, even within a sample. We believe this variability is due to a practical problem in obtaining vesicles in their equilibrium state, when using the electroformation method. Vesicles with a broad variety of tensions are presumably the result of this method. This agrees well with the observation of a heterogeneous population of floppy (lots of thermal fluctuations) vesicles together with vesicles showing no resolvable fluctuations, within the same sample.

The measured forces can be used to calculate the radius of the membrane tube and the tension of the vesicles by using the equations that relate the tube force, the membrane tension, and the bending rigidity with each other (Equations (3.8) to (3.10)). For DOPC vesicles the radius of a tube is below the resolution of the microscope. However, for a tube force of 18 pN, and using the bending rigidity for pure DOPC vesicles [95] of 85 pNnm (~ 4.1 pNnm = $1 k_b T$ at room temperature), we can use Equation (3.10) to estimate a tube radius of ~ 30 nm. It should be noted here that, to be able to attach the streptavidin beads to the vesicle, we incorporated 3 mol% of biotinylated DOPE lipids into the bilayer. We assume this does not significantly influence the bending rigidity of the membrane and the spontaneous curvature, since the DOPE lipids are most likely distributed equally over the membrane. The membrane tension can also be determined when the bending rigidity and the force are known. Using Equation (3.9), an average tension of $\sim 6.2 \cdot 10^{-2}$ pN/nm can be inferred. Note that this is the tension for a vesicle with a small tether. Because the membrane tube is short, we can assume that the area of the membrane (and therefore the tension) did not significantly increase. The tension we find for the DOPC vesicles is inside the entropic regime (see Figure 3-4).

As the bending rigidity and the tension determine the plateau force, in the following sections we will vary these two parameters and study the effect on the plateau force.

Cholesterol increases the plateau force

We experimentally determine the effect of the incorporation of cholesterol into the membrane on the tube force. Cholesterol increases the bending rigidity of membranes, and it is important for cellular membranes where it, for example, controls water transfer over the bilayer.

Forces required to maintain membrane tubes

Cholesterol is also thought to be relevant for preventing the crystallization of the lipids, thereby preserving the fluid nature of the membrane, and it is an important component for the formation of micro-domains (rafts) in the membrane [8].

To study the effect of cholesterol on the plateau forces we made DOPC giant vesicles with 40 mol% cholesterol (DOPC-chol), close to the saturation value. It has previously been shown that cholesterol increases the bending rigidity of membranes (see below). Therefore one would expect that the plateau force would increase according to Equation (3.9). Practically, this (putative) higher plateau force and the corresponding higher overshoot force (see chapter 4) makes experiments with DOPC-chol vesicles more difficult. The difficulty is that the membrane that is attached to the bead detaches more quickly at higher forces, due to the dissociation of biotin-streptavidin bonds [103]. Moreover, the lipids themselves could be pulled out of the membrane at these higher forces [104]. From the successful experiments, we do find an average plateau force of 43 ± 18 pN for the DOPC-chol vesicles (see Table 3.1). This is graphically presented in Figure 3-10, where we show a force-extension curve for a vesicle containing cholesterol, together with a DOPC vesicle, and a vesicle with pores in the membrane (see below). Compared to the average plateau force of vesicles containing no cholesterol (18 pN), the tube force is 2.4 fold higher.

If we assume that the membrane tensions of the DOPC vesicles with and without cholesterol are similar after electroformation, we can use the tension determined for the DOPC vesicles to estimate the bending rigidity for vesicles with cholesterol. Inserting the tension of $6.2 \cdot 10^{-2}$ pN/nm and the force of 43 pN in Equation (3.9), we find a bending rigidity of 376 pNnm for DOPC vesicles with 40% cholesterol. This is a 4.4 fold increase in bending rigidity (as compared to DOPC vesicles with no cholesterol). This 4.4 fold increase is a bit high, but consistent with literature data on the effect of the addition of cholesterol to vesicles made of other lipids, where the rigidities were determined by several different methods. For example, for vesicles made of SOPC + 50% cholesterol, a 2.7 fold increase was found with the pipette suction technique [94], for SOPC + 50% cholesterol a 2.8 fold increase was found with the tether pulling technique [105], a 2.3 fold increase was found for SOPC + 30% cholesterol by fluctuation spectrum analysis [106], and for DMPC vesicles with 30% and 50% cholesterol, respectively a 3.2 fold and a 4.7 fold increase were reported by inspection of the fluctuation spectrum [107].

Forces required to maintain membrane tubes

Pores in the vesicle lower the tension and the plateau force

The DOPC and the DOPC-chol vesicles studied so far have different tube forces because of the difference in bending rigidity. From these experiments we have concluded that the vesicles have a significant membrane tension before forces are applied. This tension corresponds to a small osmotic pressure difference between the inside and the outside of the vesicles, even though our vesicles were created and used in iso-osmotic buffers. The membranes of the DOPC and DOPC-chol vesicles studied above are impermeable to solutes like sucrose and glucose (present respectively inside and outside of the vesicle), and are thus unable to release this initial tension. To eliminate this initial tension, we introduced the peptide streptolysin O (SLO) into the membrane. This peptide forms pores of ~ 30 nm in the membrane (see Figure 3-7, [108, 109]).

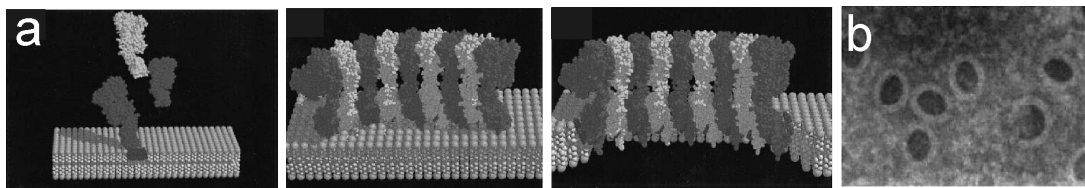


Figure 3-7. (a) Putative mechanism by which streptolysin forms pores in a bilayer [108]. First the peptide binds to cholesterol in the bilayer, next an oligomer is formed that subsequently gets inserted in the membrane. (b) Electron microscopy image of the ~ 30 nm pores in a membrane [109].

These pores allow for the exchange of solutes between the inside and outside of the vesicle, removing the osmotic component. The vesicle can now adjust its (fluctuating) shape to the energetically most favorable configuration, thus releasing the initial tension. We verified the presence of pores by enclosing sulforhodamine ($2\mu\text{M}$) inside the vesicles. As expected, this hydrophilic fluorescent dye was observed to diffuse out of the vesicles shortly after the addition of SLO (data not shown). After SLO was introduced, the vesicle started showing pronounced thermal fluctuations. Interestingly, as an additional effect we observed that the anomalous strings present in vesicles (see remark in section 3.2) disappeared and got incorporated into the vesicle membrane (Figure 3-8). Note that, in addition to the tension release by pore formation, the incorporation of additional membrane material can also make vesicles more floppy [110].

Forces required to maintain membrane tubes

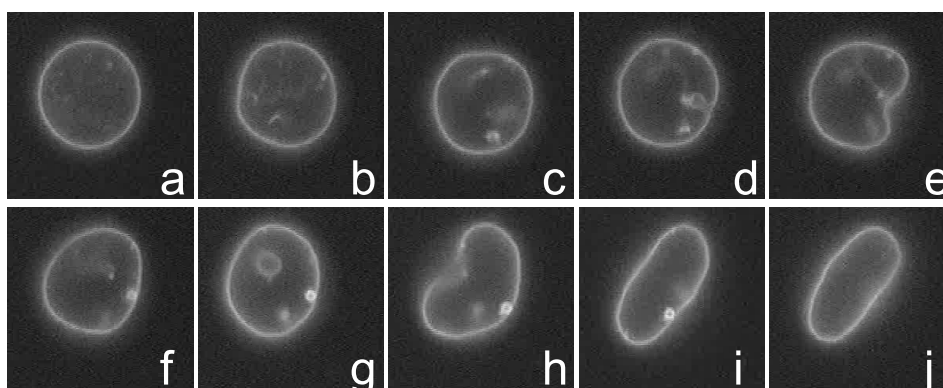


Figure 3-8. A series of snapshots of a vesicle ($\sim 10 \mu\text{m}$ diameter) into which streptolysin is being incorporated. Over a period of approximately 10 minutes (a-j), the membrane fluctuations increase. Moreover, as is clearly visible in (d-e) and (h-i) strings and smaller vesicles present inside the vesicle fuse with the membrane.

A practical problem concerning SLO vesicles is that they do not sediment. As there is no difference in density between the intravesicular and extravesicular buffer solutions, they will be distributed throughout the whole flow-cell (also in the z-direction). In addition, the contrast due to the difference in refractive index of sucrose and glucose disappears, which makes it more difficult to find the vesicles. However, after such a vesicle has been found a bead can be attached to it, and subsequently it can be moved down to the surface of the coverslip. For the remainder, the protocol for tube formation studies is the same as for DOPC vesicles.

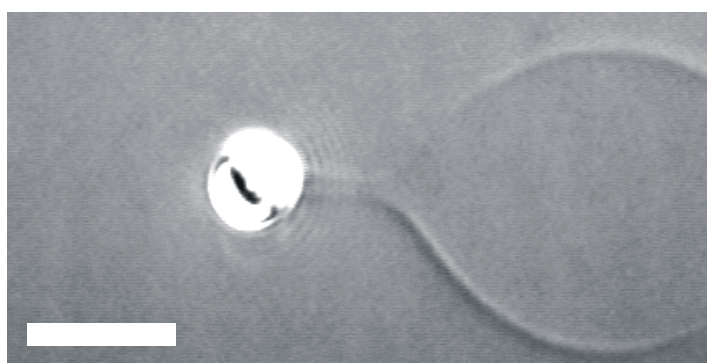


Figure 3-9. A membrane tube formed from a vesicle with streptolysin pores. This is the "steady state" and not due to a dynamic process. Note that the radius of the tube is resolvable. The bar is $5 \mu\text{m}$.

Forces required to maintain membrane tubes

The first finding for tube formation from SLO vesicles (see Figure 3-9) is that a tube can be formed at all. Membrane tension is essential for the formation of a tube (see above), and without it no tube can be formed. One would expect that the tension for SLO vesicles would become negligibly small, when it is let free to fluctuate. The key for understanding this is that the attachment (and displacement) of a trapped bead will impose boundary conditions on the vesicle. This will remove the freedom of the thermal fluctuations, and will therefore create a membrane tension (see section 3.2).

Interestingly, the tubes that are formed have a large diameter, which can be up to 1 μm large. This large tube diameter can be understood when one considers that the membrane tension of these vesicles is very small (Equation (3.8)). The forces that are required to hold a SLO tube are in the 1 pN regime, much smaller than the forces required to maintain tubes from DOPC or DOPC-chol vesicles. For a tube length of ~ 10 μm , we find an average plateau force of 0.73 pN with a standard deviation of 0.22 pN (6 vesicles, see Table 3.1). In Figure 3-10 a typical force-extension curve for a SLO vesicle is shown (together with force-extension curves for DOPC and DOPC-chol vesicles, for comparison).

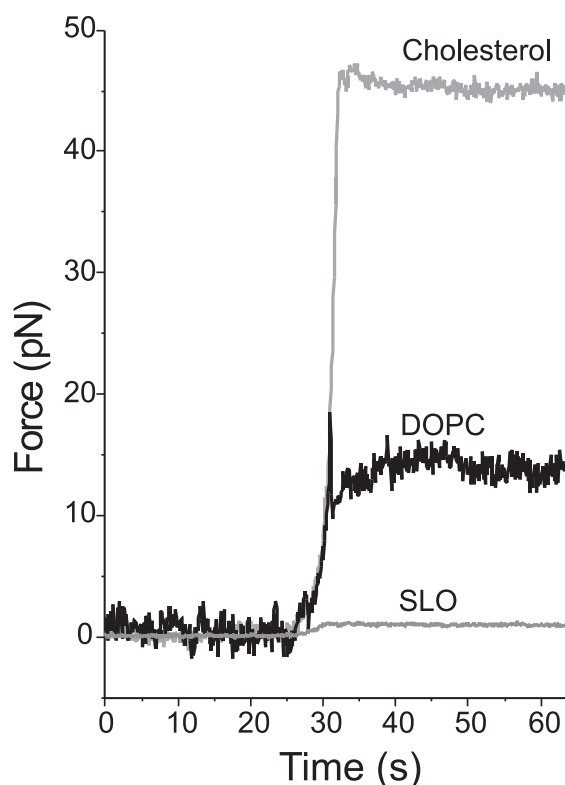


Figure 3-10. Examples of plateau forces for tubes pulled from vesicles with different properties.

Forces required to maintain membrane tubes

If the tension is caused by the suppression of membrane undulations, one would expect that a further extension of a membrane tube will further suppress the fluctuations of the bilayer, and therefore increase the membrane tension. This should result in an increasing tube-force with extension. To study this phenomenon we extended a tube to a length of 40 μm in 10- μm steps. The force corresponding to this stepwise extension is shown in Figure 3-11.

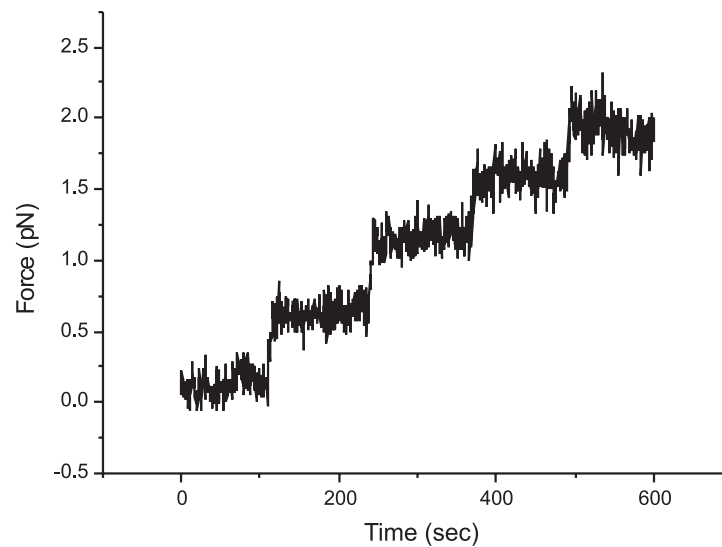


Figure 3-11. An example of the force on a bead when a tube is extended to 40 μm in four 10 μm steps. After each extension of 10 μm the tube is held at this length for ~ 100 seconds. A stepwise increase on the force of the bead can be observed.

We do indeed measure an increase in plateau force with extension. Because the radius of the membrane tube is sufficiently large to be determined with (DIC) microscopy, we can estimate the bending rigidity of our SLO vesicles. The tube force is inversely proportional to the radius of the tube, where the bending rigidity defines the slope (Equation (3.10)): $f_0 = 2\pi\kappa / R_0$. Consequently, if we now plot the tube force versus $2\pi/R_0$ for an SLO vesicle, the slope of the curve yields the bending rigidity (Figure 3-12). We find a bending modulus of 55 pNm. For the insertion of the streptolysin peptide into the membrane and the formation of pores, it was necessary to add 40% cholesterol to the membrane. For vesicles with cholesterol we found a stiffness of 376 pNm, so the subsequent addition of SLO lowers the membrane stiffness by a factor of ~ 6.8 . Since the peptide forms microscopic pores in the membrane, the total surface area that is bent is smaller (the density of lipids per surface area is lower) than for vesicles

Forces required to maintain membrane tubes

without pores. This may explain that the bending modulus decreases. A similar effect has previously been suggested in [99].

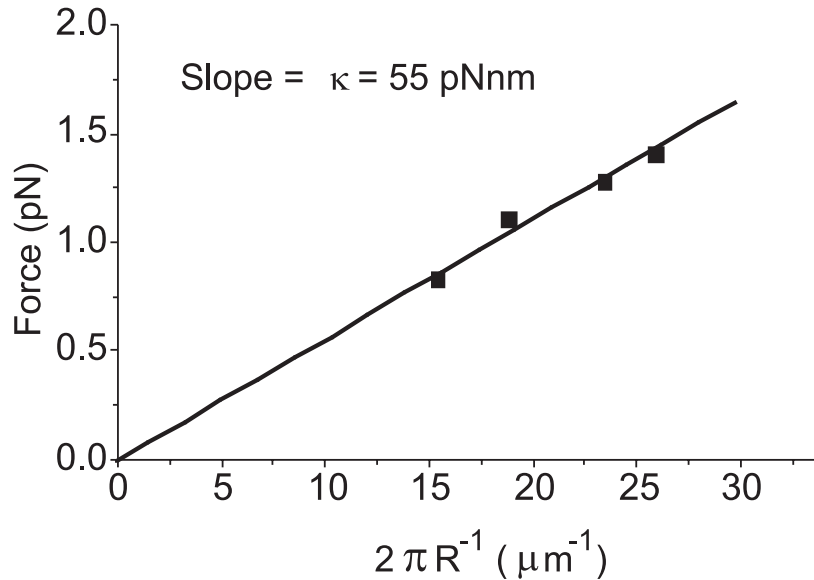


Figure 3-12. Force versus inverse tube radius. For each extension of the tube, an increase in force and a decrease of the radius was observed.

The experiments on SLO vesicles show that the initial tension plays an important role for the magnitude of the tube forces. The addition of streptolysin removes this initial tension. In a separate attempt to vary the tube forces, we tried to vary the initial tension by extravascular buffers of different osmolarities. The use of different concentrations of glucose should result in osmotic swelling and shrinking. We conducted force measurements for positive- and negative osmotic differences (+25 mOsm and -25 mOsm) on DOPC vesicles. One would expect water to flow through the vesicle membrane on a timescale of minutes [111], thereby changing the area-to-volume ratio. Unfortunately, we did not detect a significant tube-force dependence on osmolarity of the buffer, nor did we visually observe an enhancement (decline) of the membrane fluctuations for higher (lower) extravascular osmotic values. In fact, the forces were $13.4 \pm 5.1 \text{ pN}$ (average \pm SD, 10 vesicles) for the vesicles in a buffer with a lower osmolarity (which was expected to increase the tube force, since water will be pulled in, effectively removing area). For the vesicles in a higher extravascular osmotic buffer we measured forces of $14.7 \pm 6.0 \text{ pN}$ (12 vesicles), even though one would expect lower tube

Forces required to maintain membrane tubes

forces here. We lack an explanation for these results and can only speculate on the cause of this absence of an effect. One possibility is that the osmotically induced volume increase for lower osmotic values outside the vesicle forces the membrane to open up temporary pores due to a high tension [112]. Such short-lived pores in the bilayer would allow for the exchange of solutes of the intra- and extravesicular buffers (removing the induced tension). For the hyperosmotic buffer outside the vesicle, the expected increase in “free” area could possibly disappear due to the formation of (“hidden area”) inclusion objects. More experiments are clearly required to satisfactorily explain these results.

3.4 Discussion

We presented measurements on the forces required to maintain membrane tubes after they were formed from giant unilamellar vesicles. From energy minimization arguments it follows that this force should be determined by the bending rigidity (the parameter that determines the energy cost for a membrane to assume a curved shape), and the membrane tension (the parameter that determines the energy cost to increase the surface area). To verify this dependence we determined the tube forces required to maintain membrane tubes for three different kinds of vesicles. First, we determined the (static) forces required to hold membrane tubes that were formed from DOPC vesicles. These forces had an average of 18 pN, with a large spread due to a broad distribution of the initial tension of the vesicles. The force agrees well with previously studied plateau forces for membrane tubes [86, 90, 102, 113]. Interestingly, it was recently shown that the plateau forces required to form tubes from the (cell free) endoplasmic reticulum membrane [45] is ~18.6 pN (for Golgi membranes a lower force of 11.4 pN was reported). This shows that the force regime we studied is the biologically relevant one.

In our experiments, when tubes were formed from vesicles that had 40 mol% cholesterol incorporated in the bilayer, we found a higher average tube force of 43 pN. Cholesterol has been shown to increase the bending rigidity of bilayers [94, 105, 107], and should therefore result in a higher plateau force, in agreement with our results.

For the measurements on vesicles with streptolysin pores in the membrane we found very low forces of an average of 0.73 pN. We believe the vesicles obtained from the

Forces required to maintain membrane tubes

electroformation preparation have an initial tension, which (partly) causes the higher tube forces for DOPC and DOPC vesicles with cholesterol. Streptolysin forms pores in the membrane that remove the volume constraint, which is normally enforced by osmotic pressure is released. This allows the vesicles to reach their preferred configuration (at the energy minimum). Such vesicles are an interesting model system because they should have no initial membrane tension, unlike closed vesicles.

In this chapter we studied the basic properties of vesicles that are important for the forces involved in tube formation. In the next chapter we will use these results to study the force-extension curve for DOPC vesicles in more detail. We will focus on the force barrier that has to be overcome to form a tube (e.g. the peak around 30 seconds in Figure 3-6), and show how the height of this barrier depends on the size of the membrane area that attaches to the bead. In addition, these results will be used to interpret our experiments with motor proteins that form tubular networks in chapter 5.

4 Force barriers for membrane tube formation

In the previous chapter we discussed that the bending rigidity and the tension of a membrane determine the force that is required to maintain a tube. In this chapter we will show that a force that is significantly larger than the plateau force needs to be overcome for the initial formation of a tube. Our experiments with optical tweezers show that the height of this force barrier increases linearly with the radius of the area on which the pulling force is exerted. The force grows with extension while the membrane is steadily deformed until, at the moment of tube formation, the force drops down to the lower plateau force through a first-order transition. The reincorporation of an existing tube in the vesicle shows a smaller retraction overshoot due to hysteresis of the force extension curve. We confirm these experimental results with Monte Carlo simulations and theoretical calculations. These findings demonstrate that the formation of membrane tubes, in for example biological cells, strongly depends on the details of how forces are applied.

4.1 Introduction

Cellular membranous compartments frequently have a tubular shape (see chapter 1). New membrane tubes are formed from the Golgi apparatus as precursors for transport intermediates [46, 48] and the characteristic morphology of the endoplasmic reticulum is dynamically maintained by the constant formation and retraction of membrane tubes [37, 38]. For a better understanding of the relevant physics involved in tube formation, several experimental techniques have been used to pull tubes from cell membranes and synthetic vesicles. These techniques include hydrodynamic flow [113], micropipettes [114], optical and magnetic tweezers [45, 98, 115-121], and also motor proteins and polymerizing microtubules [121-123]. Most studies have either focused on the static force of extended tubes, or have examined dynamic effects that occur when elongating tubes at high speeds [102]. However, what determines in practice (i.e. in cells) whether a tube can be formed, is the force barrier connected with the initial deformation of the membrane.

Force barriers for membrane tube formation

Recent theoretical studies have focused on the "transition zone" around the critical deformation at which a tube forms [80, 87, 124] (see also [125]). These studies provide predictions for the different shapes a membrane assumes when a force is applied to a single point. They show that the force required for moving the point away increases while the membrane is being deformed. At a certain extension a transition to a configuration with a less deformed membrane and a tubular protrusion occurs. This conformation requires a lower plateau force, f_0 , to be maintained (see Figure 3-2). The value of the overshoot force (the force barrier for tube formation), f_{over} , was predicted to be $\sim 13\%$ higher than f_0 [87, 124], for a point force application (see Figure 3-2b). Under certain conditions, the shape transition was furthermore predicted to be discontinuous (first order) [80, 87, 126].

In reality, a force is never applied to a single point as was assumed in these theoretical studies. When using beads to pull tubes, a certain number of molecular links will be formed between the membrane and the bead, corresponding to a finite attachment area. The same is true in living cells, where (clusters of) molecular motors and required cofactors like accessory proteins and/or lipid domains, may be expected to occupy an area of significant size. In this chapter, data are presented on the force-extension curve for membrane tube formation (see also chapter 3). The experiments with optical tweezers demonstrate the existence of a force barrier and show that a finite attachment area (patch size) significantly increases the value of the force overshoot. The data show a linear increase of the force overshoot with the patch radius, R_p . We also performed simulations and theoretical calculations³. The experimental results are consistent with the prediction from simulations and theory that the $f_{over}-R_p$ curves for different vesicles collapse onto one curve when normalized by, respectively, f_0 and the radius of the formed tube, R_0 .

Based on the theoretical description one would expect hysteresis of the force extension curve. At the end of the chapter we will show preliminary results on the retraction overshoot, which is the small force jump that is encountered when a tube is reincorporated into the vesicle. This analysis shows a higher than expected retraction overshoot.

³ The Monte Carlo simulations were done by Angelo Cacciuto and the theory was developed by Imre Derényi. I am grateful for their contribution to this work.

4.2 Theoretical analysis of overshoot forces

The different shapes and the corresponding forces involved when a tube is formed from a membrane can be described theoretically. The shape transition that occurs at the moment of tube formation consists of a deformed vesicle that jumps to a state consisting of a less deformed vesicle and a tube. Before the transition, the shape of the membrane is best described by a catenoid [87, 124, 126] (see Figure 4-1a, top).

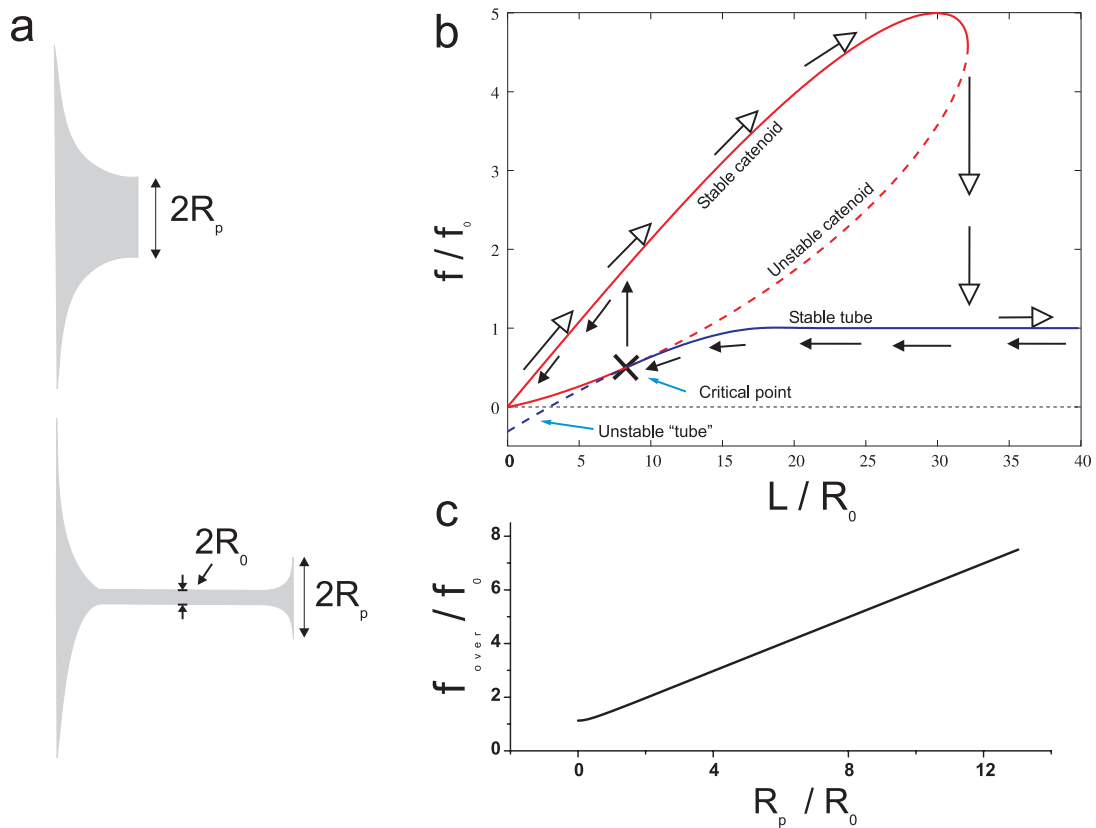


Figure 4-1. (a) (top) Sketch of a membrane which is deformed into a catenoid shape by a force exerted on a large patch. (bottom) Sketch of the membrane system after a tube has formed. (b) Theoretical force-extension curve for tube formation from a flat membrane of radius $100R_0$ with a patch size, R_p , of radius $10R_0$. f/f_0 is the normalized force. The open arrows indicate the typical path that is followed for tube formation, and the closed black arrows indicate the path for tube retraction. (c) The overshoot force, f_{over} , is expected to depend linearly on the radius of the pulling area.

Force barriers for membrane tube formation

In our experiments, this catenoid is superimposed on the sphere of the vesicle, and the end ring of this catenoid can be identified as the rim of the (approximately circular) patch. Around the extension at which tube formation occurs, the catenoid can support forces up to about $2\pi R_p \sigma$. When σ is subsequently expressed in terms of f_0 and R_0 (see section 3.1), this yields $f_{\text{over}} = 0.5f_0 R_p / R_0$. At the moment that the pulling force exceeds this value, the membrane collapses onto a tube of radius R_0 (Figure 4-1a, bottom). Thus, the ratio between the radii of the patch and the tube is expected to determine the overshoot force relative to the plateau force.

To be able to correctly impose the zero contact angle boundary condition at the rim of the patch, the shape equations have been solved numerically with the same technique as used for point forces in [87]. Figure 4-1b shows the result of such an analysis for a patch of radius $10R_0$ pulled from a flat circular piece of membrane of radius $100R_0$. When the patch is moved away from the membrane (open arrows in Figure 4-1b), the stable catenoid curve is followed and the force increases. If the tube is extended further, the catenoid cannot exist anymore and a tube is formed, at that moment the force drops to the stable tube curve. When an existing tube is retracted, the force will follow the stable tube curve while it is shortened (black arrows in Figure 4-1b). When the critical point is reached (the black cross) the tube is not stable anymore and the stable catenoid shape is assumed again. Accordingly, the force jumps up to the stable catenoid line, resulting in a retraction overshoot force that is lower than the initial overshoot force needed to create a tube. When the force extension curve is determined numerically for many different patch sizes, a patch-size dependent overshoot force is found which can be described by: $f_{\text{over}} = f_0 + 0.5f_0 R_p / R_0$ (see Figure 4-1c). Thus, a linear dependence in the large R_p limit is expected, which is the regime where experiments can be conducted.

4.3 Experimental results and simulations

To measure the force-extension curve of membrane tubes we used a procedure similar to the one presented in chapter 3. We first immobilized a biotinylated giant vesicle (doped with 0.2 mol% fluorescent rhodamine labeled DOPE, see section 2.1) on a coverslip, with a

Force barriers for membrane tube formation

streptavidin coated polystyrene bead. Subsequently, another bead was brought into contact with the vesicle for a short time with the tweezers. The vesicle was then moved away with a piezoelectric stage for 10-15 μm at constant velocity (0.5 $\mu\text{m}/\text{s}$) and a tube was formed (Figure 4-2). Faster pulling resulted in a significant dynamic component in the force (for details see Figure 4-5).

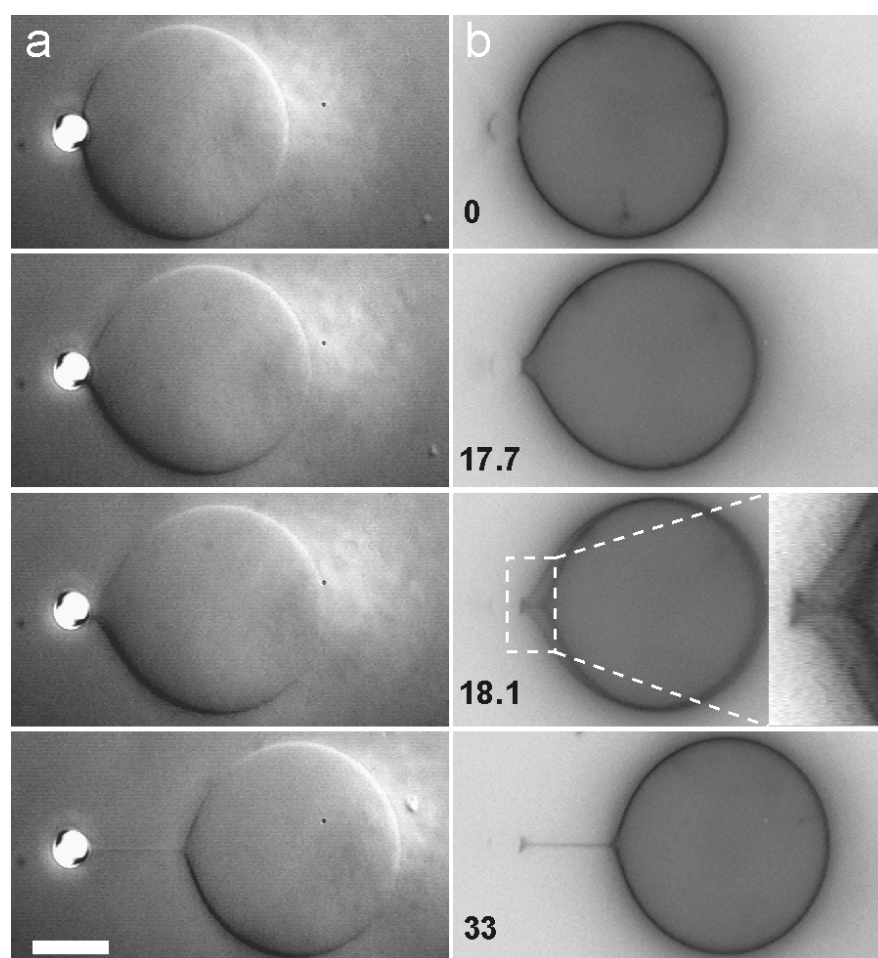


Figure 4-2. Tube formation from a vesicle. (a) Snapshots from DIC microscopy. From top to bottom: a vesicle in a spherical state when no force is exerted on it, the vesicle deformed with the tweezers, the transition point, and a vesicle with a tube. (b) Inverted contrast fluorescence images of the same vesicle. By integrating the signal (160 ms), we can observe the overlapping image of the vesicle just before and just after tube formation in the third picture from the top. The zoom (contrast enhanced) on the right side in this picture shows that the attachment area does not change during tube formation. Time is in seconds. Scale bar is 10 μm .

Force barriers for membrane tube formation

The vesicle was moved back and forth several times to pull and retract tubes. Because after each retraction more biotin-streptavidin bonds can be created between the vesicle and the bead, we expected this to result in an increased patch size for each subsequent tube formation. Since the patch itself was not visible with DIC microscopy, we used fluorescence microscopy to evaluate the patch size each time after a tube had formed. The number of repeated pulls was restricted by experimental limitations. First, photobleaching of the fluorophores in the membrane reduces the intensity of the fluorescence signal, which made it eventually impossible to determine the size of the patch. Second, the formation of a too large patch on the bead causes difficulties. A large patch size resulted in tube formation on the side anchored to the surface, the detachment of the other bead that provides the linkage to the surface, or overshoot values that were too high to measure with the tweezers.

A successful experiment resulted in multiple tube pulls during which different patch sizes could be observed and evaluated. Figure 4-3a shows inverted contrast fluorescence images of tubes with different patch sizes formed from the same vesicle. The bead itself is not fluorescent but is nevertheless visible due to a combination of scattering from the fluorescence signal of the tube and vesicle, and the attachment of small fluorescent particles. The corresponding force measurements are shown in Figure 4-3b. First, there is no contact between bead and vesicle and the force on the bead is zero. Next, the bead and vesicle are brought into contact and a (negative) force pushes the bead in the direction away from the vesicle. After the attachment has been established the bead and vesicle are moved apart and the force on the bead increases. At a certain (patch-size-dependent) displacement and force, a transition occurs from a vesicle in a deformed state to a more spherical vesicle with a tube. At this shape transition the force drops down to a lower plateau value. For the different tube pulls shown in Figure 4-3, overshoot forces that are much larger (up to 40 pN) than the plateau value (~ 4 pN for the same vesicle) can be observed. Finally, the vesicle and bead are moved towards each other again. This results in a shortening of the tube until a critical distance from the membrane is reached, where the vesicle abruptly assumes a catenoid shape again. During this retraction we observe a smaller “retraction overshoot”, which is due to the hysteresis effect for a first order transition that was predicted in Figure 4-1b (see also [80, 87]). We study this hysteresis in more detail in the end of the chapter (Figure 4-9).

Force barriers for membrane tube formation

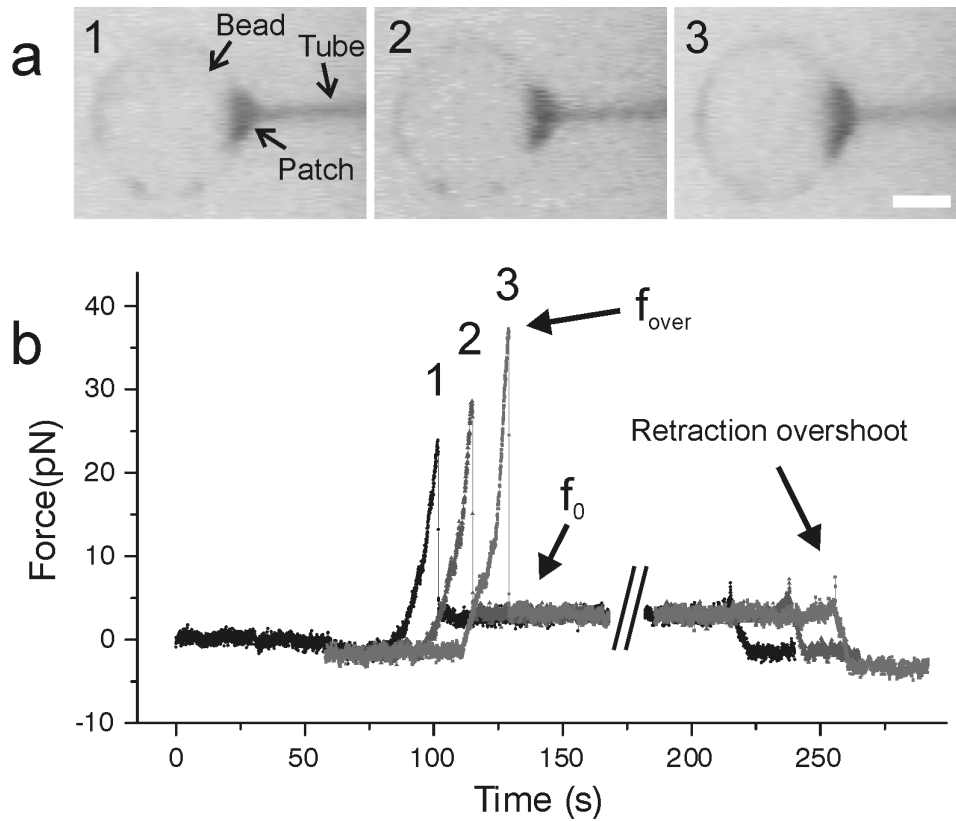


Figure 4-3. Subsequent tube pulls from the same vesicle. (a) Inverted contrast fluorescence images of an increasing attachment area after subsequent tube pulls. Scale bar: 2 μm . (b) The force on the bead during tube formation for the different pulls. The three curves correspond to the three patches in (a). In each pull the stage is moved for 20 s (10 μm) during which the force grows until at f_{over} a tube is formed and the force drops to f_0 . After the stage movement has stopped, the patch size is evaluated in fluorescence (at the break), and subsequently the stage is moved back 10 μm while the tube retracts.

After each tube had formed, we determined the patch radius by drawing a straight vertical line along the patch and counting the pixels. Depending on the quality of the image, we estimate that this results in 2-4 pixels ($\sim 150\text{-}300$ nm) uncertainty on the patch radius. Using fluorescence microscopy we also verified that the patch size stays constant during the formation of a tube (Figure 4-2).

To study the relationship between the patch size and the force overshoot in more detail, we plot the overshoot values versus the patch radius, R_p , for different vesicles in Figure 4-4. At $R_p = 0$, the value of the plateau force is plotted. This value is close to the expected force overshoot for a point force.

Force barriers for membrane tube formation

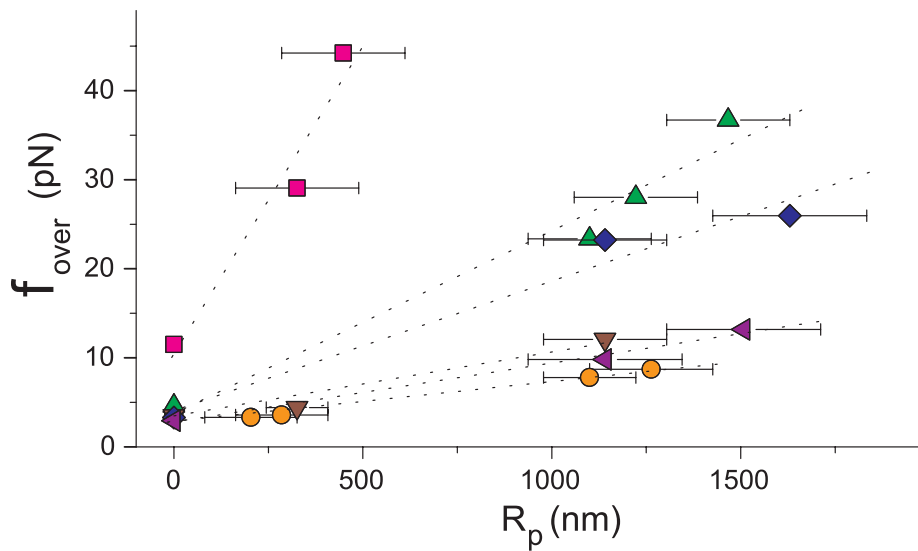


Figure 4-4. The overshoot force as a function of the radius of the patch (R_p) for 6 different vesicles. The larger slopes correspond to vesicles with higher plateau forces (plotted at $R_p = 0$). The dashed lines are linear fits to the data.

The data suggest a linear dependence of the force overshoot on the patch radius, with a slope that is higher for larger plateau forces. Higher plateau forces correspond to higher tensions, which are slightly different between different vesicles (see chapter 3). The relative errors on the overshoot forces (not shown) are small ($\sim 10\%$) because the displacements corresponding to these forces are high compared to the uncertainty in the bead position. We will compare these results with Monte Carlo simulations and the theoretical analysis. First, we will however discuss the effect of the pulling speed on the overshoot force in the following intermezzo.

Intermezzo: the overshoot force depends on the pulling speed

The formation of a membrane tube requires the strong deformation of a vesicle, and consequently it involves the reorganization of the lipids in the bilayer. Since this reorganization may be a time-dependent process we decided to determine the effect of the pulling speed on the overshoot force. To examine this, we formed tubes at a range of pulling speeds ($0.1 \mu\text{m/s} - 10 \mu\text{m/s}$), and we found that the overshoot force increases with larger pulling speeds (see Figure 4-5).

Force barriers for membrane tube formation

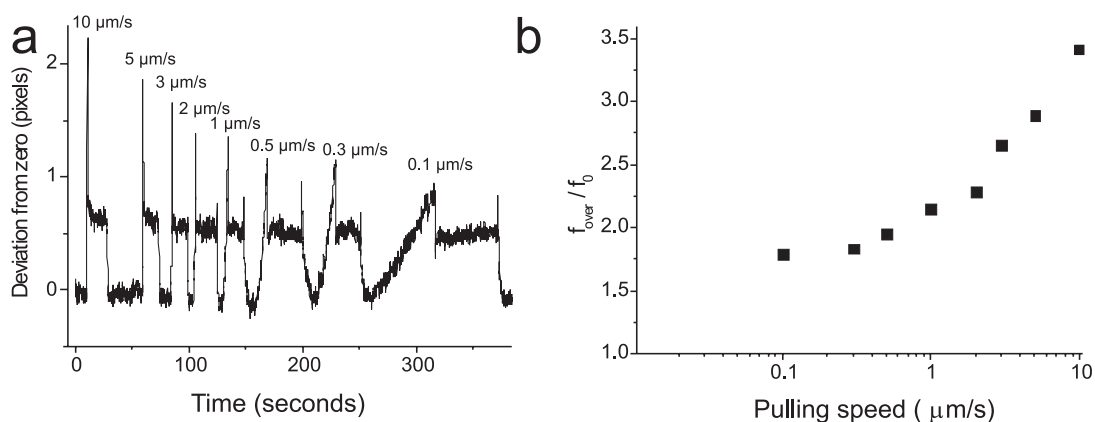


Figure 4-5. Effect of pulling speed on the overshoot force. (a) Force-extension curves for tube formation with several pulling speeds (ranging from 0.1 $\mu\text{m/s}$ to 10 $\mu\text{m/s}$). A significant dynamic component is present at pulling speeds higher than 0.5 $\mu\text{m/s}$. Due to sampling problems when pulling at high speeds, the actual peaks are underestimated for speeds larger than $\sim 2 \mu\text{m/s}$. (b) The pulling speed dependence of relative overshoot force for the several force extension curves in (a). The data is plotted on a logarithmic scale for clearness.

In a similar study [102], the extension of existing membrane tubes at high speeds ($\sim 100 \mu\text{m/s}$) was examined. It was found that the friction that arises due to the relative motion of lipids of the two monolayers in the vesicle-tube junction results in a dynamic component to the force. Even though in our experiments the tube has not yet formed at the moment that the overshoot force is present (the tube only arises when the force drops down to the plateau force), the reorganization of the lipids in the bilayer may be an explanation for the pulling speed dependence. It should be noted here that the velocity-dependent Stokes force on the bead ($F_{Stokes} = 6\pi\eta av$) is negligible. Inserting $\eta = \text{viscosity} = 10^{-3} \text{ N}\cdot\text{s}/\text{m}^2$, $a = \text{radius of bead} \sim 2 \mu\text{m}$, and $v = \text{velocity} = 0.5 \mu\text{m/s}$, yields a Stokes drag force of $\sim 0.02 \text{ pN}$, whereas all relevant measured forces are 2 to 3 orders of magnitude larger (see e.g. Figure 4-3).

An alternative explanation (in the slow pulling regime) for the pulling speed dependence of the overshoot comes from thermal fluctuations. In the vesicle-tube system the vesicle itself fluctuates (see section 3.2), the tube diffuses on the vesicle surface, and the tube fluctuates due to its small persistence length ($\sim 100\text{-}200 \text{ nm}$ [87]). A stochastic fluctuation may momentarily lower the energy barrier to form a tube. If an experiment lasts long (this is the case for lower pulling velocity), the probability for a stochastic fluctuation that pushes the system over the energy barrier for tube formation will increase. This effect of the interplay

Force barriers for membrane tube formation

between force and time is comparable to the extensively studied forces of molecular bond breaking [127, 128], where the correlation between force and probing time has been clearly demonstrated. However, as the energy barrier for tube formation is already large for a point force application [87], thermal activation may only be relevant for very slow pulling.

To exclude contributions to the force due to viscous drag between the monolayers, one would in principle want to determine the overshoot force at sufficiently small velocities. However, from a practical point of view a pulling speed of less than $0.5 \mu\text{m/s}$ is not workable, since experimental disturbances will interfere with the quality of the experiment (and possibly the force-time coupling described above). Therefore we decided to form tubes at speeds of $0.5 \mu\text{m/s}$ for the determination of the overshoot force (Figure 4-3), bearing in mind that in this case a small dynamic viscous component ($\sim 10\%$) may be present. An advantage of doing experiments at this pulling speed of $0.5 \mu\text{m/s}$, is that it is close to the velocity with which motor proteins form tubes (see chapters 5 and 6), which may be helpful for a proper comparison.

Monte Carlo simulations of overshoot forces

To check our experimental results, we performed Monte Carlo simulations of tube formation (Figure 4-7), using a simple model for a membrane introduced in [129]. The model consists of N hard spheres, of diameter d , connected by flexible links to form a triangulated network. The angle between two normals of adjacent triangles (Figure 4-6a) determines the bending energy contribution. The total bending energy is determined by the addition of all contributions from of all nearest-neighbour triangles.

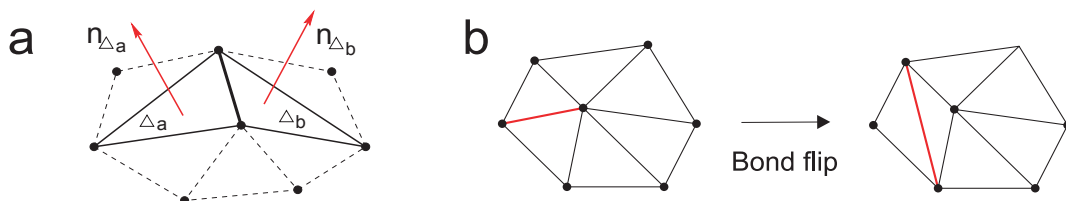


Figure 4-6. The triangulated network describing the membrane, adapted from [130]. (a) The curvature energy is determined by the angle between the normals, $n_{\Delta a}$ and $n_{\Delta b}$. (b) A bond separating two triangles can be flipped to form two new triangles.

Force barriers for membrane tube formation

The connectivity of the network is dynamically rearranged to simulate the fluidity of the membrane [131] (see Figure 4-6b). This bond-reorganization allows for the spheres to “diffuse” through the network and for the number of bonds per sphere to vary, when this is energetically favorable. Figure 4-7a shows a graphical sketch of a membrane tube formed in the simulation. The simulations show that the overshoot force increases with the patch size (Figure 4-7b). By analyzing the force needed to form a tube as a function of the radius of the patch-size in the Monte Carlo simulations we again find a linear behavior for patches larger than the tube diameter, where the slope increases with membrane tension (Figure 4-7c).

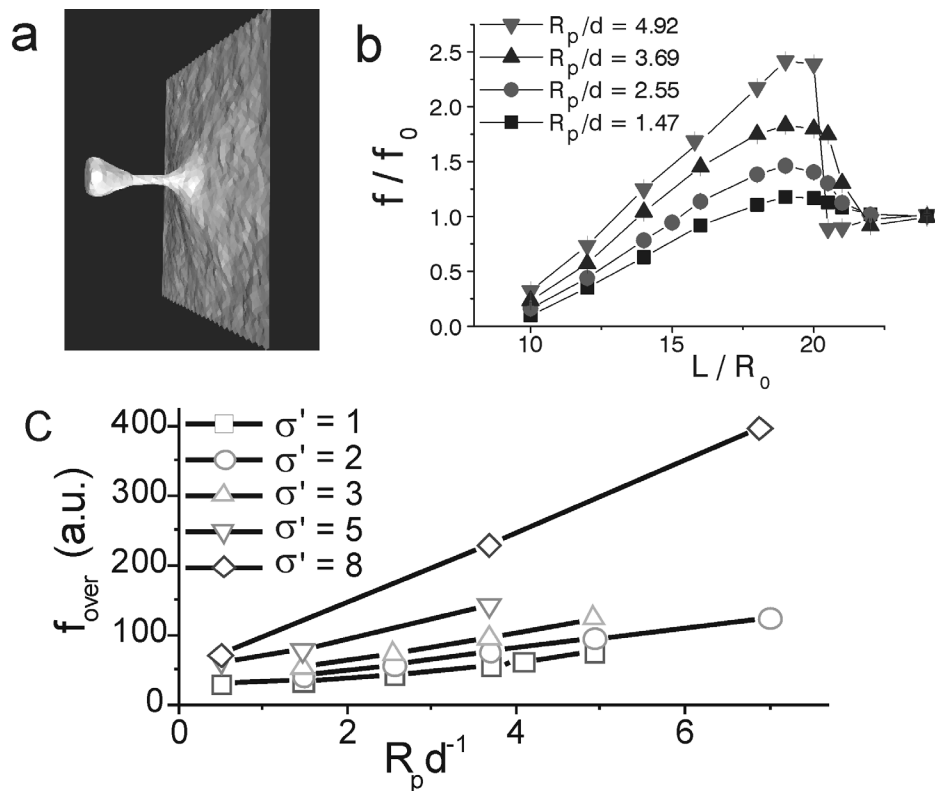


Figure 4-7. Overshoot forces from the Monte Carlo simulations. (a) Graphical presentation of a tube pulled in a simulation. (b) Force-extension curves for different patch sizes (R_p/d). The extension, L , is normalized to the tube radius R_0 . (c) The overshoot force as a function of the patch radius for membranes with several relative surface tensions (σ').

If the results from the Monte Carlo simulations are properly normalized, they confirm the prediction for the patch size dependence of the overshoot force (see stars in Figure 4-8).

Force barriers for membrane tube formation

Normalizing the experimental overshoot force and patch size

The simulations and theory predict that the relative overshoot value is determined by the ratio of the patch size and the tube radius. In Figure 4-8 we have plotted the theoretical prediction for this dependence (solid line, see Figure 4-1c) together with the results from the Monte Carlo simulations (stars). To establish whether our experimentally measured overshoot forces are consistent with this prediction, we normalized the patch size with respect to the radius of the tube and the overshoot force with respect to the plateau force. The radius of the tube is below the resolution of the microscope, but it can be derived from the plateau force by using Equation (3.10): $R_0 = 2\pi\kappa / f_0$. Hence, we can use the bending rigidity and the plateau force to estimate the tube radius. Since the bending rigidity for the vesicles used in our experiments has not been measured, we took the bending rigidity of 85 pNm for pure DOPC vesicles [95]. This is a reasonable assumption since it may be expected that the bending rigidity does not change much after the addition of 3% lipids with a different head group. The incorporation of 3% lipids with a long PEG-chain attached to the head group increased the rigidity less than $1 k_bT$ (~ 4.1 pNm) in [132].

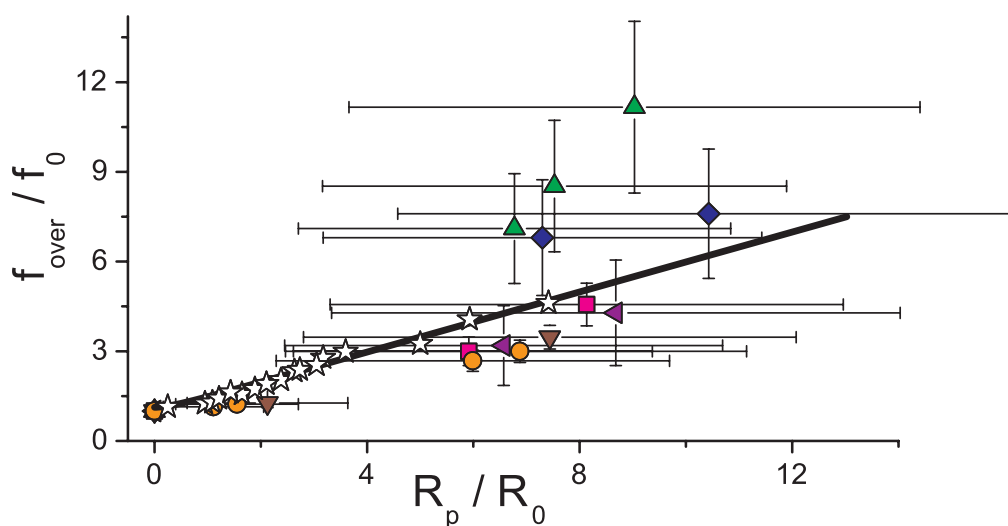


Figure 4-8. The relative overshoot versus the patch radius normalized with the radius of the tube. The experimental data are consistent with the results from the Monte Carlo simulation (open stars) and the theoretical calculations (solid line).

Force barriers for membrane tube formation

Because of the limited force the tweezers can exert, we use vesicles with a relatively low plateau force ~ 5 pN. This allows us to measure the high force barriers of tubes with patches of resolvable size. A consequence of the low plateau forces is that the measurement error on them will be relatively large ($\sim 20\%$). The total error on the ratio between R_p and R_0 (Figure 4-8) is large due to a combination of measurement errors on the patch size and the plateau force, and uncertainty in the bending rigidity. Despite this, the experimental data are, without the use of any fitting parameters, consistent with the theoretical prediction and the results from the simulations.

It has to be noted that in the simulations and in the theoretical calculations the surface tension is assumed constant. A change in the surface-to-volume ratio around the shape transition in our experiments might increase the surface tension slightly, which will increase the overshoot force. This could explain the deviation of some of the experimental data from the predicted curve in the large patch regime. The formation of a short membrane tube (< 10 μm) is not expected to significantly change the surface tension because the total area increment will be small ($< 1\%$) due to the small radius of the tubes (< 200 nm). As discussed above, enough area is stored in the thermal fluctuations of the membrane [94] and some possible hidden area [97].

Retraction overshoot

In our experimental force measurements (Figure 4-3b) we observed a hysteretic behavior, with a small retraction overshoot. This retraction overshoot can be understood from the theoretical force-extension curve presented in Figure 4-1b. When a force that is exerted on a membrane is moved further away, the stable catenoid curve is followed until a catenoid cannot be maintained anymore and the force drops down to the stable tube force when a tube is formed (open arrows in Figure 4-1b). When an existing tube is subsequently shortened, by moving the patch closer to the membrane (closed black arrows), it will follow the stable tube curve. However, at the critical point (where the stable tube line and the unstable catenoid line cross) the catenoid shape is assumed again, and the force jumps up to the force corresponding to the stable catenoid. If the distance between the “pulling patch” and the membrane is decreased further, the force will follow the stable catenoid path. This hysteretic behavior of the force-extension curve leads to the prediction of a smaller, but significant, retraction

Force barriers for membrane tube formation

overshoot. We plot both the force-extension curve and the force-retraction curve for the same vesicle and for two different patch sizes in Figure 4-9.

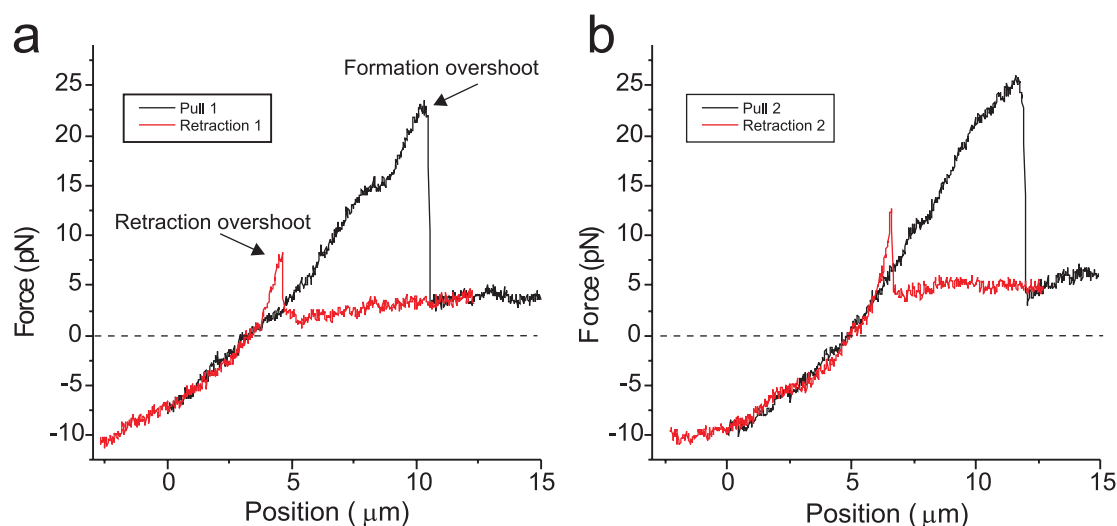


Figure 4-9. Force extension curves for tube formation and retraction for two patch sizes ($R_p = 1.14 \mu\text{m}$ in (a) and $1.63 \mu\text{m}$ in (b)) from the same vesicle. Force-extension curves are in black and retraction curves in gray.

According to the theoretical prediction (Figure 4-1b) the plateau forces and the “stable catenoid” parts of the tube formation and retraction force-curves should overlap. However to make these two parts overlap, the retraction curves needed to be shifted approximately $2 \mu\text{m}$ to the left on the position axis (Figure 4-9). This shift should not be necessary and the reason for it is presumably due to movement of the vesicle (possibly partial detachment and reattachment of the vesicle). Interestingly, even after this shift, it is not possible to have the stable catenoid part, the plateau force *and* the retraction overshoot all overlap with the tube formation curve, whereas this is expected based on the theory. An explanation for this discrepancy could be that the dynamic reorganization of the lipids in the bilayer creates a temporary (~ 1 second here) additional force that increases the retraction overshoot force. However, we do not have experimental support for this, and it requires further investigation.

4.4 Discussion

We have shown that the force barrier for the formation of a membrane tube grows linearly with the size of the area the force is exerted on. The results from the different approaches (experiments, simulations and theory) are consistent and indicate that the relative force barrier is determined by the ratio of the radius of the pulling area and the radius of the formed tube. These results should be taken into account in studies where the tube formation force is used to characterize mechanical properties of membranes of for example cells. They could be responsible for the large variety of force-overshoots observed in previous studies, e.g. [115, 117-119]. For example, in a study by Li et al., tubes that were formed from different sides of a cell [115] resulted in different overshoot forces, and it was concluded that this was due to differences in the cytoskeletal cortex. We expect that the presence of a cortical cytoskeleton will influence the force overshoot value, but an additional component on the tube formation force due to different patch sizes should also be expected. These different patch sizes could for example be caused by a different affinity for the probing bead on different sides of the cell.

We plan to analyze the full hysteretic force extension curves, including the retraction overshoot and the different distances from the membrane at which a tube forms and is reincorporated. A proper understanding of the forces exerted on a tube when it is close to the membrane, may shed light on the parameters and processes that play a role in membrane fusion and fission. After all, a conformation quite similar to the tube-membrane system studied here, is confronted when a tubulovesicular transport-intermediate fuses with, or pinches off from a membrane compartment [126]. The forces on such a piece of membrane will determine the incorporation speed and can be expected to influence the details of the functioning of fusion and fission machinery [49, 50].

Force barriers for membrane tube formation

5 Tubular membrane networks formed by dynamic association of motor proteins

The tubular morphology of intracellular membranous compartments is actively maintained through interactions with motor proteins and the cytoskeleton. Moving along cytoskeletal elements, motor proteins exert forces on the membranes to which they are attached, resulting in the formation of membrane tubes and tubular networks. To study the formation of membrane tubes by motor proteins, we developed an in vitro assay consisting of purified kinesin proteins directly linked to the lipids of giant unilamellar vesicles. When brought into contact with a network of immobilized microtubules, membrane tubes and tubular networks are formed. We study the mechanism involved by systematically varying the kinesin concentration and membrane composition. We show that a threshold concentration of motor proteins is needed, and that a low membrane tension facilitates tube formation. As the forces involved in tube formation (chapters 3 and 4) are higher than the force that individual motor proteins can exert, multiple motors must be working together to pull tubes. We propose a simple mechanism by which individual motor proteins can dynamically associate into clusters that provide the force needed for the formation of tubes.

5.1 Introduction

Lipid bilayer membranes play an important role in the functional compartmentalization of the interior of the cell where membrane compartments of different shapes and sizes can be found. A prominent example is the endoplasmic reticulum (ER), which is contiguous with the outer nuclear membrane and forms an elaborate network of interconnected tubes that extends throughout a large part of the cell [37]. Membrane tubes have also been observed in connection with the formation of cargo carriers from the Golgi apparatus [46], suggesting that the formation and maintenance of membrane tubes is also important for intracellular trafficking. *In vivo* [38, 133] as well as in cell-free extracts [42-44] a close colocalization between the membrane tubes of the endoplasmic reticulum and the cytoskeleton is observed.

Tubular membrane networks formed by dynamic association of motor proteins

The tubular membrane networks are dynamic in the sense that new tubes are continuously formed and existing ones disappear (see also chapter 1). The dynamic nature and the colocalization suggest that motor proteins in concert with the cytoskeleton play an important role in the formation and/or maintenance of the tubular membrane structures. This idea is supported by experiments in which the expression of the kinesin heavy chain was suppressed [16] or microtubules were depolymerized [39], which showed the ER retracting towards the cell center while no tubes were newly formed. These results suggested that motor proteins exert forces on membranes while moving along the cytoskeleton, and in this way shape the characteristic tubular membrane networks. The exact mechanism by which motor proteins are able to exert forces on the membrane, and consequently how the cell may regulate this process, is however not understood. Note, also, that it has been shown that elaborate tubular membrane networks can be formed independently of cytoskeletal filaments [134], and that polymerization forces generated by the cytoskeleton itself can provide an alternative to motor proteins [38, 135].

Thus far, most studies on the formation of membrane networks were conducted either *in vivo* or in cytoplasmic cell extracts, making it difficult to determine which components are essential for the process. Recently, Roux et al. [123] reported the formation of membrane tubes from synthetic vesicles by purified motor proteins. In this work, clusters of motor proteins were formed by attaching kinesin motors to small beads. These beads were subsequently linked to the vesicles. It was concluded that multiple motors that are statically linked together are a prerequisite for tube formation and that attaching individual motor proteins to the lipids of the vesicle is not sufficient for the formation of tubes. We show here instead that an *in vitro* system, consisting of purified kinesin directly linked to synthetic lipid vesicles, is sufficient for the formation of membrane tubes and tubular networks when the vesicles are brought into contact with a network of stabilized microtubules. To elucidate the mechanism involved we systematically vary different parameters and study the resulting changes in the dynamics or the morphologies of the membrane structures that arise. We find that a critical concentration of motor proteins is needed for tube formation and that motor proteins form tubes more easily when the membrane tension is low (as verified by the optical tweezers experiments in chapter 3). From our results we also conclude that multiple motors have to cooperate in the process of tube formation, but that in contrast to the findings by Roux et al. [123], these motors can do so without being physically linked to each other. We suggest a mechanism by which the membrane-bound motor proteins can spontaneously associate into stable clusters that exert enough force to form tubes.

5.2 Experimental results

Methods

To study the motor induced formation of membrane tubes we used the following protocol. First, microtubules (stabilized with taxol) were introduced into a flow-cell and incubated for 5 minutes to adhere to the polylysine-dipped coverslip (see section 2.2). Microtubules that did not stick to the surface of the flow-cell were removed by rinsing twice with MRB40 buffer (40 mM K-PIPES, 4 mM MgCl₂, 1 mM EGTA, pH = 6.8) containing 10 μM taxol, 112 mM glucose to osmotically match this solution with the intravesicular buffer (verified with a 3MO Micro-osmometer, Advanced Instruments, MA), and α-casein (2.5 mg/ml) to minimize the interaction of the vesicles with the glass surfaces. Vesicles were resuspended in MRB40 with 112 mM glucose and centrifuged (7000 rpm, 1 min) to increase the concentration. 3 μl of this solution with giant vesicles was mixed with 1 μl streptavidin (50 μg/ml, see section 2.2) (Molecular Probes, the Netherlands) and incubated for 5 minutes. Next, 1 μl of biotinylated kinesin (section 2.1) was added at the required concentration (0.1-100 μg/ml) and incubated for 5 minutes. The mixture was completed by adding 5 μl of MRB40 with 3 mM ATP, 0.4 μM C8-BODIPY 500/510-C5, 0.4 μM biotin, 20 μM taxol, 109 mM glucose, and 8 mM DTT, 0.4 mg/ml catalase, 0.8 mg/ml glucose oxidase as an oxygen scavenger system. Finally, in some experiments, streptolysin O was added to a final concentration of 500 Units/ml. This mixture was introduced into the flow-cell. In some experiments, fluorescent streptavidin (streptavidin, Alexa Fluor 488 conjugate, Molecular Probes) was used as a dye instead of BODIPY; this did not change the results.

Motor proteins and microtubules form a minimal system for tube formation from giant vesicles

Within a few minutes after the kinesin-coated vesicles sedimented onto a network of randomly positioned, taxol-stabilized, microtubules, membrane tubes were observed to be formed from the vesicles (see Figure 5-1, and see Figure 5-2a for a schematic representation). This typically occurred at a velocity that is lower than the velocity with which beads are

Tubular membrane networks formed by dynamic association of motor proteins

moved by this kinesin in a bead assay (between $\sim 0.6 \mu\text{m/s}$, [136] and $\sim 0.8 \mu\text{m/s}$, [137]), or MTs were moved in a gliding assay ($0.75 \mu\text{m/s}$, [61]).

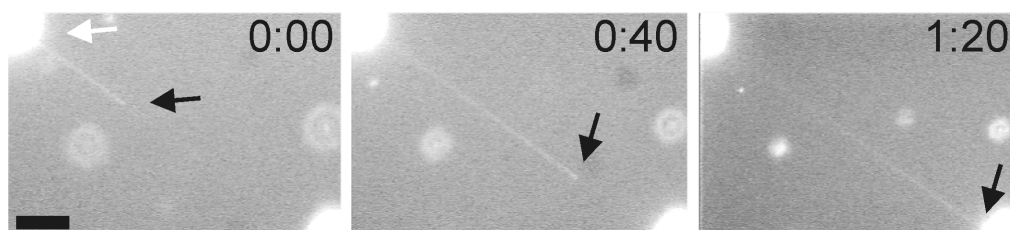


Figure 5-1. Fluorescence images of a membrane tube that is pulled from a vesicle at $\sim 0.4 \mu\text{m/s}$ by motor proteins that move along a microtubule. The white arrow indicates the vesicle and the black arrows point to the tip of the membrane tube where the motors are pulling (motors and MTs are not visible). Time is in minutes and seconds and the bar is $10 \mu\text{m}$.

Frequently, new tubes were observed to branch from existing tubes by the movement of motor proteins on crossing microtubules, leading to the formation of three-way junctions (see Figure 5-2b). Often, membrane tubes were observed to partly retract, after which the tube would elongate again. In addition, multiple tubes (up to three have been observed) would sometimes form on the same microtubule (this has been studied in more detail in [123]). After a while (>20 minutes) this resulted in an elaborate network of membrane tubes (Figure 5-2c).

Tubular membrane networks formed by dynamic association of motor proteins

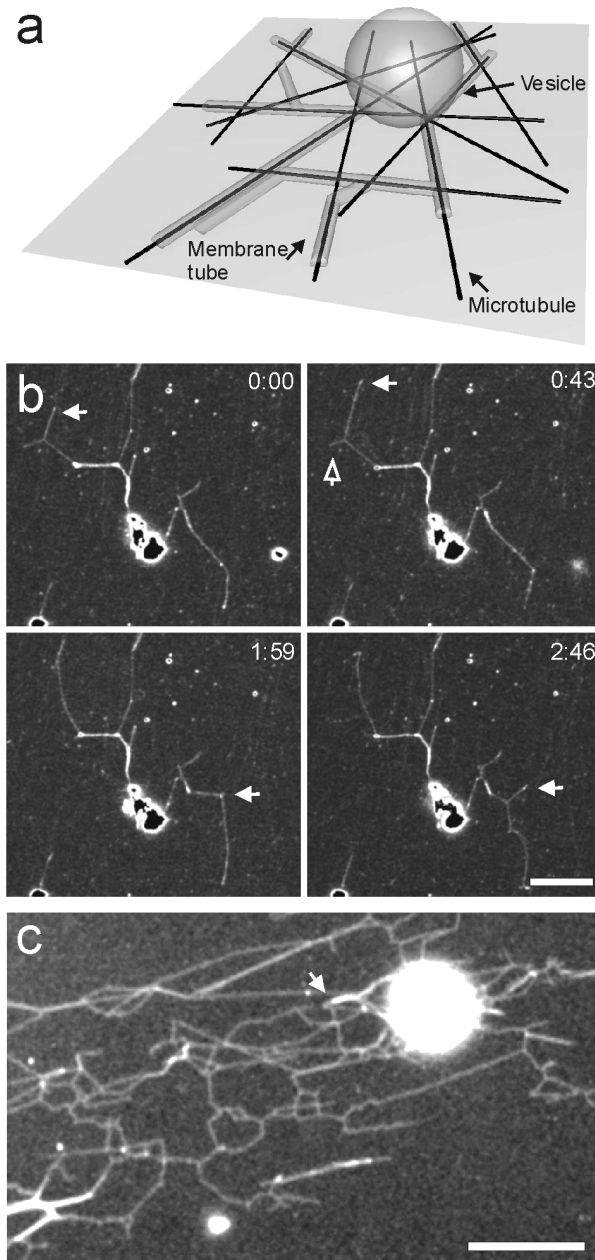


Figure 5-2. Overview of the experimental system. (a) Schematic representation of the assay (not to scale). Membrane tubes are formed from a vesicle that lies on top of a random network of microtubules attached to the surface. (b) Time sequence of scanning confocal microscopy images of membrane tubes during the early stage of network formation (approximately 10 minutes after sample preparation). The network is dynamic: existing tubes disappear (open arrow) and new tubes appear and grow (white arrows) giving shape to three-way junctions. The fluorescence is due to fluorescently labeled streptavidin. Neither microtubules nor motor proteins are visible. Time in minutes and seconds. Bar 5 μm . (c) Fluorescence image of a large network of membrane tubes (with streptolysin). After two hours, multiple three-way junctions can be observed and multiple membrane tubes are formed alongside each other, as can be seen from a stepwise increase in fluorescence (see arrow). Membranes are stained with BODIPY. Bar 10 μm .

Tubular membrane networks formed by dynamic association of motor proteins

To elucidate the mechanism by which motor proteins are able to cooperate and exert the forces needed for tube formation, we varied the number of motors on the vesicle and the properties of the vesicle that determine the force needed to pull a tube (see chapter 3). We quantified the extent of network formation by monitoring the total length of all the tubes in a network under different conditions, as a function of time.

The extent of tube formation depends on the kinesin concentration

The first parameter we varied was the density of motor proteins on the vesicle. Since a larger number of motor proteins is likely to be able to exert a higher force, one may expect that more extensive networks will be formed at high motor densities.

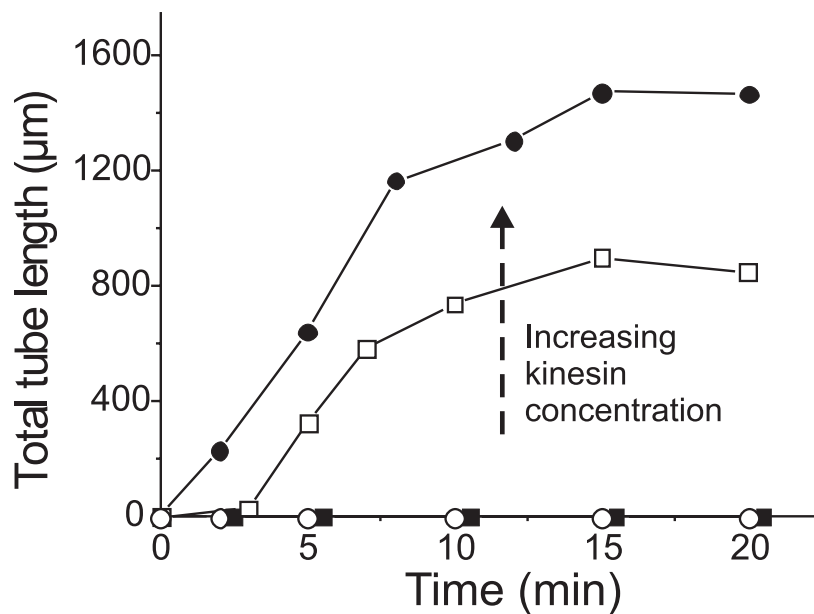


Figure 5-3. Evolution of a tubular network. The time dependence of the total length of membrane tubes pulled from vesicles for different final concentrations of kinesin in the sample: 10 µg/ml (filled circles), 3 µg/ml (open squares), 1 µg/ml (open circles) and 0.1 µg/ml (closed squares). In each sample approximately 15 vesicles were present in the field of view. Time 0 corresponds to the end of sample preparation. No tubes are formed at the lower concentrations whereas for the higher concentrations tubes start to form immediately after sedimentation.

Tubular membrane networks formed by dynamic association of motor proteins

To quantify the extent of tube formation, we determined the total length of membrane tubes in a $300 \times 500 \mu\text{m}^2$ field in the sample (see section 2.4), defined as the total tube length, for several concentrations of motor proteins. Figure 5-3 shows the time dependence of the extent of tube formation for the different concentrations of motor proteins. We found that more and longer tubes were formed for higher motor concentrations, while below a certain threshold concentration no tubes were formed at all (Figure 5-3). In all cases, after some time the total tube length did not increase anymore and a plateau was reached (typically around 20 minutes after start). In this plateau phase, the tubular network was still dynamic: existing tubes disappeared and new ones were formed. This indicates that the depletion of ATP was not the cause of the stalling of network growth.

An important issue for this experiment is how many motors eventually attach to the streptavidin on the vesicle, and accordingly what the final surface density of motors on the vesicles is. In this assay, we control the concentration of kinesin motors that are added to the vesicle solution. This results in the concentration indicated in Figure 5-3. We do not, however, control the surface density of active motors on the vesicle. There are several reasons for this. First, we do not know what percentage of the motor proteins will become inactivated by sticking to the surface of the coverslip. Second, it is unclear what percentage of the motor proteins is functional: some part of them may for example be in a rigor state. Finally, the number of vesicles in a sample varies, and the percentage of biotinylated lipids in a membrane as well as the density of streptavidin may also be subject to variability. If we ignore these uncertainties, and assume that all motor proteins introduced in the sample are active and do attach to the vesicles, we can make an estimation of the surface density. For the DOPC vesicles in Figure 5-3, tubes form at a kinesin concentration of $3 \mu\text{g/ml}$. Typically, there are approximately 15 vesicles, with a surface area of $\sim 1000 \mu\text{m}^2$ each, present in a field of view of $300 \times 500 \mu\text{m}^2$ (this total vesicle area may be an underestimate since there are many smaller lipid objects of an undefined size present in the sample, as judged from fluorescence microscopy). As the flow-cell is approximately $100 \mu\text{m}$ high, the volume above this surface area is $\sim 15 \cdot 10^6 \mu\text{m}^3$ ($= 15 \cdot 10^{-3} \mu\text{l}$). This leads to $45 \cdot 10^{-12} \text{ g}$ of motor proteins per 15 vesicles. Finally, with the molecular weight of kinesin ($\sim 50 \cdot 10^3 \text{ g/mole}$), this yields the (high) density of $\sim 10^7$ motors per vesicle ($\sim 10^{16} \text{ motors/m}^2$). Recently, in a similar assay, a protocol was developed with which it was possible to determine the concentration of motor proteins on the vesicles [136]. In that study, a threshold motor density of $\sim 10^{14} \text{ motors/m}^2$ for tube formation was predicted. Assuming this number is also applicable to our experiments, this suggests that only part of the motors introduced in the sample eventually adhere to the vesicles ($\sim 1\%$).

Tubular membrane networks formed by dynamic association of motor proteins

The total tube length pulled from vesicles depends on the initial tube force

The second parameter we varied was the initial membrane tension. This parameter, together with the membrane bending rigidity, determines the force needed to pull a tube from the vesicle (chapter 3). In practice our DOPC vesicles had a non-zero tension even before any tubes were formed, presumably due to an osmotic pressure difference between the inside and the outside. The peptide streptolysin O (SLO) was used to form pores in the bilayer of the vesicle, making them permeable to solutes and thereby eliminating the initial tension, thus lowering the tube force. In Figure 5-4, the total tube-length pulled by kinesin motors (2 $\mu\text{g/ml}$) from vesicles with SLO pores is plotted together with data for the total tube length pulled from control vesicles with no SLO. Many tubes were pulled from the vesicles with pores (filled circles), whereas far fewer tubes were formed from the DOPC vesicles (filled squares). The formation of tubes also continued for a longer time and no clear plateau was reached within the time of observation (40 minutes) for the SLO vesicles. For SLO to be functional, we added 40 mol% cholesterol to the membrane. Cholesterol increases the bending rigidity of the membrane, and thereby increasing the tube formation force (see chapter 3). In fact, when 40 mol% cholesterol was added without SLO (open circles) even fewer tubes were formed than from DOPC vesicles.

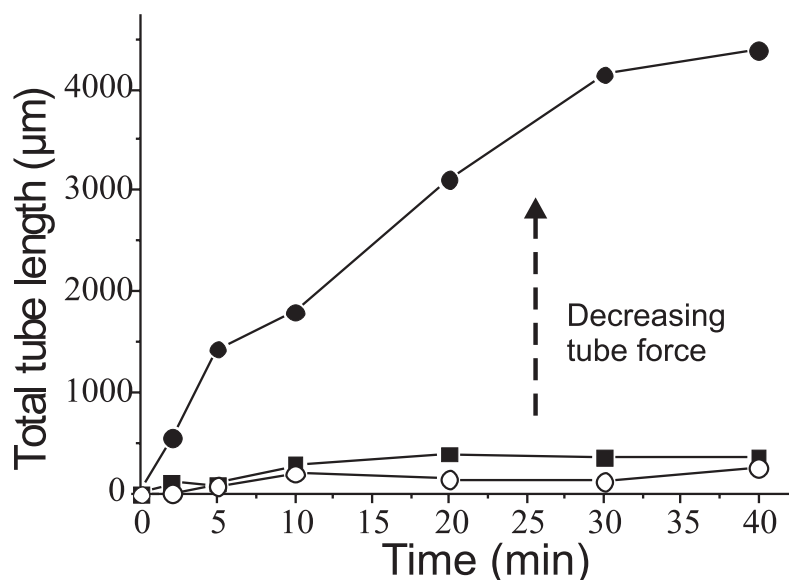


Figure 5-4. Total tube length pulled from vesicles with the pore-forming drug streptolysin O and cholesterol (filled circles), DOPC vesicles (filled squares), and vesicles with only cholesterol (open circles). These results are consistent with the force measurements presented in chapter 3, which showed that in the presence of SLO the forces needed to pull tubes are much lower than for DOPC vesicles, whereas with only cholesterol present they are higher. The kinesin concentration is 2 $\mu\text{g/ml}$.

Tubular membrane networks formed by dynamic association of motor proteins

We also attempted to vary the initial membrane tension by using buffers of different osmolarity. Since the membrane is permeable to water on experimental timescales [111], osmotic swelling and shrinking of the vesicle should result in different area-to-volume ratios. When more area is available, the initial tension should be lower, and conversely when less area is available, the initial tension is expected to rise (see section 3.2). We varied the osmolarity difference between the intravesicular and extravesicular buffer between -25 mOsm and +25 mOsm. Although we had some indication that a high osmolarity buffer facilitated tube and network formation, these experiments showed too much spread to support strong conclusions. Complementary force measurements (chapter 3) on vesicles in buffers of different osmolarities in fact also showed too large a spread to detect a clear force difference. As discussed above, we believe that this was due to the practical problem of obtaining vesicles in their equilibrium state using the electroformation method. The tension in the vesicles may not be strictly related to the imposed area-to-volume ratio, as small uncontrollable amounts of area seem to be stored in “hidden reservoirs” of lipids (see chapter 3). Moreover, if a large amount of excess area is created by the osmotic pressure difference, the fluctuations of the membrane together with the streptavidin may result in the formation of cross-linked invaginations. This would effectively remove excess area, and increase the tension again. On the other hand, when the initial excess area is removed from the vesicles by the osmotic pressure difference, the tension in the membrane may become so high that (short lived) openings in the membrane could form [112]. This would effectively tend to lower the tension closer to the initial state, and in addition would allow for the exchange of solutes between the intravesicular and extravesicular solution, which removes the pressure difference.

The threshold concentration of motors for tube formation depends on the tube force

Since the concentration of motor proteins (Figure 5-3) and the tube force (Figure 5-4) determine the extent of tube formation, it may be expected that the threshold concentration of motor proteins required for forming membrane tubes depends on the tube force as well. This threshold concentration was studied for the two types of vesicles for which the tube forces lie furthest apart: cholesterol vesicles and streptolysin vesicles (see Figure 3-10). The total tube length was determined for several motor concentrations, 20 minutes after introducing the motor-coated vesicles. The results are shown in Figure 5-5.

Tubular membrane networks formed by dynamic association of motor proteins

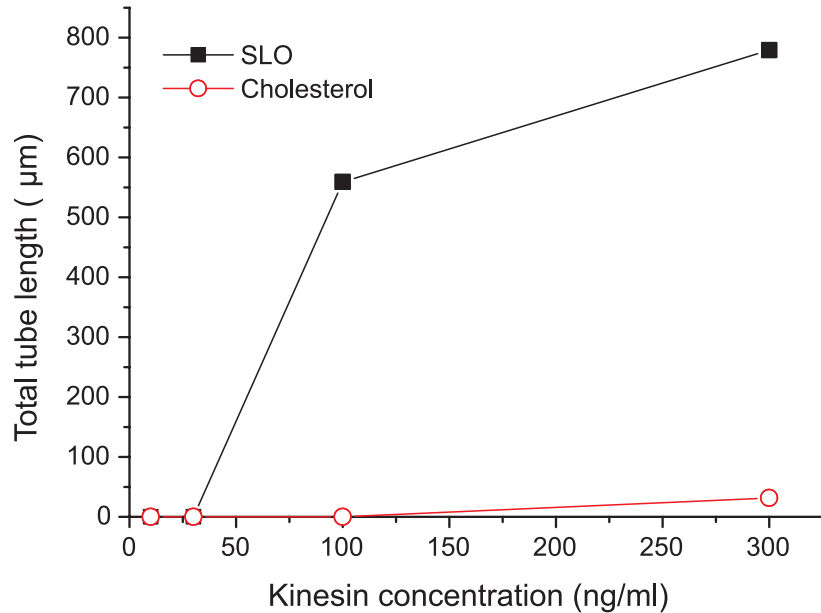


Figure 5-5. Motor concentration thresholds for tube formation. Tubes are formed from streptolysin vesicles at ~50 ng/ml, whereas for the cholesterol vesicles no significant tube formation occurs for the concentrations studied here.

The data indicate that tubes can already be formed from SLO vesicles at kinesin concentrations of ~50 ng/ml. For the cholesterol vesicles no significant tubulation occurs in the whole concentration regime studied here (but note that some tubes are present at 300 ng/ml). A large difference in the tube formation threshold of motor proteins may be expected when taking into account the large (~60x) difference in average tube force (chapter 3). The rare tubes observed for cholesterol vesicles at 300 ng/ml could be due to the large spread in tube forces (determined in section 3.3). As the total tube length is determined from ~15 different vesicles in the field of view, the tube force and therefore the motor threshold will be less well defined because the ease with which tubes can be formed will vary, even among vesicles of the same kind.

5.3 Dynamic association of motor proteins

In this chapter we have demonstrated that motor proteins can pull membrane tubes from giant vesicles, while moving along microtubules, when directly linked to the bilayer through streptavidin. We believe that multiple motor proteins are working together in the formation of membrane tubes for several reasons. First, at low motor concentrations we do not observe any tube formation, even though the probability of having one kinesin pulling should still be significant. A rough estimate suggests that more than 10,000 motors per vesicle are still present at the lowest motor concentration used. Second, tubes are moving over much longer distances (sometimes $>100\ \mu\text{m}$) than the known run length ($\sim 1\ \mu\text{m}$) of one kinesin motor, especially when taking into account the decrease of a motor's processivity when a force is exerted on it [32, 138, 139]. When multiple motors are pulling, the connection with the microtubule can be maintained for longer distances. Finally, from the force measurements presented in chapter 3 and 4, it follows that the forces involved in tube formation from DOPC vesicles are higher than the stall force of one kinesin protein ($\sim 6\ \text{pN}$) [30-32]. In addition, note that the tube formation forces we measured with the tweezers give a lower estimate of the forces involved in the formation of tubes by motors since the attachment of streptavidin (and kinesin) to the bilayer is likely to increase the bending rigidity of the membrane and therefore the tube formation force.

Modeling dynamic association

Since we conclude that multiple motor proteins must be working together, and since in our experiments the motor proteins are not physically linked to each other, we hypothesize in this section on a mechanism by which individual motor proteins could dynamically form clusters that are able to exert enough force to form tubes. As shown schematically in Figure 5-6a, we assume that motor proteins can participate in tube formation as soon as they are attached to a microtubule near the end of a membrane tube. The motors present at this location form a dynamic cluster, which constantly exchanges motors with the pool of motors attached to the vesicle. A stable cluster can only be formed if at any time the number of motors leaving the cluster is balanced by the number of motors arriving. If, in addition, the force per motor is lower than the stall force, a tube can be formed. Motor proteins can diffuse laterally on a

Tubular membrane networks formed by dynamic association of motor proteins

vesicle because of the liquid nature of the bilayer. When a diffusing motor protein is in the proximity of a microtubule, there will be a probability to attach, which will result in a certain number of motors arriving in the cluster per second: the arrival rate. This arrival rate is expected to increase linearly with the concentration of motor proteins. Motor proteins that are attached to a microtubule also have a probability of detaching from the microtubule. This detachment probability becomes higher when a force is exerted on the motor protein [32, 138, 139]. The total number of motor proteins that detaches from the microtubule and leaves the cluster per second defines the departure rate. Figure 5-6b illustrates the conditions under which a stable cluster of motor proteins at the leading end of a membrane tube can survive.

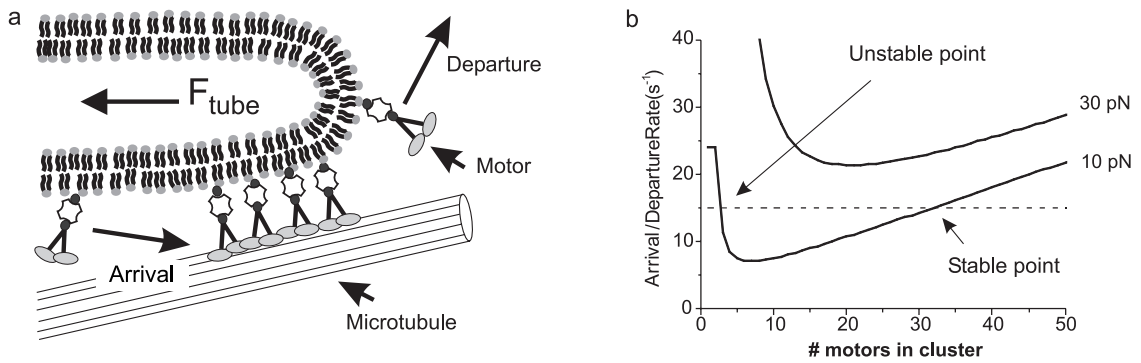


Figure 5-6. The mechanism of dynamic association. (a) Sketch of the mechanism of dynamic association of motor proteins. A cluster of motor proteins exerts a force on the tip of a tube. Each motor protein has a certain probability of detaching from the microtubule and leaving the cluster. This probability is force-dependent and will result in a certain departure rate. Motor proteins in the proximity of the microtubule also have a probability of attaching and joining the cluster, characterized by an arrival rate. (b) Graph showing the feasibility of the formation of a stable clusters by dynamic association. The solid curves show the departure rate of motors from a cluster for two different forces (10 pN and 30 pN), as a function of the number of proteins present in the cluster (see text). The dashed line depicts a constant arrival rate. For the tube force of 10 pN, there is a stable point where a cluster can be formed. For high forces (e.g. a tube force of 30 pN) the departure rate is too high and no stable cluster can be formed.

The motor arrival and departure rates are plotted as a function of cluster size. We assume an exponential force dependence of the detachment probability for one motor: $k_{\text{off}} = Ae^{\alpha F_m}$, where F_m is the force per motor protein and the constants $A=0.38 \text{ s}^{-1}$ and $\alpha=0.69 \text{ pN}^{-1}$ are obtained from a fit to results by Parmeggiani et al. [140], see also [138]. Note that the exact value of

Tubular membrane networks formed by dynamic association of motor proteins

the constants is not critical for the mechanism. When N motors are present in the cluster this leads to the following expression for the departure rate: $k_{dep} = Nk_{off} = NAe^{\alpha F_{tubc}/N}$, where we have assumed that the motors in the clusters share the load of the tube equally. In Figure 5-6b we plot the departure rate for two different tube forces (10 pN and 30 pN). The shape of these curves can be understood in the following way: if a low number of motors is present in the cluster, the force per motor is high and the detachment probability as well as departure rate will be high. If the number of motors in the cluster is high, the force per motor will be low and the detachment probability per motor will approach the spontaneous detachment rate A . However, when the number of motors in the cluster increases, even spontaneous detachment will result in a high departure rate ($k_{dep} = NA$). In contrast to the departure rate, the arrival rate will be independent of the size of the cluster, and only dependent on the local motor concentration (in Figure 5-6b an arbitrary value for the arrival rate was chosen). When the arrival and departure rates are equal, the cluster stays constant in size. For the tube force of 10 pN (Figure 5-6b), there are two points for which this is the case. One point (on the left) is unstable since small fluctuations in the number of motors in the cluster will enhance the difference between the arrival and departure rates. The other point represents a stable cluster. Here changes in the rates due to small fluctuations in the cluster size tend to drive the cluster back to the stable size. When the forces in the system become higher (e.g. 30 pN), the departure rate rises and no steady state clusters can be formed anymore.

This simple model does not take into account any geometrical constraints that may limit the number of motors in a cluster. A microtubule has multiple tracks along which motor proteins can move (13 filaments), but the number of filaments of a microtubule that are accessible to the motor proteins in our assay will presumably be at most six or seven since the microtubule is attached on one side to the coverslip. Due to the liquid nature of a lipid bilayer, only motors near the tip of a tube can exert force. It is not known, however, how these motors will interact and how the force will be distributed over the different filaments and rows of motors.

Despite these simplifications, the proposed mechanism of dynamic association is in qualitative accordance with the observed dependence on the motor concentration (Figure 5-3), membrane composition (Figure 5-4), and the threshold concentration of motors for different membrane compositions (Figure 5-5). If the motor concentration is too low for a given membrane composition, the arrival rate is too low for stable clusters to survive. When the concentration is increased, the arrival rate eventually passes a threshold value, after which

Tubular membrane networks formed by dynamic association of motor proteins

stable clusters and membrane tubes can be formed (Figure 5-3). The composition of the membrane affects tube formation through the influence it has on the tube formation force. As demonstrated in chapter 3, the membrane tension and rigidity together determine the tube formation force. In the presence of SLO the initial membrane tension is very low, leading to an initial tube formation force that is about 25-fold lower than for DOPC vesicles (Figure 3-10). Consequently, membrane tubes form much more easily in the presence than in the absence of SLO (Figure 5-4 and Figure 5-5). When, in the absence of SLO, the bending rigidity is increased by the addition of cholesterol, the force instead goes up, on average by a factor of 2.4, explaining why even fewer tubes are formed from these vesicles. The model also explains why network formation may stall. When more and longer tubes are being pulled from a vesicle, the membrane tension is expected to rise above the initial tension (Figure 3-12). For vesicles without SLO, this is first of all due to the fixed area-to-volume ratio of the vesicles [74]. In addition, when increasing amounts of membrane material are withdrawn, the (visible and non-visible) thermal undulations of the membrane are reduced, leading to an increase in membrane tension both for vesicles with and without SLO ([91, 93, 94], see also section 3.2). The rise in tension leads to a rise in force, which will increase the departure rate until the survival of a stable cluster that can support the tube is no longer possible. The collapse of a tube will release some of the tension, enabling the growth of a new tube. Thus, a dynamic steady state is reached. Due to the lack of volume constraints, the tension will rise less steeply in SLO vesicles, explaining the longer continuation of network growth.

Dynamics of motor-cluster formation studied by computer simulations

The simple model for dynamic association introduced above predicts a steady state cluster of motor proteins (if the arrival rate is high enough to balance the departure rate). In reality, stochastic fluctuations will play an important role in the behavior of such a system, especially when the fluctuations are large with respect to the steady state number of motors in the cluster. Furthermore, the motor-vesicle system does not initially find itself at the mean cluster size, but the number of motors in the cluster is zero at the start. It will therefore take a certain time to reach the (fluctuating) steady state cluster size, if it can be reached at all. Here we present some first results on the dynamics studied with kinetic Monte Carlo (KMC)

Tubular membrane networks formed by dynamic association of motor proteins

simulations⁴. Such a KMC study can supplement the steady state analysis of the model described above by providing values for the timescales involved.

For this analysis, the inverse arrival rate is set as the dimensionless unit of time. The detachment probability per motor protein per second is exponentially dependent on the force, as in the steady state approach: $k_{off} = Ae^{\alpha F}$, where A and α are constants. The dynamics are, as expected, dependent on the constants and the force. Depending on the exact values for A , F , and α , we find three regimes: (I) a regime where the off-rate is too high for a cluster to be formed, (II) a regime where a stable cluster is formed, and (III) a regime in which the cluster is present for finite time intervals. In Figure 5-7 we present examples from regimes II and III. Figure 5-7a shows a typical curve in which the number of motors in the cluster rises rapidly to the steady state value after which there are fluctuations around this average number. For a higher value of A , the interesting situation arises in which a cluster is temporarily stable, and then vanishes due to stochastic fluctuations in the number of motors (Figure 5-7b). If the number of motors in the cluster decreases due to a fluctuation, the force per motor and therefore the detachment rate will increase. This may ultimately lead to a total disappearance of the cluster. However, the cluster can be restored when a fluctuation pushes the number of motors over a threshold value, and a cluster is again present for a finite time interval. This observation may explain the repeated elongation and retraction that we observed for membrane tubes in our experiments.

The probability distribution of the number of motors in the clusters was determined from many simulations (Figure 5-7c and d). When the width of the distribution is relatively large with respect to the average number of motor proteins, stochastic fluctuations may result in significant variations in the force per motor. *In vitro* [123] as well as *in vivo* [35], variations in the (force dependent) velocity of membranous organelles have been observed. The stochastic nature of a cluster, which consists of a low number of motors, could provide an explanation for this.

In Figure 5-7f, the data from the simulations are plotted together with the curves for the same parameters from the steady state analysis (Figure 5-6). As expected, the peaks of the distribution are centered around the point where the departure rate and the arrival rate are equal. For the highest spontaneous off rate ($A = 0.6 \text{ s}^{-1}$), the distribution is bimodal with peaks around 14 motors and 1 motor.

⁴ I am grateful to Thijs Vlugt for the simulations.

Tubular membrane networks formed by dynamic association of motor proteins

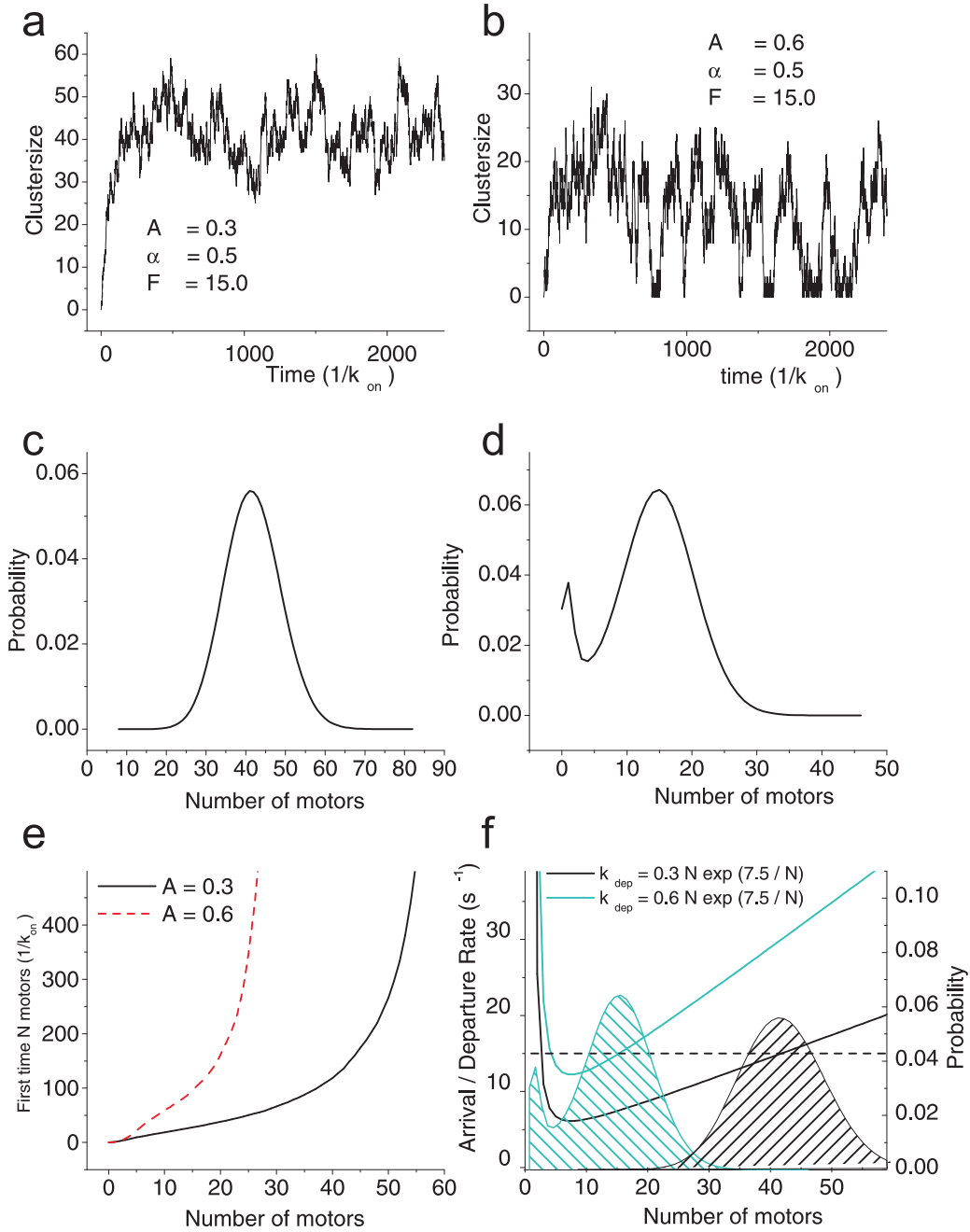


Figure 5-7. Analysis of the kinetic Monte Carlo simulations of cluster formation. (a) and (b) Time traces of the number of motor proteins in a cluster. In (a) a stable cluster is formed ($A = 0.3$, $\alpha = 0.5$, $F = 15$), and in (b) a metastable cluster is formed ($A = 0.6$, $\alpha = 0.5$, and $F = 15$). (c and d) Probability distribution of the number of motor proteins. In (c) the distribution of the number of motors for $A = 0.3$ is shown with on average ~ 42 motors, and in (d) the bimodal distribution for the metastable cluster (cluster size is 14). (e) The average time until a certain number of motors is reached for the first time for these two studies (dark line for the stable cluster, light dashed line for the unstable cluster). (f) The data from the Monte Carlo simulation plotted together with the steady state analysis (compare with Figure 5-6). The solid lines are the departure rates for $A = 0.3$ (black) and 0.6 (gray). The dashed line is the arrival rate, and the two distributions from (c) and (d) are plotted in the same graph.

Tubular membrane networks formed by dynamic association of motor proteins

Finally, the KMC study allows for the determination of the (average) time required to reach a certain cluster size for the first time (Figure 5-7e). This time could give predictions on the expected incubation time for membrane tubes to start being formed in experiments, and the dependence of these dynamics on several parameters may be a valuable test for dynamic association.

5.4 Discussion

We have demonstrated that single membrane tubes and networks of tubes can be formed by the action of motor proteins. No additional factors are required. Several parameters have been varied in order to analyze the mechanism of tube formation. The tube formation force measurements presented in the chapters 3 and 4 led us to conclude that individual motor proteins cannot exert enough force to pull the tubes. As the motor proteins are not physically linked to each other, to explain our results we proposed the mechanism of dynamic association of motor proteins.

The results presented in this chapter seem to be in contrast to the results of Roux et al. [123], who concluded that static linkers (beads), with multiple motors attached to them, are a prerequisite for the formation of tubes. Although we agree that multiple motor proteins are needed for the formation of tubes (and these could in principle be statically bound clusters) we believe that in our assay these clusters arise from the dynamic association of motor proteins. If, as an artifact, kinesin aggregates were present in our sample, tubes should still occasionally be formed at very low kinesin concentrations: however, this was not observed. The absence of tubes after using individual motor proteins in the experiment of Roux et al. may be due to a higher initial tension of their vesicles, opposing the formation of stable clusters. Their alternative way of introducing motors, by pre-binding them to the microtubules before the introduction of vesicles, may also have resulted in a lower motor concentration on the vesicles in those experiments.

An interesting point raised in Roux et al. [123] was that the cross-linking of the motor proteins to beads in their experiments could distribute the force exerted by the motor proteins over several lipids, thereby preventing the lipids from being pulled out of the membrane. Lipids are pulled out of a bilayer in a few seconds when piconewton forces are exerted on

Tubular membrane networks formed by dynamic association of motor proteins

them perpendicularly to the plane of the bilayer [104]. When the motors are directly attached to the lipids through streptavidin (as in our experiments), the force exerted on a lipid may be high and could also be present for a significant time. In this respect, it is important to note that (on average) kinesin motor proteins will detach from the microtubule even faster than the lipids will be extracted, when a force is present. Nevertheless, due to the stochastic behavior of motors and lipids, some lipids will still be pulled out. When, however, a motor (attached to a lipid withdrawn from the bilayer) detaches from the microtubule after a short run, the diffusion of the lipid in the proximity of the membrane in combination with the hydrophobicity of the lipid tail should result in a quick reincorporation of the lipid and motor.

More recent experiments by the same group (of Patricia Bassereau at Institut Curie, Paris) have confirmed the finding that membrane tubes can be formed from giant vesicles when motor proteins are linked directly to them through streptavidin, and beads are not an absolute requirement. In these follow-up studies, lipids were used that were biotinylated as well as fluorescent. This allowed for the visualization of the distribution of motor proteins on the membrane tubes, which confirmed that motor proteins dynamically associate to form tubes. These results compare well with a more refined theoretical study of dynamic association that was developed in that work [62, 136].

6 Competition between plus-end and minus-end directed motors

A large variety of motor proteins is present in the cell, which can move in opposite directions on the cytoskeleton. There is evidence that plus- and minus-end directed motor proteins are both present on cellular membranes. This is important for the spatial distribution of large organelles such as the ER and the Golgi. Also, many smaller organelles show bi-directional movement due to the presence of the oppositely directed motors. It is poorly understood how (and whether) these motors coordinate their efforts, and how they are prevented from ending up in a tug-of-war that results in the hindrance of movement in both directions. In this chapter, an assay is introduced that allows for a study of the membrane morphologies that arise when both plus- and minus-end directed motors are present, and that should allow for a better understanding of the basic interaction mechanisms between oppositely directed motors. In this study, we expand the system presented in chapter 5, where kinesin was attached to giant vesicles, by the additional attachment of biotinylated ncd, which is a non-processive minus-end directed motor. In the first part of this chapter we will present preliminary results that for example show that non-processive motors are also able to pull tubes. It will become clear that for a proper understanding of the competition of the activity of plus- and minus-end directed motors, it is important to control the organization of the microtubules. In the second part of the chapter, we will discuss several procedures that could be used to order the microtubules in vitro.

6.1 Introduction

In vivo, motor proteins move on an organized and polarized cytoskeleton (see chapter 1), which is crucial for the proper spatial distribution of organelles in cells. Some motors exert forces on organelles while moving towards the plus-end, whereas others move in the minus-end direction. The details of the activity of these two opposing groups of motors determine the shape and spatial distribution of membranous compartments. For example, membrane tubes are formed from the endoplasmic reticulum by kinesin and dynein [1], and the positioning of the Golgi apparatus is dependent on the presence of plus- and minus-end directed motor proteins [14, 16, 141]. From the Golgi, plus-end directed motors are responsible for the formation of membrane tubes, which are important transport intermediates. These tubes can presumably only be formed if there is a high enough counterforce, which keeps the Golgi in place. This force may be provided by minus-end directed motor proteins [13, 141] or by factors that statically link the Golgi to cytoskeletal filaments [15].

Interestingly, many (smaller) organelles move bi-directionally, altering their direction frequently. This bi-directional movement suggests that both plus-end directed and minus-end directed motors are present on an organelle. Several data demonstrate that this is indeed the case, and that both types of motor proteins are attached to the organelles at the same time [26, 36, 142]. How and whether the activities of the plus and minus motors are coordinated is not clear. One possibility is that coordination machinery is present that actively switches one kind of motor off when the other is active [36, 142]. An alternative coordination mechanism may be competition between (clusters of) motor proteins pulling in opposite directions on the same vesicle. Fluctuations in the number of active motor proteins could then determine the direction. When one group of motors pulls in one direction, the other motors would tend to detach from the microtubule, and *vice versa*. Thus far, it has proven difficult to discriminate between these two mechanisms [36, 142].

To shed light on how the competition between plus- and minus-end directed motor proteins could contribute to the spatial organization of membranes, we developed an assay in which plus- and minus-end directed motors compete under controlled circumstances. Motors of opposite directionality are, at the same time, attached to a giant vesicle, which is subsequently positioned on a microtubule with the optical tweezers (see Figure 6-1). In the following section we will discuss some preliminary results from this assay, and speculate on the interpretation.

Competition between plus-end and minus-end directed motors

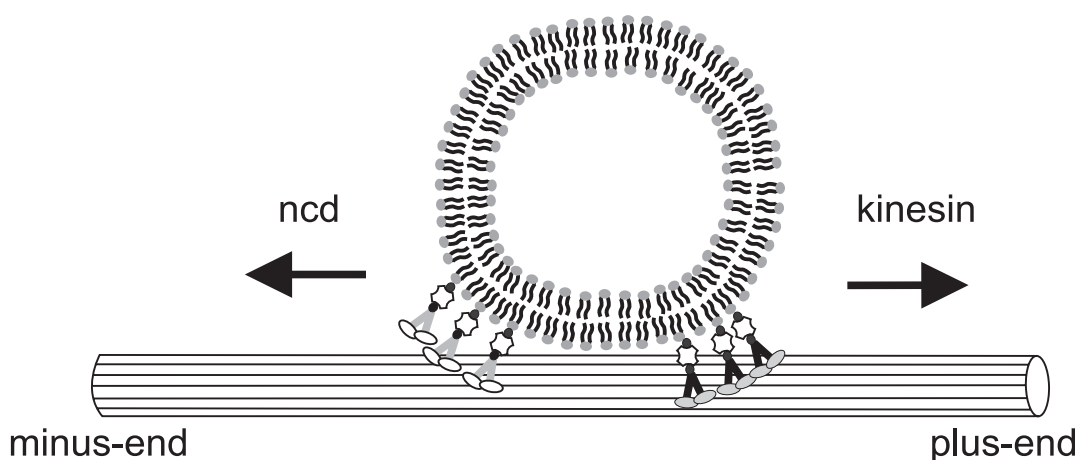


Figure 6-1. Sketch of the model system to study competition between plus and minus end directed motor proteins (not to scale).

6.2 Preliminary experimental results

The assay that we developed in order to study plus- and minus-end directed motor protein competition is similar to the one described in chapter 5. In that chapter, kinesin motor proteins were attached to giant vesicles, which subsequently sedimented on a randomly oriented network of microtubules immobilized on a coverslip. However, some changes with respect to this assay were made for the current study. First, in addition to the kinesin motors, minus-end directed motors were attached to the vesicles as well. Dynein has been suggested as the dominant minus-end directed motor for membrane organization *in vivo*. Dynein is a complex of many different proteins [26], which makes it difficult to handle *in vitro*. Since we are interested in the general interaction between plus- and minus-end directed motors in this study, we used a minus-end motor that is easier to work with in experiments. A “home-made” biotinylated version of the kinesin-like motor ncd (see chapter 2) was used. As the plus-end motor we used the biotinylated kinesin introduced in chapter 5. The second change with respect to the assay presented in chapter 5, was that the dense network of randomly oriented microtubules was replaced by a lower density of microtubules immobilized to the coverslip. A dense MT network makes it complicated to discriminate between the activity of plus- and minus-end directed motors, since forces will be exerted in all directions, even if only one kind

Competition between plus-end and minus-end directed motors

of motor is present. In principle, it is also important to control (or at least know) which the plus- and minus-ends of the microtubule are. In our preliminary studies, presented in the next section, we did not control this polarity. In section 6.3 we will discuss several attempts to organize the microtubules, where we will focus on the close-to-biological organization of a microtubule aster.

Methods

MTs were grown and stabilized with taxol and subsequently introduced in a polylysine coated (PL-dip) flow-cell. After ~15 minutes incubation of the MTs, sequentially (5 minutes intervals) casein (2.5 mg/ml), BSA (5 mg/ml), and again casein (2.5 mg/ml) were flown in to coat the surface and to prevent any interactions with the vesicles. If the vesicles were to adhere to the surface, the competition between plus- and minus-end motors would be influenced, as the motors would (partially) exert their force against the surface attachment point. Although it cannot be excluded that there is some residual interaction of the vesicle with the surface or with the microtubule, our observations of uninterrupted long distance movement of vesicles on MTs suggest that this interaction is minimal.

It is appropriate to mention some experimental challenges before discussing the results. We used polylysine to attach the MTs to the surface. MTs attach to polylysine because it is positively charged whereas MTs are negatively charged. We experimented with three methods of applying the polylysine to the surface (see also section 2.2): (a) the coverslips were dipped in diluted polylysine in ethanol (PL-dip), (b) diluted polylysine was spin-coated on the coverslip (PL-spin), or (c) “pure” polylysine was flown in before the microtubules (PL-flow). Methods (a) and (b) in practice only immobilized part of the MTs, (a) slightly better than (b). This could be seen from the fact that MTs moved and became buckled after the motor-coated vesicles were flown in. The third method, (c), resulted in a strong attachment of the MTs to the surface. However, even after coating the surface with casein/BSA/casein, the negatively charged vesicles adhered to the positively charged surface. We compromised on the use of the PL-dip method (a) to attach the MTs to the coverslip, since some mobility of the microtubules was not critical for the preliminary studies presented here, and vesicle attachment to the surface was minimal after coating with casein and BSA. After the microtubules had adhered to the polylysine-coated coverslip, and the surface was coated with casein/BSA/casein, the vesicles coated with plus- and minus end motors were flown in, in the presence of 1mM ATP.

Competition between plus-end and minus-end directed motors

These motor-coated vesicles were prepared using the same protocol as described in section 2.2 for the tube formation assay with only kinesin. In the current study, kinesin and *ncd* were first mixed, and then incubated with the streptavidin-coated vesicles.

*Activity of *ncd**

Before studying the competition between the two oppositely directed motors, we first checked the activity of *ncd* by attaching only *ncd* to giant vesicles with streptolysin pores. Membrane tubes were observed to be formed when these vesicles came into contact with a random network of microtubules on the surface. As *ncd* is a non-processive motor, this is an interesting result, which shows that non-processive motors can also work together for tube formation, and that they do not need to be connected through a rigid backbone in order to generate this long-distance movement. However, the tube formation potential of *ncd* was less than kinesin (Figure 6-2): a higher concentration of *ncd* than of kinesin was required for the formation of a comparable length of tubes. Approximately ~100 times more (g/l) *ncd* than kinesin was required for a comparable tube formation potential.

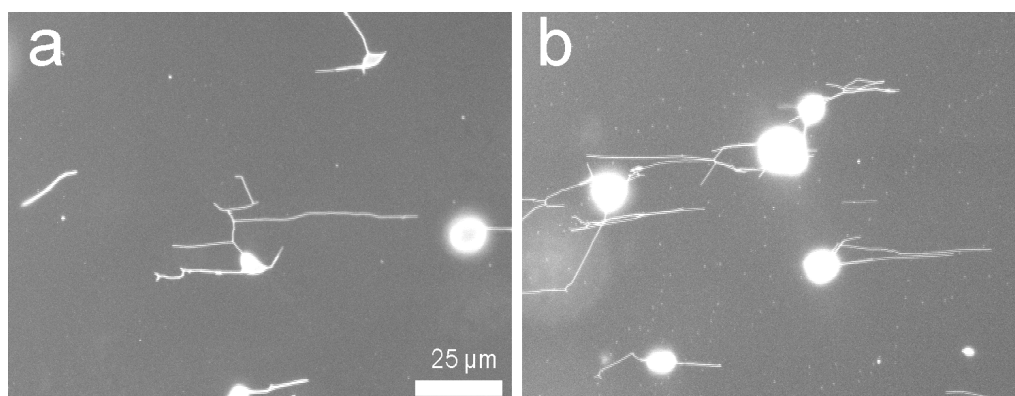


Figure 6-2. Ncd forms tubes from giant vesicles with streptolysin pores. Ncd is less efficient than kinesin. Ncd at 10 $\mu\text{g/ml}$ (a) forms a similar amount of tubes as kinesin does at 0.08 $\mu\text{g/ml}$ (b).

Due to the low velocity of *ncd*, and the photodamage done when observing it with fluorescence microscopy, it was difficult to determine the speed of membrane tube formation by *ncd*. From one measurement we determined the low speed of 0.03 $\mu\text{m/s}$ (compare with the

Competition between plus-end and minus-end directed motors

tube formation velocity by kinesin of $\sim 0.5 \mu\text{m/s}$ in chapter 5). This velocity seems small compared with earlier reports where ncd moved microtubules in a gliding assay at $\sim 0.15 \mu\text{m/s}$ [23] and beads in a bead assay at $\sim 0.2\text{-}0.3 \mu\text{m/s}$ [69, 143]. The low tube formation velocity is not surprising however, since the velocity of motor proteins decreases when a force is exerted on them (e.g. [32]), and the tube force can be of a significant magnitude (chapter 3).

Competition between motor proteins

Having verified that ncd is able to exert forces when adhered to vesicles, we wanted to determine whether kinesin and ncd can be active at the same time on a vesicle. The simplest geometry to study this is that of one immobilized MT. Tube formation or movement in opposite directions on the same MT would then provide evidence for the simultaneous activity of both kinesin and ncd on the same vesicle. Because membrane tubes form more easily at high motor concentrations (Figure 5-3), we used the high motor concentrations of $10 \mu\text{g/ml}$ kinesin and $65 \mu\text{g/ml}$ ncd (concentration in the sample).

Due to the low number of microtubules on the surface, it was improbable that vesicles would spontaneously sediment at a position where a microtubule was situated. Therefore, after a vesicle was found, we used the optical tweezers to move it on top of the microtubule. For these experiments we used somewhat smaller vesicles ($\sim 2 \mu\text{m}$ diameter) than in the experiments presented in chapters 3-5, since these vesicles are more easily manipulated with the tweezers and their behavior is more easily observed with microscopy. Although vesicles often did not interact with the microtubule, sometimes a vesicle started moving along the microtubule (Figure 6-3).

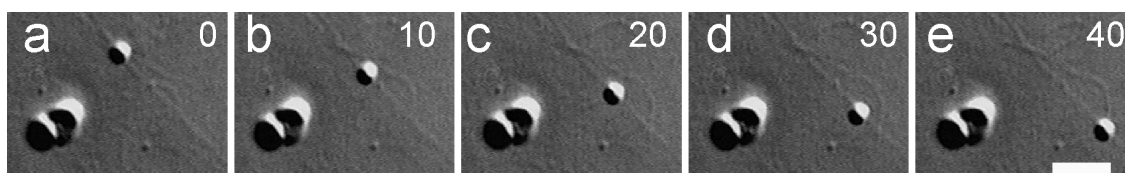


Figure 6-3. A small vesicle with kinesin ($10 \mu\text{g/ml}$) and ncd ($65 \mu\text{g/ml}$) attached, moves along a microtubule. In the background a microtubule can be observed to buckle. Bar is $5 \mu\text{m}$ and time in seconds.

Competition between plus-end and minus-end directed motors

The movement of an object along a microtubule by the activity of one kind of motor protein has been well studied in bead assays (e.g. [19, 63]), which have become a standard method for studying the activity of motor proteins. In our assay, however, plus- and minus-end directed motor proteins are both present on the vesicle, therefore one may expect bi-directional movement [143]. However, this was not observed. A possible sign of plus- and minus-end motor competition could be that this vesicle (Figure 6-3) moves at a velocity of $\sim 0.25 \mu\text{m/s}$. This velocity is lower than the velocity with which membrane tubes were formed ($\sim 0.5 \mu\text{m/s}$) by kinesin, and the speed that was reported for these kinesin motor proteins in a bead assay (between $0.6 \mu\text{m/s}$ [136] and $0.8 \mu\text{m/s}$ [137]). In agreement with those experiments, the velocity of vesicle movement by kinesin alone in our assay is on average faster than $0.5 \mu\text{m/s}$. In this sample (Figure 6-3), *ncd* was present at $65 \mu\text{g/ml}$ and kinesin at $10 \mu\text{g/ml}$. Even though kinesin should be more “active” at this concentration ratio (Figure 6-2), it is possible that a cluster of *ncd* is pulling the vesicle in the minus-end direction. Alternatively, an explanation for the lower speed in this case may be that the force exerted in the direction opposite to the vesicle movement lowers the velocity of kinesin.

Whether bi-directionality should be expected will presumably depend on the concentrations of the plus- and minus-end directed motors. Based on the concept of dynamic association introduced in chapter 5, these concentrations should determine whether a cluster is stable (which would result in unidirectional movement), or metastable (bi-directional movement). It is reasonable to believe that once one motor type has formed a cluster and is dragging the vesicle along, it is no longer possible for the other motor protein to nucleate a new cluster because the force per motor will be high and attached motors will detach swiftly again (possibly slowing down the movement). For bi-directional motion, the experimental study should therefore be conducted at lower concentrations of motor proteins, which will make the stochastic fluctuations significant with respect to the mean number of motors in a cluster, and allow for the switching of direction.

In a second experiment involving a larger vesicle and a lower kinesin concentration, we observed dynamics that more strongly suggested competition between forces exerted in opposing directions by the different motors. After a vesicle (coated with $3 \mu\text{g/ml}$ kinesin and $65 \mu\text{g/ml}$ *ncd*) had been positioned on top of a microtubule, the following was observed (Figure 6-4).

Competition between plus-end and minus-end directed motors

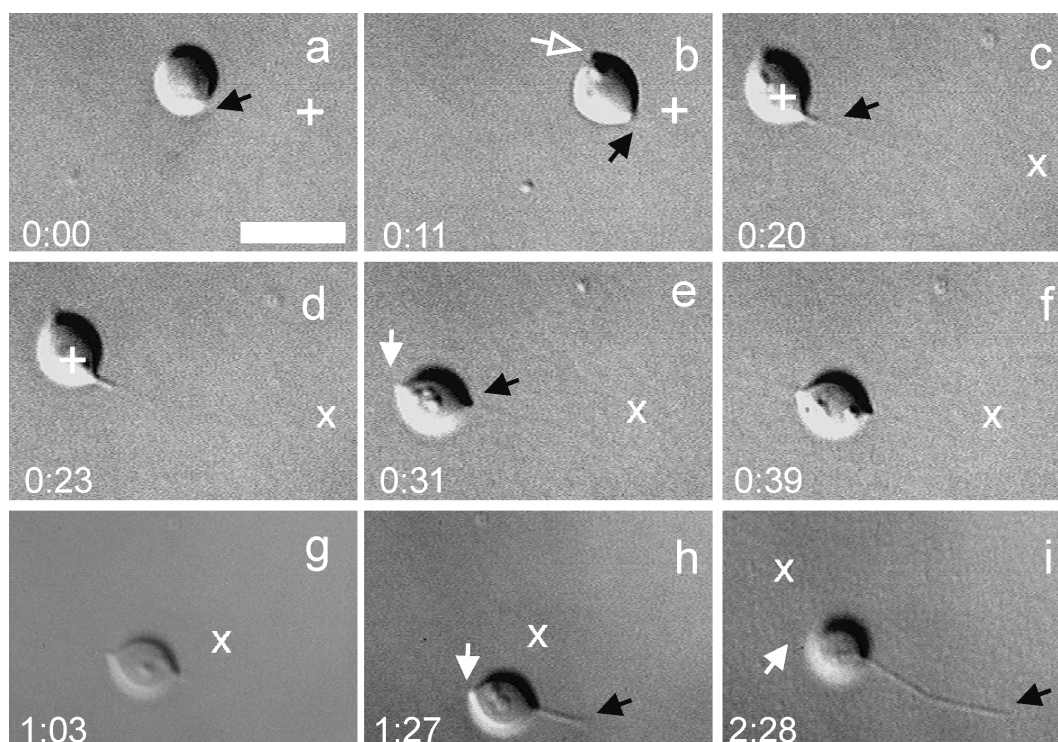


Figure 6-4. Putative plus- (black arrows) and minus-end (white arrows) directed pulling on the same vesicle. Microtubules are difficult to observe due to microscopy settings. The field of view is moved to follow the vesicle. The marks (+ and X) indicate reference points on the coverslip surface. (a) The vesicle moves along a microtubule. (b) The vesicle attaches to another MT (open white arrow) and starts getting deformed. (c) A small tube is formed along the MT. (d) The tube elongates. (e) The vesicle detaches from the second MT and moves along the original MT at $0.4 \mu\text{m/s}$, while on the trailing end a force is exerted which deforms the vesicle. (f) Continued movement. (g and h) A small tube is again formed at the leading edge, presumably because the counterforce on the trailing end has become large enough to allow this. (i) The tube extends (at $\sim 0.4 \mu\text{m/s}$). The bar is $10 \mu\text{m}$.

The vesicle started moving along a microtubule (Figure 6-4a), until hindered by the following events. First, (Figure 6-4b, c and d) a counterforce is exerted due to a second MT, where the attachment of motors to this MT provides the counterforce. The vesicle has detached from the second microtubule in Figure 6-4e, and moves along the MT. In a later stage (Figure 6-4g, h and i), the opposing force is (most-likely) exerted by oppositely directed motors, which start generating sufficient counterforce to slow the vesicle down, and subsequently a tube is formed on the leading edge of the vesicle.

Competition between plus-end and minus-end directed motors

The formation of membrane tubes when the force exerted by both motor clusters is high enough is an additional degree of freedom, which has to be taken into account when studying the competition of oppositely directed motor proteins on vesicles. Tube formation is more difficult from smaller vesicles than from larger ones, due to the presence of a smaller amount of excess area. For a study of the interaction between plus- and minus-end motors for bi-directionality, smaller vesicles may therefore be more suitable. However, to examine the role of oppositely directed motor proteins in the formation of complex membrane morphologies, large vesicles may instead be more appropriate.

The observations described here suggest that opposing motors are pulling in different directions. However, we cannot exclude that the force on the trailing edge of the vesicle is due to an aspecific interaction between the vesicle and the microtubule or coverslip. For more explicit proof of motor-competition, movement of a vesicle or tube formation in both directions needs to be directly observed. To find the parameters for which bi-directional movement of a vesicle is the case, it is important to find the correct (ratio of) concentrations of kinesin and ncd. The use of vesicles with streptolysin pores should facilitate tube formation in both directions on a microtubule, although these vesicles are more difficult to handle (see section 3.3). A proper analysis of the concentrations of different motor proteins can be facilitated by the organization of microtubules on the surface, especially when the polarity of the microtubules is defined. In the next section we will discuss various attempts to organize the microtubules on the surface in a controlled manner.

6.3 Organizing microtubules

For a proper study of the competition between plus- and minus-end motor proteins, it is necessary to control the polarization and organization of the microtubules. This polarity plays a crucial role in the organization of the living cell [8]. In this section several approaches will be discussed that may be used to arrange microtubules *in vitro*. Once this is achieved, motor-coated vesicles may be introduced to the system of controlled MT shapes.

Competition between plus-end and minus-end directed motors

Centrosomes as microtubule nucleators

In animal cells, the microtubules are organized in a radial array with all the plus-ends pointing outwards (see Figure 1-2a). This is due to a structure in the cell that nucleates microtubules: the centrosome. To achieve both organization and polarity control in our studies, we studied how such centrosomes could be used as organizing centers of MTs. Centrosomes can be isolated from cells (human lymphoblastic cell line, gift from the Bornens lab, Institut Curie, Paris) and can subsequently be used *in vitro*, in a mixture with purified tubulin and GTP. This results in approximately 5-30 microtubules growing from the centrosomes in all directions in the three-dimensional space of the flow-cell. Although a 3D microtubule distribution may be interesting for future experiments, it will make a study with microscopy more complicated, and the shapes that may arise will be more complex than those that can arise in a 2D plane. Therefore, we aimed for a 2D aster structure that was attached to the coverslip (see Figure 6-5). We will address several challenges encountered in preparing the MTs in such a 2D aster configuration.

The first method we employed was to grow asters from centrosomes in bulk (in an Eppendorf tube) and stabilize them with taxol. Next, these full-grown asters were transferred to the flow-cell (PL-dip). A problem with this method is that the MTs are presumably torn off from the centrosomes by the shear forces that are present when inserting them into the flow-cell. We tried to make the linkage between MTs and centrosomes stronger by cross-linking them with glutaraldehyde. This, however, did not result in more MTs being left on the centrosomes after flowing them in.

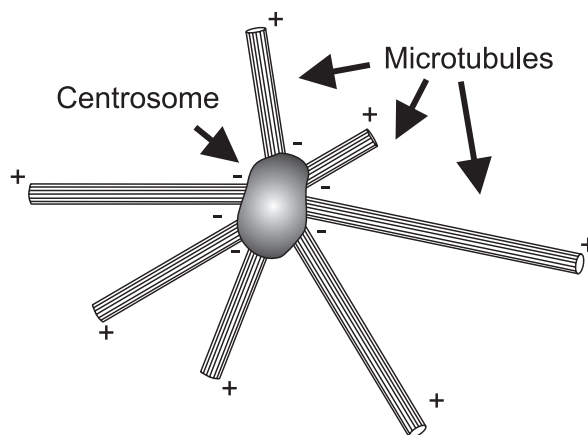


Figure 6-5. Sketch of a microtubule aster grown from a centrosome, with all the plus-ends of the MTs pointing outwards.

Competition between plus-end and minus-end directed motors

A logical solution is to grow the centrosome-asters inside the flow-cell. The centrosomes will naturally attach to the surface of the coverslip, without any surface treatment. To prevent tubulin from attaching to the surface, casein and BSA was flown in before the addition of tubulin. Clear 3D asters have been shown to be formed using this method [144, 145], but MTs radiate out in the full hemi-plane of the flow-cell and are not attached to the surface. In our assay, many of the MTs that point in the z-direction disappeared after a new solution was flown in, due to shear forces that break the microtubules from the centrosomes. For a proper analysis of the competition between the activity of plus- and minus-end directed motors, it is essential to attach the MTs strongly to the surface. Microtubules buckle at forces of typically ~ 5 pN [10] and a couple of motor proteins will therefore already easily buckle MTs. We examined several methods to grow and attach MTs to the coverslip surface.

As discussed before, there are several methods for applying polylysine to the surface. These result in different attachment strengths of the MTs. When we used a PL-dipped coverslip (and then subsequently flowed in centrosomes, casein, and tubulin), the asters that were formed nucleated 5-20 microtubules, but the MTs were only slightly immobilized. After the vesicles and motors were flown in, many of them started gliding and buckling on the surface. When polylysine was applied by PL-flow, the MTs adhered stronger. This attachment, however, did not prevent the typical aster shape from being distorted by the flow (Figure 6-6a), which is not necessarily a problem, since for our purpose it is not critical to have a perfectly shaped aster. However, even coating with excessive casein and/or BSA did not prevent the vesicles from adhering to the surface. This was the reason why we used the PL-dip method to apply polylysine to the coverslip in the study in section 6.2.

In another effort to attach the microtubules to the surface we used avidin instead of polylysine to coat the surface. This resulted in acceptable “aster-like” shapes (Figure 6-6b). However, the filaments that radiated outwards were very thick, and most likely consisted of bundles of microtubules, which stick together through avidin. An essential additional problem with this method is that the vesicles we use are biotinylated and therefore would strongly adhere to the microtubule aster. This method therefore cannot be used.

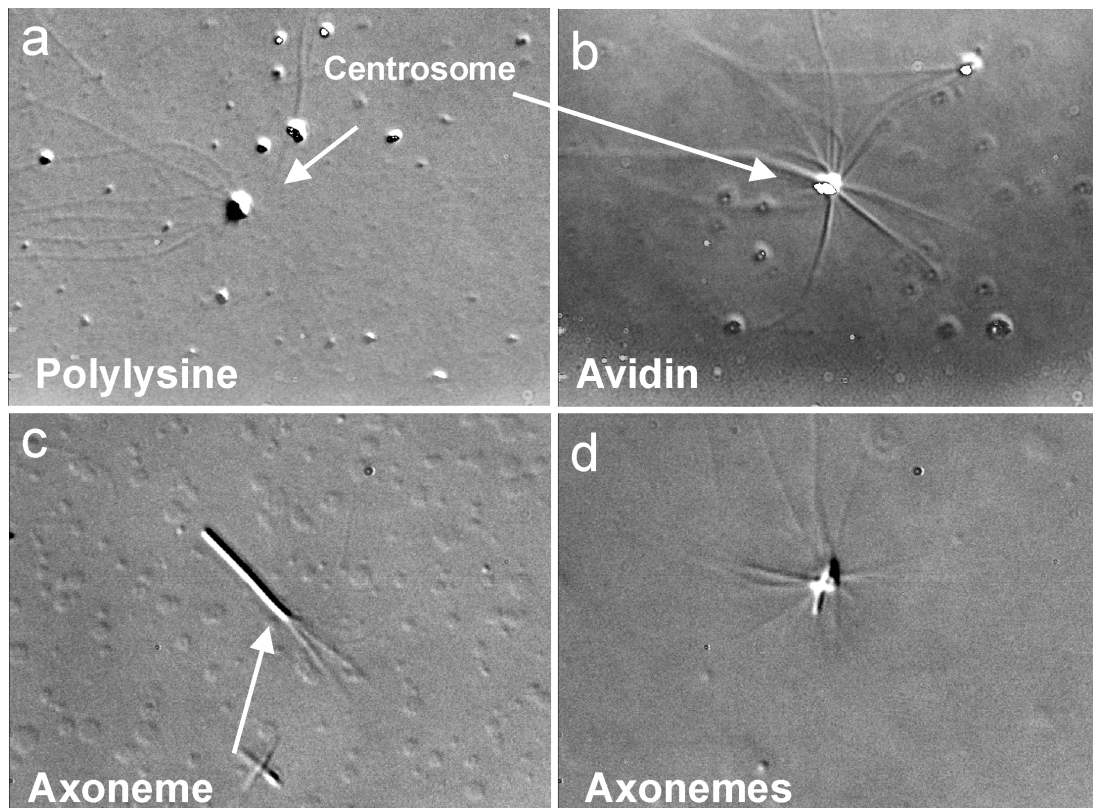


Figure 6-6. Several approaches to organize the distribution of microtubules.

Alternatives for organizing microtubules

We experimented with two other methods to control the MT organization.

- Asters were grown from clusters of short length axonemes. An axoneme consists of a bundled complex of microtubules organized in a cylindrical way. We used the axonemes as a seed for nucleation of many microtubules, and Figure 6-6c shows microtubules growing from an axoneme. When axonemes are freeze-thawed, they break into small parts that cluster together, and promote the growth of microtubules in all directions. These could indeed be used to grow stable “aster like” shapes (Figure 6-6d). The problem with axonemes is, however, that they nucleate MTs from the plus- and the minus-end. Although the nucleation dynamics of the axonemes’ plus- and minus-end are different (e.g. [146]), the polarity of the MTs will not be well controlled.

Competition between plus-end and minus-end directed motors

- Another alternative is gold chemistry and lithography. These techniques can be used to attach microtubule seeds to nanofabricated gold patches, from which subsequently microtubules can be grown (VanDuijn and Dogterom, unpublished results). The advantage of this method is that there are many variations of possible MT organizations, since the gold structures on the surface can in principle be shaped at will. However, combining such structures with motors and vesicles results in the same kind of problems as are encountered as in the case of centrosome usage, mainly concerning the aspecific sticking/non-sticking of microtubules and vesicles.

Clearly, the organization of MTs is an important element for the kind of study proposed in section 6.2. The various attempts to organize MTs on the coverslip discussed here all have their own drawbacks. The solution has to lie in a better control of the interactions between the surface and the several components used in the experiments.

6.4 Discussion

The spatial organization of membranous compartments is determined by their dynamic interaction with motor proteins. Motor proteins that move in opposite directions are important for the morphology of the larger organelles and the spatial distribution of the smaller ones. We introduced an experimental assay, reconstituted from purified components, which should allow for a better understanding of the basic interactions between plus- and minus-end directed motors. An interesting difference between this membrane-based method and other methods, like microtubule gliding assays [147] or bead assays with motors of a different directionality [143], is the liquid nature of the membrane, which may be closer to the biological situation. This will allow the motors to reorganize themselves with respect to each other with more freedom than in the case where they are rigidly linked to the surface of a bead or coverslip.

Our first results suggest that there is a competition between motor proteins of different polarity. An additional degree of freedom in this assay is the formation of tubes. When the force that the opposing motor proteins exert on the vesicle overcomes a certain critical value,

Competition between plus-end and minus-end directed motors

tubes will form. This prevents a situation of a tug-of-war in which case neither group of motors can move. Interestingly, these tubes effectively function as a sorting tool, since only motor proteins with a certain directionality will cluster on a tube. If the tube were to subsequently pinch off from the main vesicle body, plus and minus-end directed motors would be segregated.

An interesting point here is that naively one would expect two tubes to be formed, since motors are pulling in two opposing directions. When a force above a certain threshold is exerted on a vesicle, a tube will be formed (see chapters 3 and 4). It is, however, not energetically favorable to form two tubes, since in this case two neck regions with a high curvature need to be created [80], making it more favorable to extend an already existing tube. Also, we demonstrated in chapter 4 that the force barrier required to form a tube can in fact be many times larger than the force required to extend an existing tube. As the vesicle-motor system is governed by thermal fluctuations of the membrane and the motors, whether one or two tubes are formed will presumably depend on whether the amplitude of the fluctuations is large enough to overcome the force barrier. Alternatively, if the vesicle were to become attached (to for example the coverslip or the MT), two tubes can be formed. A next step in the competition study will be to have motor-coated vesicles interact with organized MT structures, especially asters. In this case, minus-end motors may keep the vesicle positioned near the center of the aster, and multiple tubes will be formed in the radial direction by plus-end directed motors.

With respect to the bi-directional movement of smaller membrane objects, which do not tubulate, it would be interesting for future experiments to lower the number of motor proteins of both kinds on the vesicle. If two competing clusters of motor proteins are exerting a force in opposite directions, the situation arises where two opposing dynamically associated clusters of motor proteins exert forces against each other. If the number of motors is low, this may result in the rise and fall of clusters of motors of different directionality. The exact number of motors for which fluctuations will be important should be determined by properties like the arrival and departure rates (see section 5.3). Such fluctuations in the number of motors could explain the bi-directionality often observed *in vivo*. Conversely, when the number of motor proteins in one cluster is large, the opposing motor proteins will not have the opportunity to form a competing cluster since each small cluster will immediately collapse, as the force per motor is too large to stay attached for a long time. Finally, a situation can be envisaged in which a stable cluster can be formed on both sides, resulting in a futile tug-of-war (which could in fact be purposeful for cell functioning) or tube formation. It would be interesting to

Competition between plus-end and minus-end directed motors

study the dynamics of plus- and minus-end motors with computer simulations, similar to the simulations on dynamic association presented in section 5.3. Such a study should examine the interaction between two competing clusters of oppositely directed motor proteins where the forces are coupled through the membrane. Note also the similarity of the plus- and minus-end motor system studied here with the system studied in [148, 149], where the cooperative effect of individually non-directional motors resulted in effective bi-directional movement over significant length scales.

For a proper understanding of the interactions between the motor proteins, and the parameters that control these, the organization of the microtubules needs to be controlled. In this chapter, we have examined several ideas on how to organize the microtubules. It will be important to immobilize the microtubules, and at the same time prevent the vesicles from adhering. This is a big challenge since the underlying reason that MTs attach to a surface (charge), also makes the vesicles attach. A possible work-around for this issue is to use vesicles of a different charge. Alternatively, a different method may be to construct 3D structures like “walls” where MTs reach from one side to the other side, and the middle part is not in contact with the surface. Vesicles can then be brought into contact with the MT using the tweezers.

The bottom-up approach of reconstituted components presented here has the strength that one can control the ingredients present in the sample. This should allow for a systematic analysis of the relevant parameters for plus- and minus-end directed motor interaction. The ultimate challenge will however be to conduct the same kind of experiments with dynein and kinesin, together with the putative accessory coordination complex that may regulate the bi-directionality [36, 142].

Competition between plus-end and minus-end directed motors

7 Summary and general discussion

Membrane tubes are ubiquitously present in the cell. The endoplasmic reticulum forms an extensive network of membrane tubes throughout the cell [1, 37, 38], which strongly colocalizes with the microtubule cytoskeleton. Thanks to advances in GFP labeling techniques, evidence has recently been gathered that indicates that the formation of tubes also plays an important role for the construction of transport intermediates that are formed from the Golgi apparatus [46, 48, 150]. As the membrane tubes have a small diameter, their formation involves the severe bending of the bilayer, which requires significant forces. Even though there are several mechanisms through which this high curvature can be enforced [40, 41], it is evident that the movement of motor proteins on the microtubule network plays an essential role in the generation of this force (e.g. [13, 16, 38, 39]). The complexity of cells makes it however difficult to decipher the exact role that motor proteins may have in the formation of tubes. Cellular membranes consist of a multitude of different lipids and often proteins are found embedded within them. In addition, many cytosolic proteins associate with the membranes through interaction with the lipids themselves or with membrane proteins. Moreover, multiple motor proteins of opposite directionality are pulling on the membranes [36], and static linkers are also providing cross-links between the membranes and the microtubule network [151].

To shed some light on the basic mechanisms that are essential for tube formation, we studied this process in a highly simplified system that was reconstituted from purified components. The experiments were conducted with giant unilamellar vesicles, which consist of a bilayer of well-controlled lipid composition, and purified motor proteins and microtubules. We have examined different parameters that are involved in tube formation. In this chapter, we will summarize the outcome of these experiments, suggest possible follow-up studies, and finally speculate on possible implications that our findings may have for the mechanisms that govern tube formation *in vivo*.

Summary and general discussion

Forces required to maintain tubes

It has been known for a relatively long time that the physical properties of the membrane determine the force required to maintain membrane tubes [89, 113]. The most important parameters for this force are the bending rigidity and the membrane tension. In chapter 3, we used optical tweezers to determine the forces required for holding tubes that were pulled from giant vesicles of several compositions at a constant distance. The results indicate that the giant vesicles behave as theoretically expected. When tubes were formed from DOPC vesicles, we found an average force of 18 pN. When the bending rigidity was increased by the incorporation of cholesterol in the membrane, the tube force increased to an average of 43 pN. This suggests an increase in bending rigidity of a factor 4.4, in reasonable agreement with previous reports on the effect of the incorporation of cholesterol into membranes [107]. We found that the giant vesicles have on average a high initial tension, when they are formed with the electroformation method. When this initial membrane tension was removed by the addition of the pore forming drug streptolysin O, the force required to form tubes became very small (0.73 pN on average). Due to the low membrane tension, the diameter of the membrane tubes that were formed from streptolysin treated vesicles could be resolved by microscopy. This allowed us to measure the bending rigidity, which decreased by a factor of ~ 6.8 due to the addition of streptolysin.

The low initial tension of the streptolysin treated vesicles may serve as an interesting model system. As a small disturbance will cause a significant deformation, it may serve as a sensitive force probe [152, 153]. In addition, the formation of membrane tubes from giant vesicles can be used as a tool for the fabrication of tubular networks for nano-technology applications [154]. Since the streptolysin treated vesicles initially have a negligible tension, membrane tubes of a relatively large diameter may be formed. For future experiments it would be interesting to study tube formation in a set-up with both optical tweezers and a micropipette [98, 155]. This allows for direct control of the membrane tension, which should yield a better characterization of the system. Such a set-up would have the additional advantage of a better control of the immobilization of the vesicle (which will be partly sucked into the pipette by aspiration).

Summary and general discussion

Force barriers for tube formation

In chapter 4, we demonstrated that force barriers exist for the formation of membrane tubes, and that these barriers can be many times larger than the plateau force described and measured in chapter 3. When a small patch of membrane is grabbed and moved away from a vesicle, the force increases during the initial phase of membrane deformation. At a certain moment the deformation is no longer stable, and a tube is formed. At this moment the force drops down to the plateau force, which occurs through a first order transition if the pulling area is large. The height of this force barrier (or overshoot force) grows linearly with the size of the area the force is exerted on. When the overshoot force is normalized with respect to the plateau force, and the pulling area is normalized with respect to the radius of the tube, the data can be compared with theoretical calculations and Monte Carlo simulations. Together these different approaches demonstrate that the relative overshoot force is determined by the ratio between the size of the pulling area and the radius of the tube.

Membrane tubes get reincorporated into the vesicle when the separation between the pulling patch and the mother membrane is decreased to a critical distance. As membrane tube formation occurs through a first order transition, one may expect hysteresis for the force extension-curve. This is what we find experimentally, as the retraction overshoot force due to the incorporation of a tube is much lower than the tube formation overshoot. However, for a proper understanding of the mechanism of reincorporation, a more thorough analysis is required.

Even though a variety of different overshoot forces has been observed in several force extension curves [115, 117-119], they have been poorly understood. In some studies (e.g. [115]), the presence of a force barrier for the initial formation of tubes was interpreted as being the consequence of the attachment to a cortical cytoskeleton. In other reports, the plateau force was defined as the threshold force for tube formation (e.g. [156]), and the initial force barrier was not mentioned. However, as the pulling area is presumably of a significant size in these studies, a large part of the force barrier should be contributed to the intrinsic physical properties of the tube formation mechanism itself.

In future experiments it would be interesting to study how the shape of the force extension curve changes when membranes are more complex. In this respect one may think of studying tube formation from vesicles with a cortical cytoskeleton. This may be done by studies on living cells or by artificially attaching a cortex to giant vesicles (e.g. [157]). Also, it may be interesting to study how a more complex composition of the membrane (e.g. [6]) will

Summary and general discussion

influence the force extension curve. The pulling of membrane tubes may result in phase separation if different lipids have a different preferred curvature. Another approach would be to study how additional factors that can cause the curvature of the membrane [41] influence the overshoot force.

Tube formation by kinesin motor proteins

In chapter 5, we showed that membrane tubes and tubular networks can be formed by the action of motor proteins, when they are brought into contact with a random network of microtubules adhered to the coverslip. We find that these three components form a minimal system and that no additional factors are required. As the forces involved in tube formation are higher than the force one motor protein can exert (chapters 3 and 4), multiple motors need to work together in the tube formation process. In contrast to what was suggested in earlier work [123], we find that the motors need not be statically linked to each other to form tubes. We showed that a threshold concentration of motor proteins is required for tube formation and that membrane tubes form more easily when the force required to form tubes is low. Since the membrane is a two-dimensional liquid, the motor proteins need to cluster at the tip of a membrane tube to pull on it. We proposed a mechanism in which motor proteins dynamically associate into clusters that can exert enough force to pull the tubes. This mechanism of dynamic association agrees with the experimental results, and very recently the dynamic nature of the motor clusters that pull tubes has been observed experimentally [136].

The model of dynamic association predicts that clusters may become unstable if the tension rises. It would be interesting to monitor the tension in a tubular network while it is being formed. This could for example be done by pulling a “probe tube” from the vesicle, and determining the force required to maintain it. One would expect that the force at which network growth stalls depends on the concentration of motors. In the same line of thinking, it would be interesting to control the tension by external means (for example with a micropipette). It may be expected that membrane tubes collapse as the tension is increased to above a threshold value (provided that there are no additional interactions of the tube with the microtubule or the surface).

Our experiments showed the intrinsic property of the motor proteins to self-organize and dynamically associate into clusters that can form tubes. In this thesis we studied this mechanism with microtubules and kinesin, similar mechanisms may however also be relevant

Summary and general discussion

for the movement of myosin on actin. In future experiments, the challenge would be to examine whether the dynamic association of motor proteins is also responsible for tube formation in cells or cell extracts, possibly by adding a fluorescent tag to the motor proteins in the cell.

Competition between oppositely directed motors

In chapter 6, we showed preliminary results on the competition between plus-end (kinesin) and minus-end (ncd) directed motor proteins. In many cells transport objects show a bi-directional movement, where they switch the movement direction frequently. In addition, plus- and minus-end directed motors have been shown to be present simultaneously on the same transport object [142]. The basic interaction mechanisms of oppositely directed motors may be studied more easily in a reconstituted system, where the concentrations of the motors and the properties of the vesicle can be controlled.

An interesting finding from the preliminary results is that non-processive motors (ncd) can form tubes, presumably due to a cooperative effect. Furthermore, the work suggests that if the forces that the competing plus-end and minus-end directed motors exert on each other overcome a certain threshold, tube formation occurs. This may be an interesting mechanism to circumvent the static tug-of-war that may arise otherwise. At the same time, this tubulation would spatially segregate the different motors.

Much work is still needed to properly study the plus-minus end competition in this assay. Most importantly, the activity of both types of motors on the same vesicle needs to be verified. The most direct approach for this may be to vary the concentrations of kinesin and ncd on the vesicle. At lower concentrations, bi-directional movement of vesicles may be more easily observed. There are several steps that may ease the study of bi-directional movement in our assay. First of all, controlling the polarity and the reproducibility of the attachment of microtubules will greatly help such a study. Also, faster and/or more processive minus end directed motor (e.g. dynein) protein might facilitate this.

Summary and general discussion

Potential relevance for in vivo membrane organization

One has to be careful when extrapolating the results from the simplified systems studied in this thesis to the functioning of motor proteins and membranes in living cells. The composition of cellular membranes is complex, and the interaction of many known and unknown factors should be taken into account. Nevertheless, the results presented in this thesis suggest possible mechanisms through which the cell may control its intracellular membrane organization. In the following we will speculate on this.

We showed that the forces involved in tube formation are determined by macroscopic properties of the membrane like the bending rigidity and the membrane tension. Whether membrane tubes are formed from cellular membranes may therefore depend on these properties as well. A high bending stiffness may, for example, be caused by the composition of the membrane, like the presence of a high concentration of cholesterol. The cell might influence the extent of tube formation by controlling the kind of lipids and the amount of cholesterol in the membrane. The opening of pores, which removes tension, may be an efficient means to lower the tube formation force.

The strong dependence of the force barrier for the formation of tubes on the patch size may be relevant for controlled intracellular membrane tube formation. In cells, lipid sub-domains of a significant size [5] as well as clusters of proteins [41] are found on membranes. When a tube must be formed by exerting a force on one of these "patches" [158], the force required for the initial step in the formation of the tube may be too high for the force generator (e.g. kinesin, polymerizing cytoskeletal elements) to overcome. The acquisition of proteins or lipids that can cause the initial curvature [40, 41, 159], which forms the highest barrier for tube formation, may lower the overshoot value. Once the tube is formed, the force is lower and regular force generators could take over.

Our experiments on membrane tube formation by motor proteins show the intrinsic ability of motor proteins to dynamically associate and form clusters without the requirement for cofactors. However, in cells there are different mechanisms through which motor proteins may associate and join forces. An alternative mechanism could be the binding of multiple motor proteins to membrane proteins that act as scaffolds to form static multi-motor complexes [44, 123]. The presence of rafts [5] could bias the mechanism of dynamic association. Certain kinesin motor proteins have been reported to directly bind to lipids [158], and sub-domains of these lipids may function as a (dynamic) pre-clustering tool. Such rafts

Summary and general discussion

could thus combine properties of both clusters formed by dynamic association and static clusters.

An appealing possibility may be that the cell could use the factors that induce the membrane curvature as a tool to control where tubes are formed. It would be efficient if the same molecules that link the motor proteins to the membrane could also induce membrane curvature (see Figure 7-1). Interestingly, motor proteins have been demonstrated to link directly to factors that are important for the formation of a curvature inducing protein coat of a significant size [160, 161].

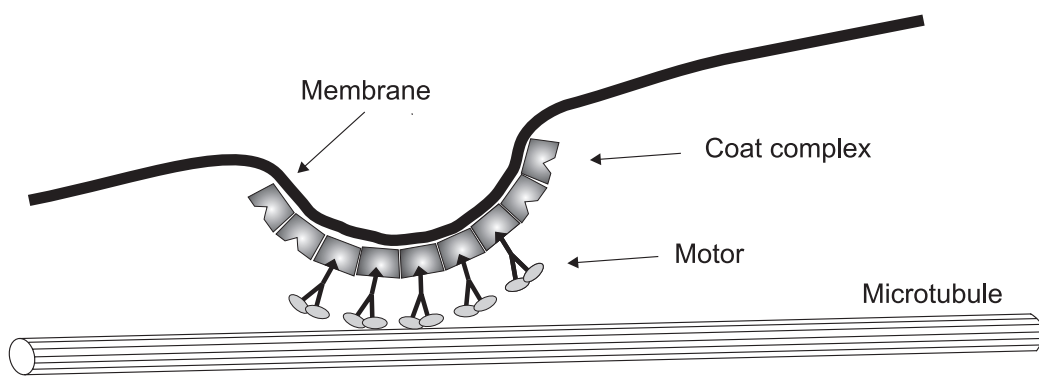


Figure 7-1. Sketch of motor proteins that attach to a (curvature inducing) coat of proteins on a membrane.

It is exciting to speculate on potential regulatory mechanisms that the cell might exploit for its membrane organization. The speculations are based on findings from our *in vitro* approach, which is a powerful method to unravel some of the basic mechanisms that govern the realm of membranes and motors. However, its strength is at the same time its weakness, as things may function differently in the more complex environment of the cell. Our speculations clearly await experimental verification *in vivo*.

Summary and general discussion

Bibliography

- [1] J. Lane and V. Allan (1999), *Microtubule-based endoplasmic reticulum motility in Xenopus laevis: activation of membrane-associated kinesin during development*, *Molecular Biology of the Cell* **10**, 1909-1922.
- [2] <http://www.people.virginia.edu/~rjh9u/cellmemb.html> (Human Biology, D. Chiras).
- [3] H. Lodish, A. Berk, S. Zipursky, P. Matsudaira, D. Baltimore and J. E. Darnell (2000), *Molecular Cell Biology*, W.H. Freeman and company, New York.
- [4] X. Buton, G. Morrot, P. Fellmann and M. Seigneuret (1996), *Ultrafast glycerophospholipid-selective transbilayer motion mediated by a protein in the endoplasmic reticulum membrane*, *Journal of Biological Chemistry* **271**, 6651-6657.
- [5] K. Simons and E. Ikonen (1997), *Functional rafts in cell membranes*, *Nature* **387**, 569-572.
- [6] T. Baumgart, S. T. Hess and W. W. Webb (2003), *Imaging coexisting fluid domains in biomembrane models coupling curvature and line tension*, *Nature* **425**, 821-824.
- [7] T. Fujiwara, K. Ritchie, H. Murakoshi, K. Jacobson and A. Kusumi (2002), *Phospholipids undergo hop diffusion in compartmentalized cell membrane*, *Journal of Cell Biology* **157**, 1071-1082.
- [8] B. Alberts, A. Johnson, J. Lewis, M. Raff, K. Roberts and P. Walter (2002), *Molecular Biology of the Cell*, Garland Publishing, New York.
- [9] M. Dogterom, M. E. Janson, C. Faivre-Moskalenko, A. Van der Horst, J. W. J. Kerssemakers, C. Tanase and B. M. Mulder (2002), *Force generation by polymerizing microtubules*, *Applied Physics A - Materials Science and Processing* **75**, 331-336.
- [10] M. E. Janson (2002), *Force generation by growing microtubules*, PhD thesis, AMOLF / Leiden University, Amsterdam.
- [11] A. Desai and T. J. Mitchison (1997), *Microtubule polymerization dynamics*, *Annual Review of Cell and Developmental Biology* **13**, 83-117.
- [12] C. Faivre-Moskalenko and M. Dogterom (2002), *Dynamics of microtubule asters in microfabricated chambers: the role of catastrophes*, *Proceedings of the National Academy of Sciences USA* **99**, 16788-16793.
- [13] V. J. Allan, H. M. Thompson and M. A. McNiven (2002), *Motoring around the Golgi*, *Nature Cell Biology* **4**, 236-242.
- [14] Y. Xu, S. Takeda, T. Nakata, Y. Noda, Y. Tanaka and N. Hirokawa (2002), *Role of KIFC3 motor protein in Golgi positioning and integration*, *Journal of Cell Biology* **158**, 293-303.
- [15] R. M. Rios, A. Sanchis, A. M. Tassin, C. Fedriani and M. Bornens (2004), *GMAP-210 recruits [gamma]-tubulin complexes to cis-Golgi membranes and is required for Golgi ribbon formation*, *Cell* **118**, 323-335.
- [16] F. Feiguin, A. Ferreira, K. S. Kosik and A. Caceres (1994), *Kinesin-mediated organelle translocation revealed by specific cellular manipulations*, *Journal of Cell Biology* **127**, 1021-1039.
- [17] J. F. Hunt, S. Weinkauff, L. Henry, J. J. Fak, P. McNicholas, D. B. Oliver and J. Deisenhofer (2002), *Nucleotide control of interdomain interactions in the conformational reaction cycle of secA*, *Science* **297**, 2018-2026.
- [18] G. J. K. Praefcke and H. T. McMahon (2004), *The dynamin superfamily: universal membrane tubulation and fission molecules?*, *Nature Reviews Molecular Cell Biology* **5**, 133-147.
- [19] J. Howard (2001), *Mechanics of Motor Proteins and the Cytoskeleton*, Sinauer Associates, Sunderland, USA.
- [20] C. Hawes and B. Satiat-Jeuemaitre (2001), *Trekking along the cytoskeleton*, *Plant Physiology* **125**, 119-122.
- [21] E. P. Sablin, R. B. Case, S. C. Dai, C. L. Hart, A. Ruby, R. D. Vale and R. J. Fletterick (1998), *Direction determination in the minus-end-directed kinesin motor ncd*, *Nature* **395**, 813-816.

Bibliography

- [22] H. B. McDonald and L. S. B. Goldstein (1990), *Identification and characterization of a gene encoding a kinesin-like protein in drosophila*, *Cell* **61**, 991-1000.
- [23] R. Chandra, E. D. Salmon, H. P. Erickson, A. Lockhart and S. A. Endow (1993), *Structural and functional domains of the Drosophila ncd microtubule motor protein*, *Journal of Biological Chemistry* **268**, 9005-9013.
- [24] M. J. deCastro (2001), *Investigation of the motile properties of the kinesin-related motor protein ncd*, PhD thesis, University of Utah, Utah.
- [25] N. Hirokawa (1998), *Kinesin and dynein superfamily proteins and the mechanism of organelle transport*, *Science* **279**, 519-526.
- [26] R. D. Vale (2003), *The molecular motor toolbox for intracellular transport*, *Cell* **112**, 467-480.
- [27] W. Hua, J. Chung and J. Gelles (2002), *Distinguishing inchworm and hand-over-hand processive kinesin movement by neck rotation measurements*, *Science* **295**, 844-848.
- [28] C. L. Asbury, A. N. Fehr and S. M. Block (2003), *Kinesin moves by an asymmetric hand-over-hand mechanism*, *Science* **302**, 2130-2134.
- [29] R. D. Vale (2003), *Myosin V motor proteins: marching stepwise towards a mechanism*, *Journal of Cell Biology* **163**, 445-450.
- [30] K. Svoboda, C. F. Schmidt, B. J. Schnapp and S. M. Block (1993), *Direct observation of kinesin stepping by optical trapping interferometry*, *Nature* **365**, 721-727.
- [31] E. Meyhofer and J. Howard (1995), *The force generated by a single kinesin molecule against an elastic load*, *Proceedings of the National Academy of Sciences USA* **92**, 574-578.
- [32] K. Visscher, M. J. Schnitzer and S. M. Block (1999), *Single kinesin molecules studied with a molecular force clamp*, *Nature* **400**, 184-189.
- [33] R. Mallik, B. C. Carter, S. A. Lex, S. J. King and S. P. Gross (2004), *Cytoplasmic dynein functions as a gear in response to load*, *Nature* **427**, 649 - 652.
- [34] M. J. deCastro, R. M. Fondecave, L. A. Clarke, C. F. Schmidt and R. J. Stewart (2000), *Working strokes by single molecules of the kinesin-related microtubule motor ncd*, *Nature Cell Biology* **2**, 724-729.
- [35] D. B. Hill, M. J. Plaza, K. Bonin and G. Holzwarth (2004), *Fast vesicle transport in PC12 neurites: velocities and forces*, *European Biophysics Journal* **33**, 623-632.
- [36] M. A. Welte (2004), *Bidirectional Transport along Microtubules*, *Current Biology* **14**, R525-R537.
- [37] C. Lee and L. B. Chen (1988), *Dynamic behavior of endoplasmic reticulum in living cells*, *Cell* **54**, 37-46.
- [38] C. M. Waterman-Storer and E. D. Salmon (1998), *Endoplasmic reticulum membrane tubules are distributed by microtubules in living cells using three distinct mechanisms*, *Current Biology* **8**, 798-806.
- [39] C. H. Lee, M. Ferguson and L. B. Chen (1989), *Construction of the Endoplasmic Reticulum*, *Journal of Cell Biology* **109**, 2045-2055.
- [40] K. N. J. Burger (2000), *Greasing membrane fusion and fission machineries*, *Traffic* **1**, 605-613.
- [41] K. Farsad and P. De Camilli (2003), *Mechanisms of membrane deformation*, *Current Opinion in Cell Biology* **15**, 372-381.
- [42] S. L. Dabora and M. P. Sheetz (1988), *The microtubule-dependent formation of a tubulovesicular network with characteristics of the ER from cultured cell extracts*, *Cell* **54**, 27-35.
- [43] R. D. Vale and H. Hotani (1988), *Formation of membrane networks in vitro by kinesin-driven microtubule movement*, *Journal of Cell Biology* **107**, 2233-2241.
- [44] V. Allan and R. D. Vale (1994), *Movement of membrane tubules along microtubules in vitro: evidence for specialised sites of motor attachment*, *Journal of Cell Science* **107**, 1885-1897.
- [45] A. Upadhyaya and M. P. Sheetz (2004), *Tension in tubulovesicular networks of Golgi and endoplasmic reticulum membranes*, *Biophysical Journal* **86**, 2923-2928.
- [46] N. Sciaky, J. Presley, C. Smith, K. J. M. Zaal, N. Cole, J. E. Moreira, M. Terasaki, E. Siggia and J. Lippincott-Schwartz (1997), *Golgi tubule traffic and the effects of brefeldin A visualized in living cells*, *Journal of Cell Biology* **139**, 1137-1155.
- [47] J. Lippincott-Schwartz, E. Snapp and A. Kenworthy (2001), *Studying protein dynamics in living cells*, *Nature Reviews Molecular Cell Biology* **2**, 444-456.

Bibliography

- [48] E. V. Polishchuk, A. Di Pentima, A. Luini and R. S. Polishchuk (2003), *Mechanism of constitutive export from the Golgi: bulk flow via the formation, protrusion, and en bloc cleavage of large trans-Golgi network tubular domains*, *Molecular Biology of the Cell* **14**, 4470-4485.
- [49] T. Kirchhausen (2000), *Three ways to make a vesicle*, *Nature Reviews Molecular Cell Biology* **1**, 187-198.
- [50] J. S. Bonifacino and B. S. Glick (2004), *The mechanisms of vesicle budding and fusion*, *Cell* **116**, 153-166.
- [51] M. I. Angelova, S. Soleau, P. Meleard, J. F. Faucon and P. Bothorel (1992), *Preparation of giant vesicles by external AC electric fields. Kinetics and applications*, *Progress in Colloid and Polymer Science* **89**, 127-131.
- [52] J.-B. Manneville (1999), *Fluctuations de membranes actives*, PhD thesis, Université Paris 7, Paris.
- [53] L. Mathivet, S. Cribier and P. F. Devaux (1996), *Shape change and physical properties of giant phospholipid vesicles prepared in the presence of an AC electric field*, *Biophysical Journal* **70**, 1112-1121.
- [54] L. A. Bagatolli, T. Parasassi and E. Gratton (2000), *Giant phospholipid vesicles: comparison among the whole lipid sample characteristics using different preparation methods: a two photon fluorescence microscopy study*, *Chemistry and Physics of Lipids* **105**, 135-147.
- [55] E. Helfer (1999), *Micromécanique de membrane solides artificielles*, PhD thesis, Université Louis Pasteur, Strasbourg.
- [56] P. Girard, J. Pecreaux, G. Lenoir, P. Falson, J.-L. Rigaud and P. Bassereau (2004), *A new method for the reconstitution of membrane proteins into giant unilamellar vesicles*, *Biophysical Journal* **87**, 419-429.
- [57] D. K. Fygenson (1995), *Microtubules: the rhythm of assembly and the evolution of form*, PhD thesis, Princeton University, Princeton.
- [58] T. E. Holy (1997), *Physical aspects of the assembly and function of microtubules*, Princeton University, Princeton.
- [59] C. J. Lawrence, R. K. Dawe, K. R. Christie, D. W. Cleveland, S. C. Dawson, S. A. Endow, L. S. B. Goldstein, H. V. Goodson, N. Hirokawa, J. Howard, R. L. Malmberg, J. R. McIntosh, H. Miki, T. J. Mitchison, Y. Okada, A. S. N. Reddy, W. M. Saxton, M. Schliwa, J. M. Scholey, R. D. Vale, C. E. Walczak and L. Wordeman (2004), *A standardized kinesin nomenclature*, *Journal of Cell Biology* **167**, 19-22.
- [60] E. Berliner, E. C. Young, K. Anderson, H. K. Mahtani and J. Gelles (1995), *Failure of a single-headed kinesin to track parallel to microtubule protofilaments*, *Nature* **373**, 718-721.
- [61] T. Surrey, M. B. Elowitz, P. E. Wolf, F. Yang, F. Nedelec, K. Shokat and S. Leibler (1998), *Chromophore-assisted light inactivation and self-organization of microtubules and motors*, *Proceedings of the National Academy of Sciences USA* **95**, 4293-4298.
- [62] A. Roux (2004), *Tubes de membrane dans le trafic intracellulaire: aspects physiques et biologiques*, PhD thesis, Université Paris 7, Paris.
- [63] J. Howard, A. J. Hunt and S. Baek (1993) in *Motility Assays for Motor Proteins*, ed. J. M. Scholey (Academic Press, San Diego), Vol. 39, 137-147.
- [64] A. Ashkin (1970), *Acceleration and trapping of particles by radiation pressure*, *Physical Review Letters* **24**, 156-159.
- [65] K. Svoboda and S. M. Block (1994), *Biological applications of optical forces*, *Annual Review of Biophysics and Biomolecular Structure* **23**, 247-285.
- [66] K. Visscher, S. P. Gross and S. M. Block (1996), *Construction of multiple-beam optical traps with nanometer-resolution position sensing*, *IEEE Journal of Selected Topics in Quantum Electronics* **2**, 1066-1076.
- [67] F. Gittes and C. F. Schmidt (1998) in *Methods in Cell Biology*, ed. M. P. Sheetz (Academic Press, San Diego), Vol. 55, 129-156.
- [68] W. Roos (2000), *Optical trapping of core-shell particles and dividing Escherichia coli*, MSc thesis, AMOLF/University of Amsterdam, Amsterdam.

Bibliography

- [69] M. W. Allersma, F. Gittes, M. J. deCastro, R. J. Stewart and C. F. Schmidt (1998), *Two-dimensional tracking of ncd motility by back focal plane interferometry*, Biophysical Journal **74**, 1074-1085.
- [70] J. Gelles, B. J. Schnapp and M. P. Sheetz (1988), *Tracking kinesin-driven movements with nanometre-scale precision*, Nature **331**, 450-453.
- [71] J. M. Seddon and R. H. Templer (1995) in *Structure and Dynamics of Membranes*, eds. R. Lipowsky and E. Sackmann (Elsevier Science, Amsterdam), Vol. 1A, 97-160.
- [72] J. Kas and E. Sackmann (1991), *Shape transitions and shape stability of giant phospholipid vesicles in pure water induced by area-to-volume changes*, Biophysical Journal **60**, 825-844.
- [73] R. Lipowsky (1991), *The conformation of membranes*, Nature **349**, 475-481.
- [74] U. Seifert and R. Lipowsky (1995) in *Structure and Dynamics of Membranes*, eds. R. Lipowsky and E. Sackmann (Elsevier Science, Amsterdam), Vol. 1A, 405-463.
- [75] H. G. Dobereiner (1995), *The budding transition of phospholipid vesicles: a quantitative study via phase contrast microscopy*, Simon Fraser University, Vancouver.
- [76] H. G. Dobereiner, E. Evans, M. Kraus, U. Seifert and M. Wortis (1997), *Mapping vesicle shapes into the phase diagram: a comparison of experiment and theory*, Physical Review E **55**, 4458-4474.
- [77] W. Helfrich (1973), *Elastic properties of lipid bilayers: theory and possible experiments*, Zeitschrift fur Naturforschung **28**, 693-703.
- [78] P. B. Canham (1970), *The minimum energy of bending as a possible explanation of the biconcave shape of the human red blood cell*, Journal of Theoretical Biology **26**, 61-81.
- [79] L. Miao, U. Seifert, M. Wortis and H. G. Dobereiner (1994), *Budding transition of fluid-bilayer vesicles: the effect of area-difference elasticity*, Physical Review E **49**, 5389-5407.
- [80] V. Heinrich, B. Bozic, S. Svetina and B. Zeks (1999), *Vesicle deformation by an axial load: from elongated shapes to tethered vesicles*, Biophysical Journal **76**, 2056-2071.
- [81] B. De Kruijff and K. W. A. Wirtz (1977), *Induction of relatively fast transbilayer movement of phosphatidylcholine in vesicles*, Biochimica et Biophysica Acta **468**, 318-326.
- [82] T. M. Bayerl, C. F. Schmidt and E. Sackmann (1988), *Kinetics of symmetric and asymmetric lipid transfer between small sonicated vesicles studied by high-sensitivity differential scanning calorimetry, NMR, electron microscopy, and dynamic light scattering*, Biochemistry **27**, 6078-6085.
- [83] R. Raphael and R. Waugh (1996), *Accelerated interleaflet transport of phosphatidylcholine molecules in membranes under deformation*, Biophysical Journal **71**, 1374-1388.
- [84] U. Seifert (1997), *Configurations of fluid membranes and vesicles*, Advances in Physics **46**, 13-137.
- [85] D. J. Bukman, J. H. Yao and M. Wortis (1996), *Stability of cylindrical vesicles under axial load*, Physical Review E **54**, 5463-5468.
- [86] R. Waugh, J. Song, S. Svetina and B. Zeks (1992), *Local and nonlocal curvature elasticity in bilayer membranes by tether formation from lecithin vesicles*, Biophysical Journal **61**, 974-982.
- [87] I. Derenyi, F. Julicher and J. Prost (2002), *Formation and interaction of membrane tubes*, Physical Review Letters **88**, 238101-1 - 238101-4.
- [88] B. Bozic, V. Heinrich, S. Svetina and B. Zeks (2001), *Shapes of cylindrical, axisymmetric bilayer membranes*, European Physical Journal E **6**, 91-98.
- [89] R. E. Waugh and R. M. Hochmuth (1987), *Mechanical equilibrium of thick, hollow, liquid membrane cylinders*, Biophysical Journal **52**, 391-400.
- [90] L. Bo and R. E. Waugh (1989), *Determination of bilayer membrane bending stiffness by tether formation from giant, thin-walled vesicles*, Biophysical Journal **55**, 509-517.
- [91] W. Helfrich and R. M. Servuss (1984), *Undulations, steric interaction and cohesion of fluid membranes*, Nuovo Cimento **3D**, 137-151.
- [92] J.-B. Manneville, P. Bassereau, S. Ramaswamy and J. Prost (2001), *Active membrane fluctuations studied by micropipet aspiration*, Physical Review E **64**, 021908-1 - 021908-1.
- [93] J. B. Fournier, A. Ajdari and L. Peliti (2001), *Effective-area elasticity and tension of micromanipulated membranes*, Physical Review Letters **86**, 4970-4973.

Bibliography

- [94] E. Evans and W. Rawicz (1990), *Entropy-driven tension and bending elasticity in condensed-fluid membranes*, Physical Review Letters **64**, 2094-2097.
- [95] W. Rawicz, K. C. Olbrich, T. McIntosh, D. Needham and E. Evans (2000), *Effect of chain length and unsaturation on elasticity of lipid bilayers*, Biophysical Journal **79**, 328-339.
- [96] J.-B. Manneville, P. Bassereau, D. Levy and J. Prost (1999), *Activity of transmembrane proteins induces magnification of shape fluctuations of lipid membranes*, Physical Review Letters **82**, 4356-4359.
- [97] W. Helfrich (1995) in *Structure and Dynamics of Membranes*, eds. R. Lipowsky and E. Sackmann (Elsevier Science, Amsterdam), Vol. 1A, 691-721.
- [98] V. Heinrich and R. E. Waugh (1996), *A piconewton force transducer and its application to measurement of the bending stiffness of phospholipid membranes*, Annals of Biomedical Engineering **24**, 595-605.
- [99] W. Hackl, U. Seifert and E. Sackmann (1997), *Effects of fully and partially solubilized amphiphiles on bilayer bending stiffness and temperature dependence of the effective tension of giant vesicles*, Journal de Physique II **7**, 1141-1157.
- [100] V. Kralj-Iglic, G. Gomisecek, J. Majhenc, V. Arrigler and S. Svetina (2001), *Myelin-like protrusions of giant phospholipid vesicles prepared by electroformation*, Colloids and Surfaces A **181**, 315-318.
- [101] A. K. C. Yeung (1994), *Mechanics of inter-monolayer coupling in fluid surfactant bilayers*, PhD thesis, University of British Columbia, Vancouver.
- [102] E. Evans and A. Yeung (1994), *Hidden dynamics in rapid changes of bilayer shape*, Chemistry and Physics of Lipids **73**, 39-56.
- [103] R. Merkel, P. Nassoy, A. Leung, K. Ritchie and E. Evans (1999), *Energy landscapes of receptor-ligand bonds explored with dynamic force spectroscopy*, Nature **397**, 50-3.
- [104] E. Evans and F. Ludwig (2000), *Dynamic strengths of molecular anchoring and material cohesion in fluid biomembranes*, Journal of Physics: Condensed Matter **12**, A315-A320.
- [105] J. Song and R. E. Waugh (1993), *Bending energy of SOPC membranes containing cholesterol*, Biophysical Journal **64**, 1967-1970.
- [106] J. Henriksen, A. C. Rowat and J. H. Ipsen (2004), *Vesicle fluctuation analysis of the effects of sterols on membrane bending rigidity*, European Biophysics Journal **33**, 732-741.
- [107] P. Meleard, C. Gerbeaud, T. Pott, L. Fernandez-Puente, I. Bivas, M. D. Mitov, J. Dufourcq and P. Bothorel (1997), *Bending elasticities of model membranes: influences of temperature and sterol content*, Biophysical Journal **72**, 2616-2629.
- [108] J. Rossjohn, S. C. Feil, W. J. McKinstry, R. K. Tweten and M. W. Parker (1997), *Structure of a cholesterol-binding, thiol-activated cytolysin and a model of its membrane form*, Cell **89**, 685-692.
- [109] M. Palmer, R. Harris, C. Freytag, M. Kehoe, J. Tranum-Jensen and S. Bhakdi (1998), *Assembly mechanism of the oligomeric streptolysin O pore: the early membrane lesion is lined by a free edge of the lipid membrane and is extended gradually during oligomerization*, EMBO Journal **17**, 1598-1605.
- [110] J. Solon (2004), *Interactions entre membranes lipidiques chargées: instabilités, déformations et mouvement*, PhD thesis, Université Paris 7, Paris.
- [111] K. Olbrich, W. Rawicz, D. Needham and E. Evans (2000), *Water permeability and mechanical strength of polyunsaturated lipid bilayers*, Biophysical Journal **79**, 321-327.
- [112] O. Sandre, L. Moreaux and F. Brochard-Wyart (1999), *Dynamics of transient pores in stretched vesicles*, Proceedings of the National Academy of Sciences USA **96**, 10591-6.
- [113] R. Waugh (1982), *Surface viscosity measurements from large bilayer vesicle tether formation-analysis*, Biophysical Journal **38**, 19-37.
- [114] E. Evans, H. Bowman, A. Leung, D. Needham and D. Tirrell (1996), *Biomembrane templates for nanoscale conduits and networks*, Science **273**, 933-935.
- [115] Z. Li, B. Anvari, M. Takashima, P. Brecht, J. H. Torres and W. E. Brownell (2002), *Membrane tether formation from outer hair cells with optical tweezers*, Biophysical Journal **82**, 1386-1395.
- [116] T. Roopa, N. Kumar, S. Bhattacharya and G. V. Shivashankar (2004), *Dynamics of membrane nanotubulation and DNA self-assembly*, Biophysical Journal **87**, 974-979.

Bibliography

- [117] T. Roopa and G. V. Shivashankar (2003), *Nanomechanics of membrane undulations and DNA assembly*, Applied Physics Letters **82**, 1631-1633.
- [118] D. Raucher and M. P. Sheetz (1999), *Characteristics of a membrane reservoir buffering membrane tension*, Biophysical Journal **77**, 1992-2002.
- [119] H. Hotani, T. Inaba, F. Nomura, S. Takeda, K. Takiguchi, T. J. Itoh, T. Umeda and A. Ishijima (2003), *Mechanical analyses of morphological and topological transformation of liposomes*, Biosystems **71**, 93-100.
- [120] D. K. Fygenson, M. Elbaum, B. Shraiman and A. Libchaber (1997), *Microtubules and vesicles under controlled tension*, Physical Review E **55**, 850-859.
- [121] G. Koster, M. VanDuijn, B. Hofs and M. Dogterom (2003), *Membrane tube formation from giant vesicles by dynamic association of motor proteins*, Proceedings of the National Academy of Sciences USA **100**, 15583-15588.
- [122] D. K. Fygenson, J. F. Marko and A. Libchaber (1997), *Mechanics of microtubule-based membrane extension*, Physical Review Letters **79**, 4497-4500.
- [123] A. Roux, G. Cappello, J. Cartaud, J. Prost, B. Goud and P. Bassereau (2002), *A minimal system allowing tubulation with molecular motors pulling on giant liposomes*, Proceedings of the National Academy of Sciences USA **99**, 5394-5399.
- [124] T. R. Powers, G. Huber and R. E. Goldstein (2002), *Fluid-membrane tethers: minimal surfaces and elastic boundary layers*, Physical Review E **65**, 1901.1 - 1901-11.
- [125] A. S. Smith, E. Sackmann and U. Seifert (2004), *Pulling tethers from adhered vesicles*, Physical Review Letters **92**, 208101-1 - 208101-4.
- [126] V. A. Frolov, V. A. Lizunov, A. Y. Dunina-Barkovskaya, A. V. Samsonov and J. Zimmerberg (2003), *Shape bistability of a membrane neck: a toggle switch to control vesicle content release*, Proceedings of the National Academy of Sciences USA **100**, 8698-8703.
- [127] E. Evans (2001), *Probing the relation between force-lifetime-and chemistry in single molecular bonds*, Annual Review of Biophysics and Biomolecular Structure **30**, 105-128.
- [128] R. Merkel (2001), *Force spectroscopy on single passive biomolecules and single biomolecular bonds*, Physics Reports **346**, 343-385.
- [129] Y. Kantor, M. Kardar and D. R. Nelson (1986), *Statistical mechanics of tethered surfaces*, Physical Review Letters **57**, 791-794.
- [130] R. Holzlohner (1998), *Mesoscopic and statistical properties of fluctuating membranes*, MSc thesis, Technische Universitat, Berlin.
- [131] A. Baumgartner and J.-S. Ho (1990), *Crumpling of fluid vesicles*, Physical Review A **41**, 5747-5750.
- [132] E. Evans and W. Rawicz (1997), *Elasticity of "fuzzy" biomembranes*, Physical Review Letters **79**, 2379-2382.
- [133] M. Terasaki, L. B. Chen and K. Fujiwara (1986), *Microtubules and the endoplasmic reticulum are highly interdependent structures*, Journal of Cell Biology **103**, 1157-1568.
- [134] L. Dreier and T. A. Rapoport (2000), *In vitro formation of the endoplasmic reticulum occurs independently of microtubules by a controlled fusion reaction*, Journal of Cell Biology **148**, 883-898.
- [135] M. P. Yaffe, N. Stuurman and R. D. Vale (2003), *Mitochondrial positioning in fission yeast is driven by association with dynamic microtubules and mitotic spindle poles*, Proceedings of the National Academy of Sciences USA **100**, 11424-11428.
- [136] C. Leduc, O. Campas, K. B. Zeldovich, A. Roux, P. Jolimaitre, L. Bourel-Bonnet, J. F. Joanny, P. Bassereau and J. Prost (2004), *Cooperative extraction of membrane nanotubes by molecular motors*, Proceedings of the National Academy of Sciences USA **101**, 17096-17101.
- [137] E. E. F. Riemsлаг, M. F. Janson and M. Dogterom (2004), *Active motor proteins can couple cargo to the ends of growing microtubules*, Physical Biology (accepted).
- [138] C. M. Coppin, D. W. Pierce, L. Hsu and R. D. Vale (1997), *The load dependence of kinesin's mechanical cycle*, Proceedings of the National Academy of Sciences USA **94**, 8539-8544.

Bibliography

- [139] M. J. Schnitzer, K. Visscher and S. M. Block (2000), *Force production by single kinesin motors*, Nature Cell Biology **2**, 718-723.
- [140] A. Parmeggiani, F. Julicher, L. Peliti and J. Prost (2001), *Detachment of molecular motors under tangential loading*, Europhysics Letters **56**, 603-609.
- [141] J. Lane and V. Allan (1998), *Microtubule-based membrane movement*, Biochimica et Biophysica Acta **1376**, 27-55.
- [142] S. P. Gross (2004), *Hither and yon: a review of bi-directional microtubule-based transport*, Physical Biology **1**, R1-R11.
- [143] J. Yajima, M. Edamatsu, J. Watai-Nishii, N. Tokai-Nishizumi, T. Yamamoto and Y. Y. Toyoshima (2003), *The human chromokinesin kid is a plus end-directed microtubule-based motor*, EMBO Journal **22**, 1067-1074.
- [144] K. Kinoshita, I. Arnal, A. Desai, D. N. Drechsel and A. A. Hyman (2001), *Reconstitution of physiological microtubule dynamics using purified components*, Science **294**, 1340-1343.
- [145] H. Bringmann, G. Skiniotis, A. Spilker, S. Kandels-Lewis, I. Vernos and T. Surrey (2004), *A kinesin-like motor inhibits microtubule dynamic instability*, Science **303**, 1519-1522.
- [146] B. Govindan and R. D. Vale (2000), *Characterization of a microtubule assembly inhibitor from Xenopus oocytes*, Cell Motility and the Cytoskeleton **45**, 51-57.
- [147] R. Vale, F. Malik and D. Brown (1992), *Directional instability of microtubule transport in the presence of kinesin and dynein, two opposite polarity motor proteins*, Journal of Cell Biology **119**, 1589-1596.
- [148] S. A. Endow and H. Higuchi (2000), *A mutant of the motor protein kinesin that moves in both directions on microtubules*, Nature **406**, 913-916.
- [149] M. Badoual, F. Julicher and J. Prost (2002), *Bidirectional cooperative motion of molecular motors*, Proceedings of the National Academy of Sciences USA **99**, 6696-6701.
- [150] K. Hirschberg, C. M. Miller, J. Ellenberg, J. F. Presley, E. D. Siggia, R. D. Phair and J. Lippincott-Schwartz (1998), *Kinetic analysis of secretory protein traffic and characterization of Golgi to plasma membrane transport intermediates in living cells*, Journal of Cell Biology **143**, 1485-1503.
- [151] R. M. Rios and M. Bornens (2003), *The Golgi apparatus at the cell centre*, Current Opinion in Cell Biology **15**, 60-66.
- [152] E. Evans, K. Ritchie and R. Merkel (1995), *Sensitive force technique to probe molecular adhesion and structural linkages at biological interfaces*, Biophysical Journal **68**, 2580-2587.
- [153] D. A. Simson, F. Ziemann, M. Strigl and R. Merkel (1998), *Micropipet-based pico force transducer: In depth analysis and experimental verification*, Biophysical Journal **74**, 2080-2088.
- [154] M. Karlsson, M. Davidson, R. Karlsson, A. Karlsson, J. Bergenholtz, Z. Konkoli, A. Jesorka, T. Lobovkina, J. Hurtig, M. Voinova and O. Orwar (2004), *Biomimetic nanoscale reactors and networks*, Annual Review of Physical Chemistry **55**, 613-649.
- [155] J.-Y. Shao and R. M. Hochmuth (1996), *Micropipette suction for measuring piconewton forces of adhesion and tether formation from neutrophil membranes*, Biophysical Journal **71**, 2892-2901.
- [156] G. Girdhar and J.-Y. Shao (2004), *Membrane tether extraction from human umbilical vein endothelial cells and its implication in leukocyte rolling*, Biophysical Journal **87**, 3561-3568.
- [157] E. Helfer, S. Harlepp, L. Bourdieu, J. Robert, F. C. MacKintosh and D. Chatenay (2001), *Viscoelastic properties of actin-coated membranes*, Physical Review E **63**, 021904-1 - 021904-13.
- [158] D. R. Klopfenstein, M. Tomishige, N. Stuurman and R. D. Vale (2002), *Role of phosphatidylinositol(4,5)biphosphate organization in membrane transport by the Unc104 kinesin motor*, Cell **109**, 347-358.
- [159] B. J. Peter, H. M. Kent, I. G. Mills, Y. Vallis, P. J. G. Butler, P. R. Evans and H. T. McMahon (2004), *BAR domains as sensors of membrane curvature: the amphiphysin BAR structure*, Science **303**, 495-499.
- [160] T. Nakagawa, M. Setou, D.-H. Seog, K. Ogasawara, N. Dohmae, K. Takio and N. Hirokawa (2000), *A novel motor, KIF13a, transports mannose-6-phosphate receptor to plasma membrane through direct interaction with AP-1 complex*, Cell **103**, 569-581.

Bibliography

- [161] F. Buss, S. D. Arden, M. Lindsay, J. P. Luzio and J. Kendrick-Jones (2001), *Myosin VI isoform localized to clathrin-coated vesicles with a role in clathrin-mediated endocytosis*, EMBO Journal **20**, 3676-3684.

Samenvatting

Membranen worden in levende cellen door motor-eiwitten in allerlei labyrintachtige netwerken van membraanbuizen getrokken. We hebben een minimaal model systeem ontwikkeld waarmee we de vorming van membraanbuizen kwantitatief hebben kunnen bestuderen buiten de cel. Dankzij deze experimenten weten we nu hoe moleculaire motors in staat zijn gezamenlijk de krachten te leveren die voor buisvorming vereist zijn.

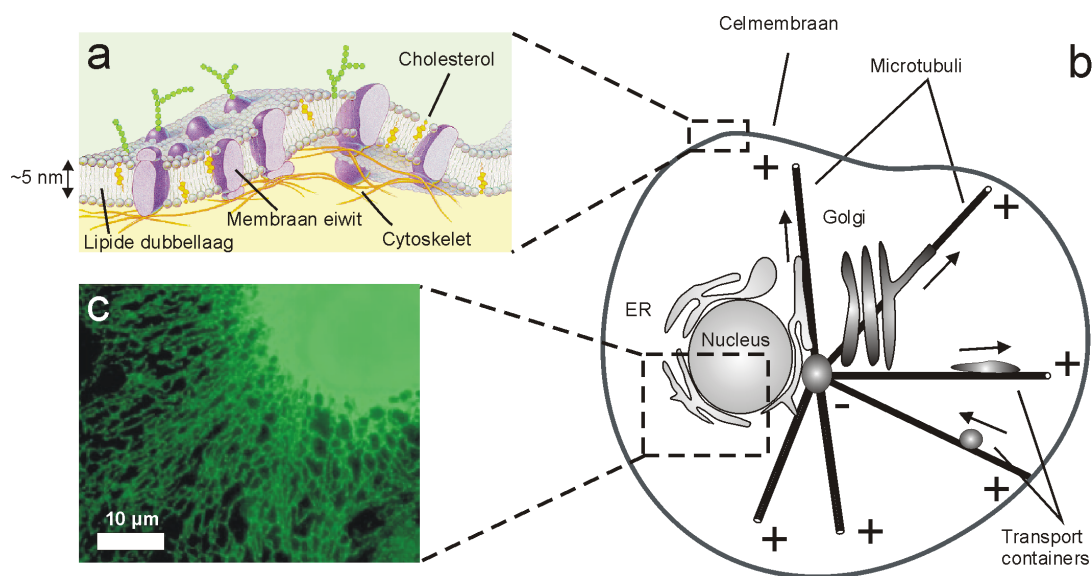
Membranen in de cel

De cel is de basis-bouweenheid van levende organismen. Planten- en dierencellen zijn typisch tussen de 10 en 50 μm groot, en een dubbellaag van lipiden die is doorspekt met eiwitten (zie figuur 8-1a) vormt de afbakening tussen de cel en de buitenwereld. De cellen zijn geen zakjes met een homogene soep van componenten. Zelfs op deze microscopische schaal is er een duidelijke organisatie, met verschillende compartimenten (organellen) voor de verschillende functies en componenten in de cel, die ook weer afgebakend worden door een membraan. Zo wordt het DNA opgeslagen in de celkern, wordt er energie aangemaakt in de mitochondriën, worden eiwitten en lipiden geproduceerd in het endoplasmatisch reticulum (ER) en dient het Golgi apparaat als een sorteercentrum voor transport tussen verschillende compartimenten (zie figuur 8-1b).

De positie en de vorm van membraancompartimenten wordt in de cel geregeld door een complex samenspel van motor-eiwitten en het cytoskelet (het skelet van de cel). Het cytoskelet verschaft stijfheid aan de cel en vormt tegelijkertijd een infrastructuur waarover motor-eiwitten kunnen bewegen. Het cytoskelet bestaat uit verscheidene componenten waarvan de zogenaamde microtubuli de dominante component voor de intracellulaire membraan-organisatie zijn (zie figuur 8-1b). Het motor-eiwit kinesine beweegt bijvoorbeeld over deze microtubuli (door ATP te verbruiken) en kan daarbij een maximale kracht uitoefenen van ongeveer zes piconewton. Wanneer een motor-eiwit zich vastkoppelt aan een membraan, kan het membraan-compartiment worden meegetrokken, of zelfs worden vervormd als deze beweging elders wordt tegengehouden. Onder bepaalde omstandigheden kunnen er zo membraanbuizen met een diameter van ongeveer 50 nm gevormd worden. Deze

Samenvatting

buizen vormen een belangrijke bouwsteen van intracellulaire compartimenten (zie figuur 8-1c) en worden bovendien gebruikt als langgerekte containers voor het vervoer tussen de verschillende compartimenten.



Figuur 8-1. (a) Schets van een celmembraan (zie tekst). (b) Schets van een cel met microtubuli en enkele van de intracellulaire compartimenten. (c) Fluorescentieplaatje van de labyrintachtige structuur van het ER.

In vitro studie van buisvorming door motoreiwitten

De correcte organisatie van membraanstructuren in de cel en het transport tussen de verschillende compartimenten is essentieel voor het gezond functioneren van cellen. Een beter begrip van de mechanismen die deze organisatie tot stand brengen zal leiden tot een beter begrip van het disfunctioneren van membranen, en de legio mogelijke consequenties daarvan.

Een belangrijk vraagstuk is hoe de organisatie gecoördineerd en gereguleerd wordt (hoe wordt bijvoorbeeld gedurende de verschillende stadia die een cel doorloopt in haar delingscyclus de ruimtelijke organisatie van membranen gereguleerd?). Alhoewel door gebruik te maken van ingenieuze technieken veel informatie is vergaard, is het door de complexiteit van de complete cel bijkans onmogelijk om de basis-reguleringsmechanismen te begrijpen. Om dit probleem te omzeilen, hebben we een vergelijkbaar systeem buiten de cel

Samenvatting

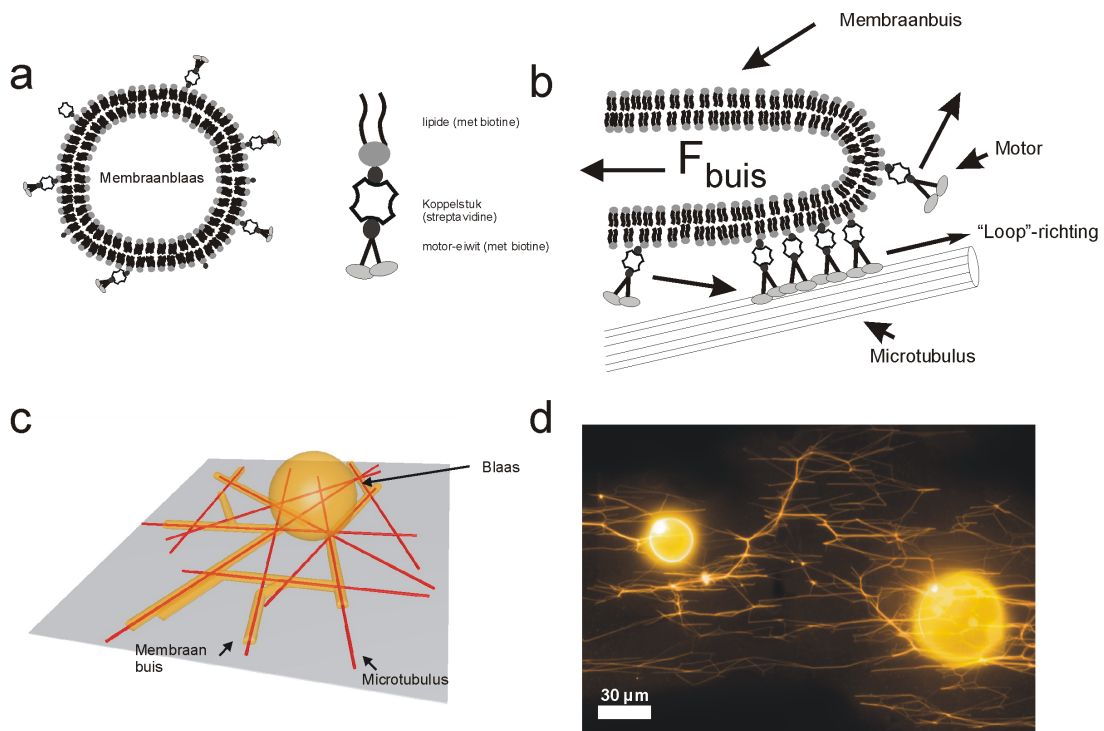
(*in vitro*) gereconstrueerd en bestudeerd. Daartoe hebben we microtubuli en het motor-eiwit kinesine uit cellen gehaald. Door gebruik te maken van de intrinsieke eigenschap van lipiden om zich te organiseren in dubbellaagen, kunnen grote (~20 µm diameter) membraanblazen worden gemaakt die bestaan uit één dubbellaag van vooraf gekozen lipiden. Deze membranen dienen vervolgens als een gesimplificeerd modelsysteem voor de cellulaire membranen. Het voordeel van het werken met een gereconstrueerd systeem is dat elk van de verschillende aanwezige componenten bekend is, in een gecontroleerde hoeveelheid. Omdat de membraanblazen relatief groot zijn kunnen ze bovendien zichtbaar gemaakt worden met geavanceerde microscopie.

Nadat de motor-eiwitten aan de membranen vastgemaakt zijn (via een biochemische truc, zie figuur 8-2a) worden ze in contact gebracht met een ongeordend en geïmmobiliseerd netwerk van microtubuli. Als de motor-eiwitten nu gaan “lopen” over de microtubuli (figuur 8-2b) zullen ze een kracht uitoefenen op de membraan. De experimenten laten zien dat dit (ook in een gereconstrueerd systeem) resulteert in de vorming van netwerken van membraanbuizen (figuur 8-2c en d).

Samenwerking door motors

Het interessante is dat de kracht die het kost om een buis te vormen meestal hoger blijkt te zijn dan de kracht die één enkel motor-eiwit kan uitoefenen (zie hieronder). De motor-eiwitten moeten dus op de een of andere manier samenwerken om voldoende kracht te kunnen genereren! Het heeft echter geen zin ergens halverwege de buis een kracht uit te oefenen aangezien de membraan vloeibaar is (lipiden kunnen vrijelijk bewegen en diffunderen in het vlak van de membraan). Wanneer een motor-eiwit halverwege de buis aan een lipide trekt zal deze daarom door de membraan heen getrokken worden totdat de punt van de buis is bereikt. Alleen de motor-eiwitten die hier kracht uitoefenen zullen vervolgens een bijdrage leveren aan de vorming van een buis.

Samenvatting



Figuur 8-2. (a) Schematische voorstelling van een membraanblaas met aangekoppelde motor-eiwitten (niet op schaal). (b) Schets van een groepje van motor-eiwitten dat gezamenlijk een membraanbuis vormt. (c) Schets van een netwerk van membraanbuizen gevormd uit een blaas op een ongeordend netwerk van microtubuli. (d) Fluorescentie-microscopie plaatje van een netwerk van membraanbuizen zoals gevormd in een experiment (de microtubuli en motors zijn niet zichtbaar).

Door in de experimenten de concentratie van motor-eiwitten en de membraaneigenschappen te variëren, hebben we dit modelsysteem kwantitatief kunnen bestuderen. De belangrijkste conclusies uit de experimenten zijn: 1) dat louter motor-eiwitten, microtubuli en membraanblazen voldoende zijn voor de vorming van buizen, en 2) dat er een drempelconcentratie van motor-eiwitten nodig is om buizen te vormen. Deze concentratie hangt af van de kracht die het kost om een buis uit de blaas te trekken (zie hieronder). De resultaten kunnen beschreven worden met een theoretisch model waarin de motors een cluster vormen die dynamisch in stand wordt gehouden. Motor-eiwitten die reeds in het groepje aanwezig zijn, zullen met een bepaalde kans loslaten (deze kans is afhankelijk van de kracht die het motor-eiwit te verduren heeft), terwijl er zich tevens per seconde een aantal motors (afhankelijk van de concentratie van motor eiwitten) bij de cluster zullen voegen. De hoeveelheid motor-eiwitten in de cluster kan alleen gehandhaafd worden als er zich voldoende

Samenvatting

motors per seconde bij de cluster voegen om het aantal dat eruit getrokken wordt te compenseren.

Wat bepaalt de kracht die vereist is om een buis te vormen?

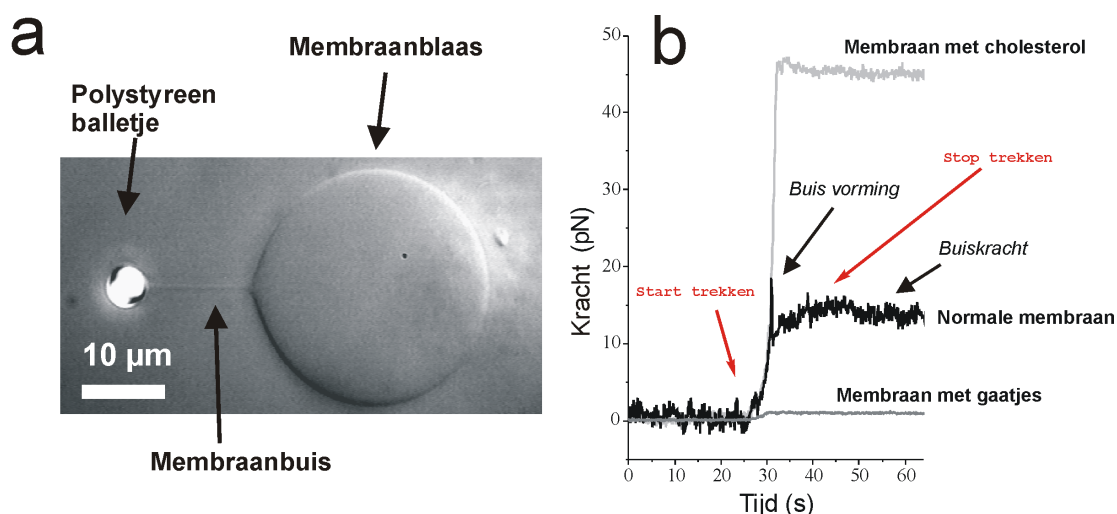
Als er een lokale kracht op een blaas wordt uitgeoefend door eraan te trekken dan zal in eerste instantie een groot deel van de membraan vervormen. Verder in het trekproces gebeurt er iets contra-intuïtiefs: in tegenstelling tot vaste elastische materialen wordt de membraan niet verder over het hele oppervlak vervormd, maar wordt er een membraanbuis met een constante diameter van enkele tientallen nanometers gevormd. Het vormen van een buis is energetisch voordeliger en dankzij de vloeibare aard van de membraan kunnen de lipiden zich makkelijk hergroeperen tot deze nieuwe configuratie.

Om dit systeem beter te begrijpen hebben we de kracht die het kost om een buis na vorming op een vaste lengte te houden (de buiskracht) gemeten voor membranen met een verschillende samenstelling. Deze krachten zijn typisch een paar (tientallen) piconewtons groot. Krachten van deze orde kunnen gegenereerd en gemeten worden met een optisch pincet. Met het optisch pincet wordt een balletje van enkele micrometers groot aan de blaas geplakt en vervolgens wegbewogen en op een vaste afstand gehouden (zie figuur 8-3a). De kracht op het balletje wordt achteraf bepaald door de verplaatsing ervan in het optisch pincet te meten.

De eigenschappen van de membraan hebben we op twee manieren gevarieerd: de membraan is stijver gemaakt door er cholesterol in op te nemen, en de spanning van de membraan is geminimaliseerd door gaatjes in de membraan te maken waardoor de osmotische druk weggenomen wordt. Als we de kracht meten die het kost om een buis te trekken na toevoegen van cholesterol, vinden we een grofweg verdrievoudiging van de kracht die het kost om een buis te vormen (van ~15 naar 45 pN, zie figuur 8-3b). Als door de gaatjes in de membraan de membraanspanning wordt geminimaliseerd vinden we een kracht die ongeveer zestig keer zo laag wordt als die voor membranen zonder gaatjes! (van ~45 pN naar ~0.75 pN, zie figuur 8-3b). Deze krachtveranderingen kunnen begrepen worden door de twee belangrijkste bijdragen aan de energie van een membraanbuis in ogenschouw te nemen: de membraanspanning en de buigingsstijfheid. Aan de ene kant vereist de vorming van het oppervlak van de buis extra energie die bepaald wordt door de grootte van de membraanspanning. Hier geldt: hoe dunner de buis, hoe voordeliger. De buigingsstijfheid van

Samenvatting

de membraan zal echter het steeds dunner worden van de buis beperken. Aangezien een membraan erg dun is (~5 nm) kost het in principe weinig energie om deze te verbuigen. Bij de vorming van een buis met een diameter van ~50 nm blijkt de buiging desalniettemin een vergelijkbare bijdrage aan de energie te leveren als die door toedoen van de membraanspanning.

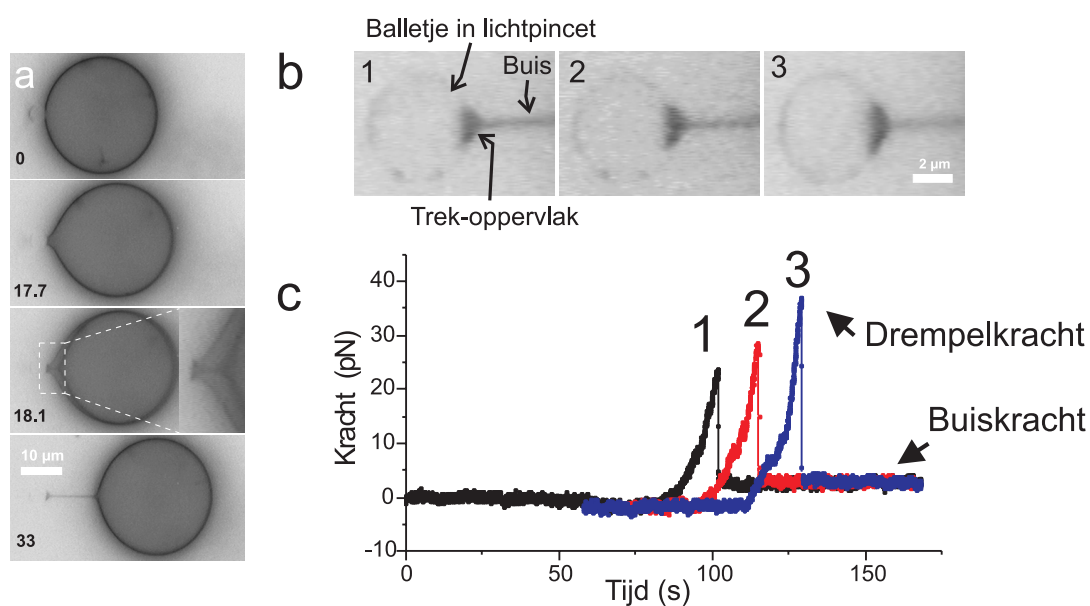


Figuur 8-3. (a) Een polystyreen balletje wordt gebruikt om een membraanbuis uit een blaas te trekken (Differential Interference Contrast-microscopie). (b) De kracht op het balletje gedurende het vormen en vasthouden van buizen uit blazen met verschillende eigenschappen.

Barrière voor vorming van membraanbuizen

De initiële kracht (de drempelkracht) die vereist is om een buis te vormen, blijkt niet hetzelfde te zijn als de kracht die nodig is om een reeds gevormde buis vast te houden. Tijdens de eerste vervorming van de membraan neemt de kracht toe tot een moment waarop de situatie niet meer stabiel is (figuur 8-4a, 2^e en 3^e plaatje van boven). Op dat moment wordt er een membraanbuis gevormd (figuur 8-4a, onderste figuur) en voor de handhaving hiervan is een lagere kracht vereist. De hoogste kracht die bereikt moet worden om een buis te vormen is de drempelkracht.

Samenvatting



Figuur 8-4. Fluorescentiemicroscopie-plaatjes van een membraanblaas die vervormd wordt door een balletje (nauwelijks zichtbaar). (b) Zoom van het oppervlak dat aan het balletje vastplakt. (c) De kracht op het balletje gedurende drie maal de vorming van een buis. De krachten corresponderen met de figuren in (b), waarin het contactoppervlak iedere keer toeneemt.

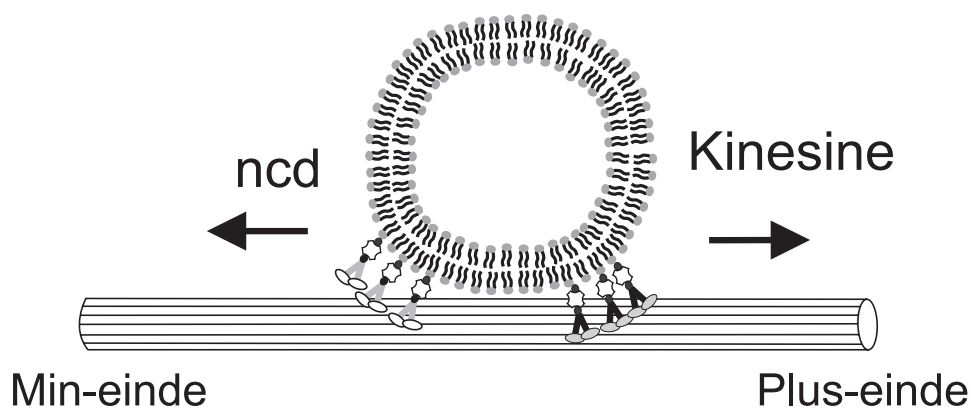
Om de drempelkracht te bestuderen hebben we verscheidene malen buizen gevormd uit dezelfde blaas. In dit experiment hebben we ervoor gezorgd dat het contactoppervlak waarop de kracht wordt uitgeoefend iedere maal dat een buis gevormd wordt toeneemt (figuur 8-4b). Deze experimenten tonen aan dat de drempelkracht voor buisvorming lineair toeneemt met de omtrek van het oppervlak waaraan getrokken wordt (figuur 8-4c), en dat de verhouding tussen de diameter van het oppervlak waaraan getrokken wordt en de diameter van de gevormde buis de drempelkracht bepaalt. Deze experimentele metingen hebben we kunnen staven met resultaten van computersimulaties en theoretische berekeningen.

Competitie tussen motor-eiwitten

Microtubuli zijn van zichzelf asymmetrisch, met één uiteinde dat het plus-einde genoemd wordt en het andere dat het min-einde genoemd wordt (zie figuur 8-1 en figuur 8-5). Deze asymmetrie wordt herkend door motor-eiwitten: sommige soorten motor-eiwitten lopen richting het plus-einde (bijvoorbeeld kinesine) terwijl andere soorten juist richting het min-

Samenvatting

einde (bijvoorbeeld ncd) lopen. In cellen zijn dikwijls beide soorten motor-eiwitten aan membraanblazen vastgekoppeld, met als consequentie een soort touwtrekken aan de membraanblaas door de verschillende groepjes motor-eiwitten. Het gevolg van dit touwtrekken is enerzijds dat membraanblazen in de cel vaak van bewegingsrichting veranderen. Het is echter niet bekend hoe de richting van de blazen gecoördineerd wordt. Anderzijds wordt het door de kracht die uitgeoefend wordt door tegengesteld gerichte motors ook mogelijk om membraanbuizen te vormen. Om inzicht te krijgen in de gevolgen die dit touwtrekken op de vorm en ruimtelijke verdeling van membraanblazen heeft, hebben we een experimenteel modelsysteem ontwikkeld. In dit modelsysteem zijn tegelijkertijd plus-eind gerichte motors en min-eind gerichte motors vastgekoppeld aan de blazen (zie figuur 8-5).



Figuur 8-5. Schets van een membraanblaas waar plus-eind gerichte en min-eind gerichte motor-eiwitten aan vastgekoppeld zijn.

Vervolgens hebben we het optisch pincet gebruikt om de blaas op een microtubulus te plaatsen, waarna het touwtrekken kan beginnen. Dit onderzoek is zeker nog niet afgerond maar er zijn al enkele resultaten. Ten eerste suggereren de resultaten dat een hoge concentratie motor-eiwitten het overschakelen tussen bewegingsrichtingen moeilijker maakt. Ten tweede is het soms zo dat grotere membraanblazen in plaats van de looprichting te veranderen buizen vormen. Om meer duidelijkheid te krijgen over dit systeem, zal het uitgebreider bestudeerd moeten worden.

Samenvatting

Relevantie van de resultaten?

In tegenstelling tot wat gedacht werd, laten onze experimenten zien dat motor-eiwitten de intrinsieke eigenschap hebben om via zelforganisatie een cluster te vormen die voldoende kracht kan uitoefenen om membraanbuizen te vormen, en dat het niet noodzakelijk is om de motors via een statische connectie aan elkaar te binden. Bovendien hebben we laten zien dat er voor buisvorming een minimale concentratie van motor-eiwitten vereist is die afhangt van de kracht die het kost om de buis te vormen. Dit suggereert dat de mate van buisvorming in de cel gereguleerd zou kunnen worden door bijvoorbeeld de concentratie van motor-eiwitten te beïnvloeden. Het is ook mogelijk dat de stijfheid of de spanning van de membraan gemodificeerd worden. Een andere suggestie vloeit voort uit onze krachtmetingen die aantonen dat voor buisvorming een hogere kracht vereist is als er aan een groter oppervlak wordt getrokken. Het is dus niet alleen de grootte van de kracht, maar ook *hoe* een kracht wordt uitgeoefend die bepaalt of membraanbuizen gevormd worden. Deze vondst suggereert dat de mate van buisvorming in de cel wellicht gereguleerd wordt door de grootte van de domeinen waarmee de motor-eiwitten verbonden zijn.

We hebben via onze *in vitro* benadering veel geleerd van de basismechanismen die de ruimtelijke organisatie van membranen bepalen. De uitdaging zal nu zijn om te bestuderen hoe deze mechanismen in de complexiteit van de levende cel daadwerkelijk gereguleerd worden.

Samenvatting

Nawoord

Veel zaken lijken moeilijk als je er alleen voor staat, maar met vereende kracht (net als motor-eiwitten doen, zie hoofdstuk 5 ;-) zijn ze vaak best te overzien. De resultaten die in dit proefschrift beschreven staan zouden dan ook niet mogelijk geweest zijn zonder de steun van, en de samenwerking met vele personen.

Ik heb mijn onderzoek uitgevoerd in de groep “bio-assembly and organization” van Marileen Dogterom, dit is een ideale plek voor het doen van onderzoek in een stimulerende en enthousiaste sfeer, maar ook met een kritische houding naar de eigen resultaten. Als ik het even niet meer zag zitten kon ik altijd spontaan langskomen en, na een grondige gezamenlijke analyse van de data weer vol nieuwe energie aan de slag. Ik wil hiervoor de huidige en vroegere groepsleden bedanken: Andrea, Astrid, Bas, Cendrine, Eva, Jacob, Gertjan, Guillaume, Henk, Laura, Liedewij, Marcel, Marco, Marileen, Martijn, Mathilde, Tatiana en Wouter.

Op AMOLF zijn er veel mensen geweest die mijn promotietijd prettig en interessant hebben gemaakt. Vele interacties waren waardevol, maar ik zal er hier slechts een paar bij naam noemen. Ik heb het nauwst samengewerkt met Martijn van Duijn. Martijn is in alle opzichten een fantastische collega, een magiër met pipet en computers die altijd vol energie en enthousiasme voor je klaarstaat, zelfs nu hij zich aan de andere kant van de wereld bevindt. Angelo Cacciuto wil ik bedanken voor een prettige samenwerking. Deze samenwerking zou er niet geweest zou zijn zonder Marco Cosentino Lagomarsino die de bijzondere gave bezit om een brug te slaan tussen theoretici en experimentalisten. Andrea Fera heeft me laten zien dat er veel tegen kan zitten, maar dat met een sterke wil niets onoverkomelijk is. Na de verhuizing naar de Overloop vanuit het oude AMOLF gebouw, hebben Ruud van Leeuwen, Ivan Coluzza en ik gedurende langere tijd gedrieën (!) een kamer gedeeld. Dit is me goed bevallen en ik wens ze alle succes met de verdere promotie.

Buiten AMOLF hebben we met Aurélien Roux, Cécile Leduc en Patricia Bassereau, regelmatig uitgebreid en openhartig gebrainstormd over de interpretatie van resultaten. Uiteindelijk hebben we zelfs gezamenlijk onderzoek gedaan, terwijl het in eerste instantie misschien wel veel logischer was geweest om in competitie te geraken. Ik denk dat de samenwerking uiteindelijk voor iedereen veel heeft opgeleverd. De COSY zomerscholen met de groep van Christoph Schmidt waren erg nuttig en gezellig, en hebben zeker het

Nawoord

drempelverlagende effect gehad waar ze (ook) voor bedoeld waren: tegenwoordig lopen we zonder probleem bij zijn lab binnen en er zijn zelfs gezamenlijke tubuline-purificaties gedaan.

Op AMOLF werd de plezierige werkomgeving niet alleen door wetenschappers gecreëerd. Het is al door velen verkondigd (maar daarom niet minder waar) dat het op AMOLF prettig toeven is door de professionaliteit en het enthousiasme van alle ondersteunende afdelingen. Ik wil hierbij iedereen bedanken voor de flexibiliteit en de snelheid waarmee problemen opgelost werden als dat nodig was, terwijl dit altijd op zeer sympathieke wijze gebeurde. Als wetenschapper ben je gauw geneigd om je enkel op je eigen vakgebied te richten. Door zowel met wetenschappers als ondersteunend personeel in de IRC en (met Dirk Vossen) in de COR actief te zijn, heb ik de kans gekregen om het efficiënt functioneren van AMOLF en FOM vanuit een heel andere invalshoek te leren kennen. Dit was een erg leuke ervaring.

Buiten het werk heb ik een fijne tijd gehad met Paul en Sander (en nog vele andere AMOLFers die “dynamisch associeerden”), de D&D groep (wat kan een grote dosis creativiteit en fantasie leuke avonden opleveren), en aan de zaterdagen met mijn schaakteam. Alteveer zal ik nog lang mooie herinneringen overhouden. Ik wil mijn ouders en broers bedanken voor hun niet aflatende steun, ik besef terdege hoe gelukkig ik met hen mag zijn. Tenslotte wil ik Jorunn bedanken: haar steun en interesse hebben veel voor me betekend en geven vertrouwen in de toekomst, waar dan ook.

Curriculum Vitae

Gerbrand Koster werd geboren op 29 september 1974 in Wageningen. Na het behalen van het VWO diploma in 1992 aan de “scholengemeenschap Reigersbos” te Amsterdam begon hij aan een studie experimentele natuurkunde. De studie werd in 1999 afgerond met een stageonderzoek naar contourintegratie door het visuele systeem met behulp van magneto-encefalografie. Dit gebeurde op het “Interuniversitair Oogheelkundig Instituut” onder leiding van Dr. P.R. Roelfsema en Prof. Dr. H. Spekreijse. In 2000 werd op het FOM Instituut voor Atoom en Molecuulfysica (AMOLF) in de groep van Prof. Dr. Marileen Dogterom zijn promotieonderzoek gestart. De resultaten van dat onderzoek staan beschreven in dit proefschrift. Gedurende de promotie was hij twee jaar lid van de Instituutsraad-commissie van AMOLF en de centrale ondernemingsraad van FOM.